

Targeted transport of active pharmaceutical ingredients into adipose tissue

Dissertation

zur

Erlangung des Doktorgrades (Dr. rer. nat.)

der

Mathematisch-Naturwissenschaftlichen Fakultät

der

Rheinischen Friedrich-Wilhelms-Universität Bonn

vorgelegt von

Zheming Niu

aus

Hangzhou, China

Bonn (August 2022)

Angefertigt mit Genehmigung der Mathematisch-Naturwissenschaftlichen Fakultät
der Rheinischen Friedrich-Wilhelms-Universität Bonn

1. Gutachter: Prof. Dr. Alexander Pfeifer
2. Gutachter: Prof. Dr. Alf Lamprecht

Tag der Promotion: 03.02.2023

Erscheinungsjahr: 2023

Acknowledgment

I would like to express my sincere gratitude to my supervisors, Prof. Dr. Alexander Pfeifer and Prof. Dr. Alf Lamprecht for providing me with these amazing projects and their invaluable advice. They handed a master's graduate from Kiel the key to open the door of “Top-notch Science” in December 2017 and elevated that young man to an entirely new level scientifically and personally.

Secondly, my sincere thanks go out to my esteemed supervisor --- Dr. Staffan Hildebrand for his great patience, treasured support, and tremendous scientific input during my PhD. Dr. Staffan Hildebrand accepted and supported me in the beginning and further guided me always in the right direction. We collaborated closely on particle synthesis, keeping animals, and attending conferences. His Office 005 is always open to me whenever I had troubles or I needed his advice.

I would sincerely express my appreciation to all the colleagues from AG Pfeifer, the Institute of Pharmacology and Toxicology. Thank you to Dr. Jelena Zurkovic for her professional techniques in various fields and her suggestions for my thesis. Thank you to Dr. Laia Reverte, Dr. Gerburg Schwärzer, and Dr. Viktoria Götz for a lot of help in the lab and for checking documents. Thank you to my close friends Dr. Stefan Löffler, Mickel Michael, and the former and current officemates from Office 008 for such a cherished time spent together and trillions of help.

Moreover, I would also like to give my special thanks to my friends and colleagues, Dr. Ehab Ali, Dr. Jan Kozak, and Mr. Sebastian Kappes from AG Lamprecht, the Institute of Pharmaceutical Technology, University of Bonn (my “second hometown” institute). From them, I received a lot of encouragement, understanding, and help. In the most challenging period of my PhD, they introduced me to their specialties and accepted me as a part of their group. Without their assistance, I could not have accomplished and gone so far.

I am also grateful to the Bonn International Graduate School of Drug Sciences (BIGS DrugS) for the PhD funding as well as to Dr. Elisabeth Mies-Klomfass for her corrections, help, regulations, and coordination.

My appreciation also goes out to all my friends and my warm family. My dear parents, 牛加堅先生和陸靜文女士, deserve special thanks for their love, continued support, countless sacrifices, and encouragement. Thank you for your 30 years of dedication to me.

由衷感謝爸爸媽媽您們對兒子一路成長的無窮關愛和無盡付出！哲明感激涕零，謝無疆焉！

Table of Content

ACKNOWLEDGMENT	5
TABLE OF CONTENT	6
LIST OF FIGURES	10
LIST OF TABLES	12
LIST OF UNITS	13
ABBREVIATIONS	14
1 INTRODUCTION.....	20
1.1 Physiology of adipose tissue.....	20
1.1.1 Obesity.....	20
1.1.2 Adipose tissue	21
1.1.2.1 White adipose tissue	21
1.1.2.2 Brown adipose tissue	22
1.1.3 Adipogenesis and lipolysis.....	23
1.1.4 Brown adipocyte activation: thermogenesis at the molecular level	24
1.1.5 Browning and whitening of white adipose tissue	25
1.1.6 Lipoprotein particles.....	26
1.1.7 G protein-coupled signaling pathways	28
1.1.8 Adrenergic receptors in adipose tissue.....	29
1.1.9 A β 3-adrenergic receptor agonist: Mirabegron	32
1.1.10 A Gq signaling inhibitor: FR900359 (FR).....	33
1.1.11 Thyroid hormones and thyroid hormone activities in adipose tissue	34
1.1.11.1 Thyroid hormone	34
1.1.11.2 Thyroid hormone-related activities in the liver and adipose tissue	35
1.2 Poly (lactic-co-glycolic acid) polymer-based delivery system	38
1.2.1 Intrinsic properties of PLGA copolymers	38
1.2.2 Biodegradation mechanism of PLGA microparticles as drug delivery carriers	39
1.3 Artificial triglyceride-rich lipoproteins uptake in adipose tissue	40
2 AIM OF THE THESIS.....	41

3	MATERIALS AND METHODS	42
3.1	Common materials and equipment	42
3.2	Cell culture and isolation of adipocytes	43
3.2.1	Materials and equipment	43
3.2.2	Isolation and immortalization of BAT-derived mesenchymal stem cells (MSCs)	44
3.2.3	Isolation of WAT-derived mesenchymal stem cells (MSCs)	45
3.2.4	Differentiation of adipocytes	45
3.2.4.1	Differentiation of brown adipocytes	45
3.2.4.2	Differentiation of white adipocytes	46
3.3	Nucleic acid methods	47
3.3.1	Materials and equipment	47
3.3.2	RNA isolation	47
3.3.3	Complementary DNA (cDNA) synthesis	48
3.3.4	Real-time quantitative PCR (RT-qPCR)	49
3.4	Protein analysis	51
3.4.1	Materials and equipment	51
3.4.2	Protein lysates from cells and tissues	52
3.4.3	Protein quantification using the Bradford method	53
3.4.4	Western Blot	54
3.4.4.1	One-dimensional SDS-polyacrylamide electrophoresis (SDS-PAGE)	54
3.4.4.2	Blotting and immunodetection	55
3.5	Oil Red O staining	56
3.6	Lipolysis	57
3.6.1	Materials and equipment	57
3.6.2	<i>In vitro</i> lipolysis	57
3.6.3	<i>Ex vivo</i> lipolysis	58
3.7	Immunohistochemistry	58
3.7.1	Materials and equipment	58
3.7.2	Tissue preparation for staining	59
3.7.3	Hematoxylin/Eosin (H&E) staining	59
3.7.4	Immunohistochemistry for UCP1 detection	59
3.8	Mitochondrial Stress Assay	60
3.9	Toxicity assays	62
3.9.1	MTT assay	62
3.9.2	ATP-based assay	62
3.10	MIR-loaded PLGA MPs synthesis method	62
3.10.1	Materials and equipment	62
3.10.2	Microparticles preparation	63
3.10.3	Drug releasing condition	64

3.10.4	Human subcutaneous white adipose tissue	64
3.11	HPLC system and Liquid Chromatography-Mass Spectrometry (LC/MS) analysis	64
3.11.1	Materials and equipment.....	64
3.11.2	HPLC methods	65
3.11.3	LC/MS method.....	65
3.11.4	Scanning Electron Microscope (SEM) analysis.....	65
3.12	The API-loaded triglyceride-rich lipoproteins synthesis method.....	66
3.12.1	Materials and equipment.....	66
3.12.1	API-loaded TRLs preparation.....	66
3.13	Animal experiments	67
3.13.1	Materials and equipment.....	67
3.13.2	Targeted delivery T3-TRLs to BAT	67
3.14	Statistics	68
4	RESULTS OF PROJECT I: MIR-LOADED PLGA MICROPARTICLES	69
4.1	Characterization of MIR-loaded microparticles	69
4.1.1	Characteristics and morphology of MIR-loaded microparticles.....	69
4.1.2	Encapsulation efficiency and drug loading of MIR-loaded microparticles	71
4.1.3	<i>In vitro</i> release profile of MIR-loaded microparticles.....	73
4.1.4	Stability of MIR-loaded microparticles.....	75
4.2	Effects of MIR-loaded microparticles on adipocytes.....	76
4.2.1	<i>In vitro</i> lipolysis induced by MIR-loaded microparticles.....	76
4.2.2	MIR-loaded microparticles induced BA thermogenesis	77
4.2.3	MIR-loaded microparticles induced iWA beiging and morphological changes	78
4.2.4	Mitochondrial stress assay on adipocytes.....	81
4.3	Toxicity tests of MIR-loaded microparticles on adipocytes	82
4.4	<i>Ex vivo</i> lipolysis induced by MIR-loaded microparticles	84
4.5	MIR-loaded microparticles induce lipolysis in human subcutaneous white adipose tissue	88
4.6	<i>Ex vivo</i> lipolysis and gene expressions in explanted human subcutaneous white adipose tissue after direct injection of MIR-loaded microparticles	91
5	RESULTS OF PROJECT II: API-LOADED TRLS.....	93
5.1	Characterization of API-loaded TRLs	93
5.2	Optimization of API-loaded TRLs.....	94
5.3	<i>In vivo</i> effects of T3-TRLs.....	97
5.3.1	Metabolic changes in mice treated with T3-TRLs	97

Table of Content

5.3.2	T3-TRLs induced effects in brown adipose tissue	99
5.3.3	T3-TRLs-induced gene expressions	100
5.3.4	Histological changes in mice treated with T3-TRLs	103
6	DISCUSSION	106
6.1	Project I: MIR-loaded PLGA microparticles	106
6.1.1	A novel combination of PLGA microparticles and MIR	106
6.1.2	The release profile of MIR-loaded PLGA microparticles	107
6.1.3	Non-toxicity of MIR-loaded PLGA microparticles in adipocytes	108
6.1.4	MIR-loaded PLGA microparticles induced effects in iWA	108
6.1.5	MIR-loaded PLGA microparticles induced oxygen consumption in adipocytes	109
6.1.6	MIR-loaded PLGA microparticles induced effects in adipose tissue	110
6.2	Project II: T3-loaded TRLs	112
6.2.1	Optimization of T3-TRLs	112
6.2.2	<i>In vivo</i> effects of T3-TRLs	113
7	SUMMARY	116
8	REFERENCES	118
	PUBLICATIONS AND ABSTRACTS	140

List of Figures

Figure 1. The mechanism of lipolysis in adipocytes via β -adrenergic receptors	24
Figure 2. Thermogenesis at the molecular level in brown adipocytes	25
Figure 3. NE-activated brown adipocytes take up TRLs from the bloodstream	27
Figure 4. Different adrenergic receptor expressions in human and rodent adipose tissue	31
Figure 5. Chemical structure of mirabegron.....	33
Figure 6. Chemical structure of FR900359	34
Figure 7. The effects of T3 in the liver.....	36
Figure 8. The function of T3 in brown adipocytes	37
Figure 9. Degradation of drug-loaded PLGA particles	39
Figure 10. Degradation of PLGA to lactic acid and glycolic acid	40
Figure 11. Assembly and characterization of MIR-loaded microparticles	71
Figure 12. Encapsulation efficiency and Drug loading of four formulations of MIR-loaded PLGA microparticles.....	72
Figure 13. <i>In vitro</i> release profiles of MIR-loaded PLGA microparticles.....	74
Figure 14. Morphological images of MIR-loaded microparticles after release.....	74
Figure 15. Scanning electron microscopic pictures of microparticles before and after 8 months of storage.....	75
Figure 16. Lipolysis of adipocytes after treatments.....	77
Figure 17. Gene expression of <i>Ucp1</i> , <i>Pparγ</i> , and <i>Fabp4</i> in BA after treatments	78
Figure 18. Changes in iWA after treatments.....	80
Figure 19. MIR-loaded microparticles induced effects on mitochondrial respiration of iWA	82
Figure 20. MTT assay for adipocytes after treatments.....	83
Figure 21. ATP assay for adipocytes after treatments	84
Figure 22. Lipolysis of adipose tissue after treatments	85
Figure 23. Lipolysis of white adipose tissue after treatments via direct injection	86
Figure 24. Prolonged lipolysis of white adipose tissue after treatments.....	87
Figure 25. β -adrenergic receptor expression in human/murine WA and WAT and <i>ex vivo</i> lipolysis of human scWAT after treatments.....	90
Figure 26. <i>Ex vivo</i> lipolysis and gene expressions in human scWAT after treatment with MIR-MPs via direct injection.....	92
Figure 27. Schematic overview of API-loaded TRLs and API-loaded TRLs preparation protocol	95
Figure 28. Optimization of T3-loaded TRLs	96
Figure 29. Optimization of FR-loaded TRLs.....	97
Figure 30. Assembly and physiological changes of mice after treatment with Vehicle-TRLs/T3-TRLs.....	98

Figure 31. Gene and protein expression in BAT after treatment with Vehicle-TRLs/T3-TRLs .	100
Figure 32. Hepatic gene expression in mice treated with Vehicle-TRLs and T3-TRLs.....	102
Figure 33. T3 regulated gene expression in the heart after treatment with Vehicle-TRLs and T3-TRLs.....	103
Figure 34. H&E staining and immunohistochemical UCP1 staining of BAT after treatments with Vehicle-TRLs and T3-TRLs	104
Figure 35. H&E staining of the liver and heart of mice treated with Vehicle-TRLs and T3-TRLs	105
Figure 36. Scheme illustration of mechanisms of MIR-MPs and T3-TRLs	117

List of Tables

Table 1. qPCR Program	49
Table 2. qPCR primer sequences	49
Table 3. Four formulations of MIR-loaded microparticles.....	70
Table 4. Characteristics of TRLs	94

List of Units

μl	Microliter
μM	Micromolar
A	Ampere
C	Celsius
d	Day
h	Hour
L	Liter
M	Molar
min	Minute
ml	Milliliter
nM	Nanomolar
V	Volt
v/v	Volume/Volume
w/v	Weight/Volume

Abbreviations

7TM	7 transmembrane domain
ACC	Acetyl-CoA carboxylase
ACMs	Artificial chylomicrons
ACSL	Long-chain Acyl-CoA synthetase
ADH	Alcohol dehydrogenase
ADRB1	Beta 1-adrenergic receptors
ADRB2	Beta 2-adrenergic receptors
ADRB3	Beta 3-adrenergic receptors
aP2	Adipocytes protein 2
APIs	Active pharmaceutical ingredients
Apo	Apolipoprotein
APS	Ammonium peroxodisulfate
ASC	Adipose-derived stem cell
AT	Adipose tissue
ATGL	Adipose triglyceride lipase
ATP	Adenosine triphosphate
AUC	Area under the curve
BA	Brown adipocyte
BAT	Brown adipose tissue
BMI	Body mass index
BSA	Bovine serum albumin
C/EBP α	CCAAT/enhancer-binding protein α
C/EBP β	CCAAT/enhancer-binding protein β
CAC	Citric acid cycle
cAMP	Cyclic adenosine monophosphate
cDNA	Complementary DNA
CGI58	Comparative gene identification-58
ChREBP	Carbohydrate-responsive element-binding protein
Cidea	Cell death inducing DFFA like effector A
Cpt1	Carnitine palmitoyltransferase
Cpt1a	Carnitine palmitoyltransferase 1A
CREB	cAMP response element-binding protein
CYP	Cytochrome
Cyp7a1	Cytochrome P450 family 7 subfamily A member 1
d.i.	Direct injection
DAB	3,3'-Diaminobenzidine

Abbreviations

DBZ	Dibenzazepine
DCM	Dichloromethane
DEPC	Diethylpyrocarbonate
DG	Diglycerol
Dgat	Diacylglycerol O-acyltransferase 1
Dio1	Iodothyronine deiodinase 1
Dio2	Iodothyronine deiodinase 2
Dio3	Iodothyronine deiodinase 3
DL	Drug loading
DLS	Dynamic light scattering
DMEM	Dulbecco's Modified Eagle Medium
DMSO	Dimethyl sulfoxide
DNA	Deoxyribonucleic acid
EA	Ethyl acetate
EDTA	Ethylenediaminetetraacetic acid
EE	Encapsulation efficiency
EGTA	Ethylene glycol-bis(β -aminoethyl ether)- <i>N,N,N',N'</i> -tetraacetic acid
ELISA	Enzyme-linked immunosorbent assay
ET-1	Endothelin-1
EtOH	Ethanol
FABP4	Fatty acid-binding protein 4
FADH2	Flavin adenine dinucleotide
FAS	Fatty acid synthase
FATPs	Fatty acid transport proteins
FBS	Fetal bovine serum
FCCP	Carbonyl-cyanide-4-(trifluoromethoxy) phenylhydrazone
FDA	Food and drug administration
FFA	Free fatty acids
FGF21	Fibroblast growth factor 21
FR	FR900359
GDP	Guanosine diphosphate
GLP-1	Glucagon-like peptide-1
GPCRs	G protein-coupled receptors
GPIHBP1	Glycosylphosphatidylinositol anchored high-density lipoprotein binding protein 1
GTP	Guanosine triphosphate
gWAT	Gonadal white adipose tissue
H&E	Hematoxylin/Eosin
HCC	Hepatocellular carcinoma
HDL	High-density lipoproteins

HFD	High-fat diet
HIF1 α	Hypoxia-inducible factor 1- α
HPLC	High-performance liquid chromatography
HPRT	Hypoxanthine-guanine phosphoribosyltransferase
HSL	Hormone-sensitive lipase
i.p.	Intraperitoneal injection
i.v.	Intravenous injection
IBMX	3-isobutyl-1-methylxanthine
ICI	ICI 118,551
IRON-TRL	Iron-oxide-nanoparticle-loaded TRLs
iWA	Inguinal white adipocyte
iWAT	Inguinal white adipose tissue
KCl	Potassium chloride
kDa	Kilo dalton
KH ₂ PO ₄	Potassium dihydrogen phosphate
L/G ratio	Lactide to glycolide residue ratio
LCAT	Lecithin-cholesterol acyltransferase
LD ₅₀	Lethal dose 50%
LDL	Low-density lipoproteins
LDLR	Low-density lipoprotein receptor
LIPC	Lipase C
LPL	Lipoprotein lipase
LV	Left ventricle
LXR	Liver X receptor
MCP1	Monocyte chemoattractant protein 1
Me1	Malic enzyme 1
MG	Monoglycerol
MGL	Monoglycerol lipase
MIR	Mirabegron
MPI	Magnetic particle imaging
MPS	Magnetic particle spectroscopy
MRM	Multiple reaction monitoring
mRNA	Message RNA
MSCs	Mesenchymal stem cells
MW	Molecular weight
MWCO	Molecular weight cut-off
Na ₂ HPO ₄	Disodium hydrogen phosphate
Na ₃ VO ₄	Sodium orthovanadate
NaCl	Sodium chloride

NADH	Nicotinamide adenine dinucleotide
NADPH	Nicotinamide adenine dinucleotide phosphate
NaF	Sodium fluoride
NAFLD	Non-alcoholic fatty liver disease
NE	Norepinephrine
NST	Non-shivering thermogenesis
OAB	Overactive bladder
OCR	Oxygen consumption rate
P/S	Penicillin/streptomycin
PBS	Phosphate-buffered saline
PDI	Polydispersity index
Pdk4	Pyruvate dehydrogenase kinase 4
PDLA	Poly D-lactic acids
PES	Polyethersulfone
PET-CT	Positron emission tomography-computed tomography
PFA	Paraformaldehyde
PGA	Polyglycolic acid
PKA	Protein kinase A
PLA	Polylactic acid
PLC	Phospholipase C
PLGA	Poly (lactic-co-glycolic acid)
PLIN1	Perilipin 1
PLLA	Poly L-lactic acids
PPARGC1 α	Peroxisome proliferator-activated receptor gamma coactivator 1-alpha
PPAR α	Peroxisome proliferator-activated receptor-alpha
PPAR γ	Peroxisome proliferator-activated receptor-gamma
PRDM16	PR/SET domain 16
PTFE	Polytetrafluoroethylene
PVA	Polyvinyl alcohol
qPCR	Quantitative polymerase chain reaction
RES	Reticuloendothelial system
RIPA	Radioimmunoprecipitation assay
RNA	Ribonucleic acid
ROCK	Rho/Rho kinase
ROS	Reactive oxygen species
Rosi	Rosiglitazone
RPL13A	Ribosomal Protein L13a
RPM	Revolutions per minute
RV	Right ventricle

RXR	Retinoid X receptor
s.e.m	Standard error of the mean
S14	Spot14
SAL	Salbutamol
SBP	Systolic blood pressure
Scarb1	Scavenger receptor class B member 1
scWAT	Subcutaneous white adipose tissue
SDS	Sodium dodecyl sulfate
SDS-PAGE	SDS-polyacrylamide electrophoresis
SEM	Scanning electron microscope
Sirt1	Sirtuin 1
SNS	Sympathetic nervous system
Srebp2	Sterol regulatory element Binding Transcription Factor 2
SVF	Stromal vascular fraction
SZ	Schizophrenia
T3	Triiodothyronine
T4	Thyroxine
TBS	Tris-buffered saline
TBST	Tris-buffered saline with 0.1% Tween® 20 detergent
TC	Tissue culture
TEMED	Tetramethylethylenediamine
TG	Triglycerides
TMEM26	Transmembrane protein 26
TNFRS9	Tumor necrosis factor receptor superfamily 9
TNF- α	Tumor necrosis factor-alpha
TR	Thyroid hormone receptor
TRLs	Triglyceride-rich lipoproteins
TSH	Thyroid-stimulating hormone
TZDs	Thiazolidinediones
UCP1	Uncoupling protein 1
UCP2	Uncoupling protein 2
UCP3	Uncoupling protein 3
UGT	Glucuronosyltransferase
ULDL	Ultra-low-density lipoproteins
UV	Ultraviolet
VAT	Visceral adipose tissue
VEGF	Vascular endothelial growth factor
VLDL	Very-low-density lipoproteins
WA	White adipocyte

Abbreviations

WAT	White adipose tissue
WHO	World health organization
WT	Wild type

1 Introduction

1.1 Physiology of adipose tissue

1.1.1 Obesity

Obesity is a condition characterized by excessive accumulation of body fat, which adversely affects health (Hoffmans, Kromhout, and de Lezenne Coulander 1988). The prevalence of obesity has already reached pandemic levels (Mitchell et al. 2011). The Global Burden of Disease (GBD) Obesity Collaborators has reported that the obesity prevalence has doubled in 2015 compared with its prevalence in 1980 (GBD 2015 Obesity Collaborators et al. 2017). Shockingly, 39% - 49% of the world's population (2.8 - 3.5 billion people) are overweight or obese (Maffetone, Rivera-Dominguez, and Laursen 2016). Modern lifestyles coupled with a combination of excessive food intake, lack of physical exercise, and genetic disposition contribute to obesity (Yazdi, Clee, and Meyre 2015; Thaker 2017).

Body mass index (BMI) is a measurement commonly used to evaluate obesity. Using bodyweight divided by the square of height, the BMI is used to determine an individual's weight status as normal, underweight, overweight, or obese. The World Health Organization (WHO) defines normal weight as a BMI $< 25 \text{ kg/m}^2$, overweight as BMI ≥ 25 and $< 30 \text{ kg/m}^2$, and obesity as BMI $\geq 30 \text{ kg/m}^2$ (Hoffmans, Kromhout, and de Lezenne Coulander 1988).

Importantly, obesity is associated with a higher risk of insulin resistance, non-alcoholic fatty liver diseases (NAFLD), type 2 diabetes, hypertension, cardiovascular diseases (arteriosclerosis, angina pectoris, inadequate cerebral blood, etc.), as well as neurodegenerative disorders and cancer (Reaven 2011; Larsson et al. 2017; Milić, Lulić, and Štimac 2014; Gallagher and LeRoith 2015; Reaven 2011). According to a recent report from the American Heart Association, the mortality from obesity-induced cardiovascular disease is even independent of other cardiovascular risk factors (Powell-Wiley et al. 2021). So far, only a few medications like orlistat (Xenical) aimed to reduce fat absorption by inhibiting pancreatic lipase are approved and used to treat obesity (Ballinger 2000). However, non-negligible gastrointestinal adverse effects are associated with orlistat, including oily stools, diarrhea, abdominal pain, and fecal spotting (Filippatos et al. 2008). Additionally, Liraglutide (Victoza) is a recently FDA-approved glucagon-like peptide-1 (GLP-1) receptor agonist for treating type 2 diabetes mellitus. It showed potential benefits for weight loss but also induced adverse effects including nausea, gastrointestinal symptoms, and a high risk of pancreatitis (Monami et al. 2012; Mehta, Marso, and Neeland 2016).

Several medications, such as Rimonabant (Acomplia) and Sibutramine (Meridia), were withdrawn or were considered unsafe by medicines agencies due to their unacceptable adverse effects (Wadman 2006; Woollorton 2002). On the other hand, as one of the surgical procedures used to treat obesity besides drugs, gastric balloon surgery showed good effectiveness in weight loss (more than 10% weight loss) after six months (Dastis et al. 2009). This can be an alternative option to reduce the size of the stomach or the length of the intestines if controlled diet, exercise, and medications are ineffective (Colquitt et al. 2014). Unfortunately, the current treatments can only relieve a small number of obese patients from their situations (Wing and Phelan 2005).

1.1.2 Adipose tissue

Adipose tissue (AT) is a type of connective tissue composed of adipocytes and the stromal vascular fraction (SVF), containing pericytes, endothelial cells, monocytes, macrophages, and adipose-derived stem cells (ASC) (Martyniak and Masternak 2017; Trujillo and Scherer 2006). AT is distributed throughout the body and is mostly found in the subcutaneous area, in the abdominal cavity, surrounding the intestines, around the heart, and in the bone marrow (Ibrahim 2010). AT serves as an energy reservoir to regulate whole-body energy homeostasis in higher vertebrates. When nutrients are abundant, excessive nutrients are stored as neutral triglycerides (TG); whereas AT releases and supplies glycerol and fatty acids to other tissues through lipolysis under nutrient-deficit conditions (Birsoy, Festuccia, and Laplante 2013). Specifically, there are two different types of AT in mammals, brown adipose tissue (BAT) and white adipose tissue (WAT) (Pfeifer and Hoffmann 2015).

1.1.2.1 White adipose tissue

The main physiological role of WAT is to store energy and maintain body homeostasis. There are two major subtypes of WAT in humans: subcutaneous WAT (scWAT) and visceral adipose tissue (VAT). The murine inguinal WAT (iWAT) corresponds to the large gluteofemoral subcutaneous AT in humans, which is distributed from the dorsolumbar region to the gluteal region (Chusyd et al. 2016). The murine gonadal WAT (gWAT) corresponds to the VAT in humans (Luong, Huang, and Lee 2019; Chusyd et al. 2016). gWAT surrounds the uterus and ovaries in female rodents, while it surrounds the epididymis and testes in male rodents (Bagchi and MacDougald 2019).

Importantly, excessive energy intake could lead to WAT hypertrophy and hyperplasia, which could further result in insulin resistance and obesity (Salans, Knittle, and Hirsch 1968).

Besides, WAT is also known as an endocrine organ. WAT secretes adipokines including adiponectin, visfatin, and resistin, which interact with other organs such as the liver and skeletal muscle (Guerre-Millo 2004). Leptin-deficient ob/ob mice can easily develop insulin resistance and obesity (Kim et al. 2007). It was further reported that adiponectin-deficient mice showed severe insulin resistance in the liver and exhibited impaired responses to thiazolidinediones (TZDs), agonists for peroxisome proliferator-activated receptor-gamma (PPAR γ) (Nawrocki et al. 2006). Moreover, WAT can also secrete tumor necrosis factor-alpha (TNF α) and monocyte chemoattractant protein 1 (MCP1), which are essential to inflammatory responses, particularly in obese individuals (Jung and Choi 2014).

1.1.2.2 Brown adipose tissue

The second type of AT is BAT, which is abundant in rodents and human infants (especially in the interscapular and perirenal regions). Recently, using positron emission tomography-computed tomography (PET-CT), BAT can be detected in the cervical area, the paravertebral area, the supraclavicular area, and the aorta in adult humans (Cypess et al. 2009).

Brown adipocytes (BA) are densely packed with a large number of iron-rich mitochondria, resulting in the brown color of the tissue, and have multiple lipid droplets. In contrast, mature white adipocytes (WA) contain a single large lipid droplet and few mitochondria (Cannon and Nedergaard 2004). BAT has a different role in metabolism compared to WAT. The main role of BAT in mammals is to maintain a constant core temperature in cold environments without shivering, known as non-shivering thermogenesis (NST) (van Marken Lichtenbelt and Schrauwen 2011). Namely, instead of storing excess energy, BAT converts chemical energy into heat through the process of thermogenesis (Himms-Hagen 1989). The sympathetic nervous system (SNS) innervates both BAT and WAT, and BAT can be activated by environmental stimuli, including cold temperatures and the digestion of food (Himms-Hagen 1984).

1.1.3 Adipogenesis and lipolysis

Adipogenesis refers to the formation of adipocytes from mesenchymal stem cells (MSCs), which involves determination and terminal differentiation (Rosen and MacDougald 2006). In the process of adipogenesis, MSCs are committed to the adipogenic lineage, meanwhile losing their potential to differentiate into chondrocytes, myocytes, or osteoblasts (Gregoire, Smas, and Sul 1998). The terminal differentiation of adipocytes involves several transcription factors and morphological changes. Adipogenic stimuli like 3-isobutyl-1-methylxanthine (IBMX) can induce the activation of protein kinase A (PKA), which further phosphorylates the cyclic adenosine monophosphate (cAMP) response element-binding protein (CREB) and subsequently results in a high expression of CCAAT/enhancer-binding protein β (C/EBP β) (Petersen et al. 2008). Additionally, the augmented expression of C/EBP β can be stimulated by dexamethasone (Matsuno et al. 1996). C/EBP β plays an important role in activating peroxisome proliferator-activated receptor- γ (PPAR γ) during the process of adipogenesis (Seale 2015). PPAR γ influences adipocyte differentiation, fatty acid-binding protein 4 (FABP4)/adipocytes protein 2 (AP2), and adiponectin levels in plasma along with CCAAT/enhancer-binding protein α (C/EBP α) (Ahmadian et al. 2013; Maeda et al. 2001; Rosen and MacDougald 2006).

As an important metabolic activity, lipolysis is regulated by several factors such as norepinephrine (NE) and adenosine in AT (Hjemdahl and Linde 1983; Ahmadian, Wang, and Sul 2010). TG released from lipid droplets is hydrolyzed to one molecule of glycerol and three molecules of free fatty acids (FFA) by several lipases during lipolysis (Zimmermann et al. 2009). Specifically, lipolysis is initiated by the activation of β -adrenergic receptors. Activated β -adrenergic receptors couple to Gs protein resulting in adenylyl cyclase-dependent increases in cAMP (Steinberg and Huttunen 1972). As a secondary messenger, cAMP increases protein kinase A (PKA) activity, which in turn activates both hormone-sensitive lipase (HSL) and perilipin 1 (PLIN1) through phosphorylation. TG hydrolysis is performed in a sequential process by three lipases. In the first step, the adipose triglyceride lipase (ATGL) enzyme activity is activated by the co-activator comparative gene identification-58 (CGI58) (Lass et al. 2006). ATGL catalyzes the conversion of TG into diglycerol (DG) and an FFA (Zimmermann et al. 2004). The activated HSL further hydrolyzes DG into mono glycerol (MG) and an FFA (Vaughan, Berger, and Steinberg 1964). In the last step, mono glycerol lipase (MGL) hydrolyzes MG to glycerol and an FFA (Figure 1).

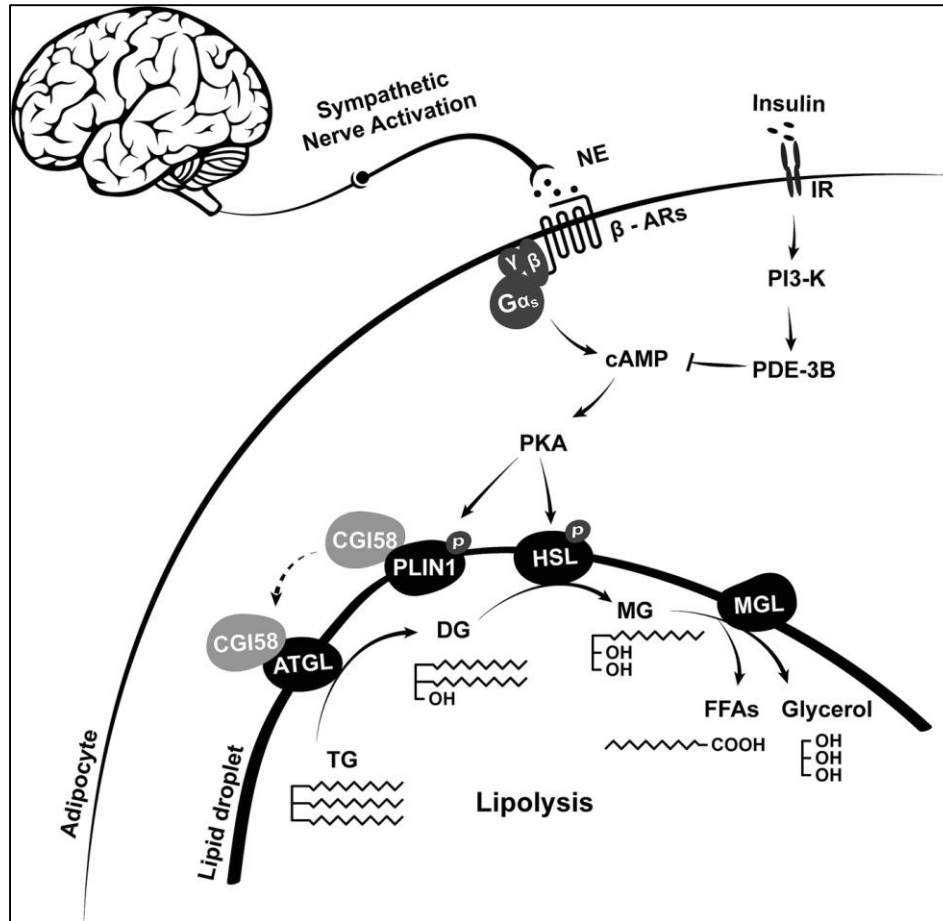


Figure 1. The mechanism of lipolysis in adipocytes via β -adrenergic receptors. Cited from Li and Sun, 2018. (X. Li and Sun 2018).

1.1.4 Brown adipocyte activation: thermogenesis at the molecular level

Uncoupling protein 1 (UCP1) is a unique protein in BA responsible for the process of thermogenesis (Argyropoulos and Harper 2002). BAT receives the efferent signal from the SNS via NE, which binds to Gs-coupled β 3-adrenergic receptors (ADRB3) on the surface of BA. The binding increases cAMP production in BA and activates the cAMP/PKA pathway. PKA phosphorylates the transcription factor of cAMP response element-binding protein (CREB) to upregulate the expression of *Ucp1* in BA (Thonberg et al. 2002). Additionally, activated PKA can also induce lipolysis (Frühbeck et al. 2014). Long-chain acyl-CoA synthetases (ACSL) activate FFA to acyl-CoA (Coleman, Lewin, and Muoio 2000). The acyl-CoA is transferred into the mitochondria matrix, where the β -oxidation and the citric acid cycle (CAC) take place, through

carnitine palmitoyltransferase (CPT1) (Brown et al. 1997). Subsequently, two reduced electron carriers, Flavin adenine dinucleotide (FADH₂) and Nicotinamide adenine dinucleotide (NADH), are generated and oxidized within the electron transport chain (respiratory chain) (Cannon and Nedergaard 2004). Protons are pumped out of the mitochondria and form the mitochondria proton gradient (a proton-motive force). As a result, UCP1 within the inner mitochondrial membrane transports protons from the inner membrane space back into the mitochondrial matrix, and the mitochondria generate energy in the form of heat (Fedorenko, Lishko, and Kirichok 2012; Azzu and Brand 2010; Nicholls 2006) (Figure 2).

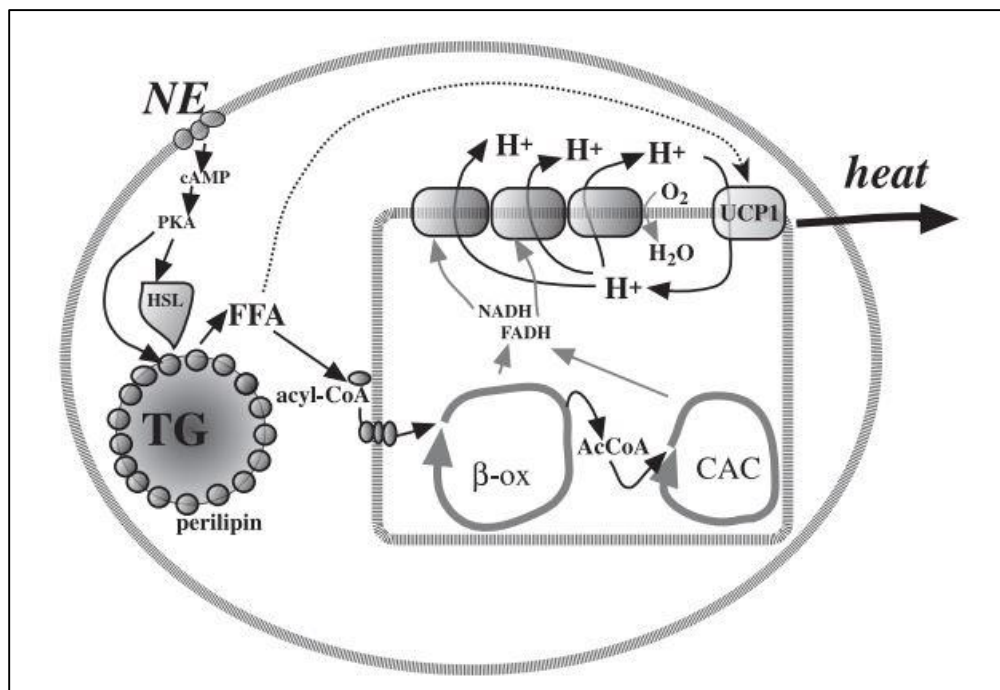


Figure 2. Thermogenesis at the molecular level in brown adipocytes. Cited from Cannon and Nedergaard, 2004. (Cannon and Nedergaard 2004).

1.1.5 Browning and whitening of white adipose tissue

Mature inguinal white adipocytes (iWA) are well-known for energy storage and their large, single droplets, but a distinct population of adipocytes, beige adipocytes, has been discovered (Petrovic et al. 2010; J. Wu, Cohen, and Spiegelman 2013). According to its characteristics such as multilocular lipid droplets and a high amount of mitochondria, beige adipocytes are another type of thermogenic adipocyte (J. Wu et al. 2012). They sporadically exist in WAT (Garcia, Roemmich,

and Claycombe 2016). Considering their thermogenic properties, beige adipocytes are intensively studied to combat obesity (A. M. Singh et al. 2020; Shabalina et al. 2013). Beige adipocytes express markers characteristic of brown adipocytes such as *Ucp1*, *Ppargc1α*, and Cell Death Inducing DFFA Like Effector A (*Cidea*); in addition to those markers, some beige adipocyte-specific genes, including tumor necrosis factor receptor superfamily 9 (*Tnfrs9*) and transmembrane protein 26 (*Tmem26*), are also expressed in murine beige adipocytes (J. Wu et al. 2012; Shabalina et al. 2013). The browning of WAT is defined as the presence of beige adipocytes in WAT, which can be induced by cold exposure and exogenous pharmaceuticals such as rosiglitazone, a PPAR γ agonist (Rong et al. 2007), and CL-316243, an ADRB3 agonist (Bartelt and Heeren 2014; Nedergaard and Cannon 2014). Fisher, F. M. *et al.* also reported that peptide hormones such as fibroblast growth factor 21 (FGF21) regulate the browning of WAT. The expression of *Fgf21* increases in WAT after cold exposure or β 3-adrenergic activation. FGF21 plays an essential role in the recruitment of beige adipocytes through regulating and stabilizing peroxisome proliferator-activated receptor gamma coactivator 1-alpha (PPARGC1 α) protein (Fisher et al. 2012). Generally, the browning of WAT is an adaptive and reversible process, in which beige adipocytes develop from WA (trans-differentiation) in response to external stimuli or they develop from WA precursors residing within WAT (Seale et al. 2008; Bartelt and Heeren 2014). Nevertheless, inflammatory microenvironments and pro-inflammatory cytokines can impair the beiging process in WAT and alter the plasticity of adipocytes (Villarroya et al. 2018).

Importantly, the beiging process is transient. The process when BA and beige adipocytes obtain characteristics of WA is called “whitening”, which can be induced by several factors including aging, obesity, high-fat diet (HFD), and high ambient temperature (Rosenwald et al. 2013; Kotzbeck et al. 2018). The whitening of BAT is characterized by the accumulation of enlarged lipid droplets in BA, loss of UCP1 expression, weakened β -adrenergic signaling, and hypoxia-induced loss of vascularity in BAT (Shimizu and Walsh 2015).

1.1.6 Lipoprotein particles

Lipoprotein particles are complex particles that transport lipids like TG and cholesterol (Richardson et al. 2005). Lipoprotein particles have a hydrophobic core mainly containing cholesterol and TG. The hydrophobic core is enclosed by a hydrophilic membrane composed of phospholipids, free cholesterol, and apolipoproteins (Feingold and Grunfeld 2000). Lipoprotein particles can be characterized into several groups according to their diameters: high-density

lipoproteins (HDL) (5 - 12 nm), low density-lipoproteins (LDL) (18 - 25 nm), very-low-density lipoproteins (VLDL) (30 - 80 nm), and chylomicrons (75 - 1200 nm) (Feingold and Grunfeld 2000).

There are two lipoprotein metabolic pathways in the body: the exogenous pathway and the endogenous pathway. The exogenous pathway initiates in the intestine, in which lipids are incorporated into chylomicrons (Feingold and Grunfeld 2000; Briand et al. 2016, 1). Chylomicrons transport TG obtained from the intestine to peripheral tissues like AT and skeletal muscle for energy storage and utilization. Chylomicrons can also deliver cholesterol to the liver (Mansbach and Siddiqi 2010). Lipoprotein lipase (LPL) is synthesized by the parenchymal cells in muscle and AT and then transported to the surface of capillary endothelial cells by the shuttle protein glycosylphosphatidylinositol-anchored high-density lipoprotein binding protein 1 (GPIHBP1) (Adeyo et al. 2012; Olivecrona 2016). In AT, LPL hydrolyzes TG carried by chylomicrons, and FFA liberated from TG hydrolysis are further transported to the adipocytes through fatty acid transport proteins (FATPs) and CD36 (Figure 3) (Hoeke et al. 2016). After hydrolysis of TG, chylomicron remnants decrease in size and can further transport cholesterol to hepatocytes for the formulation of VLDL particles and bile acids (Dallinga-Thie et al. 2010).

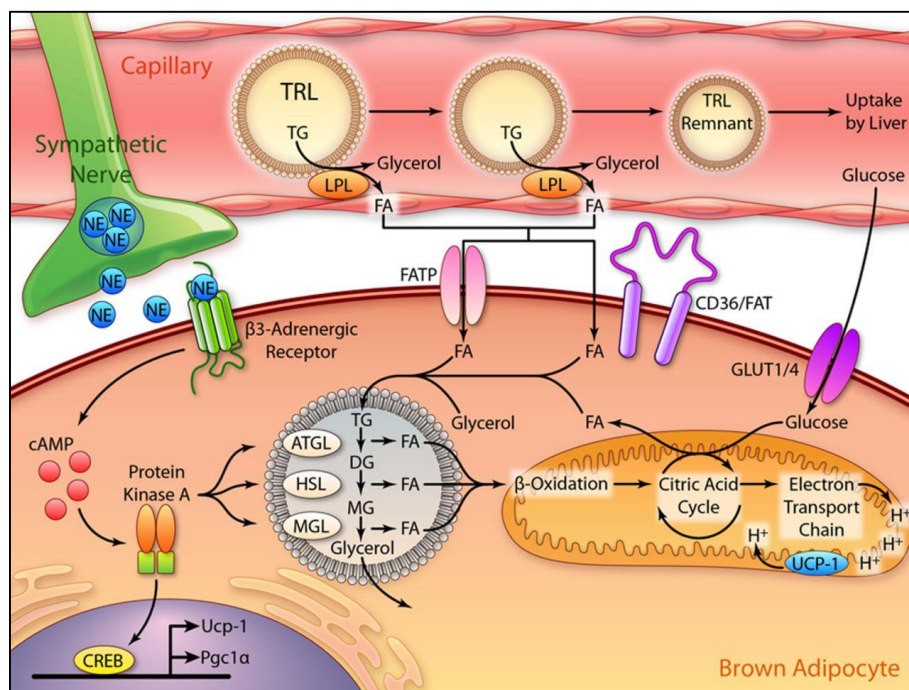


Figure 3. NE-activated brown adipocytes take up TRLs from the bloodstream. NE: norepinephrine, TRLs: triglyceride-rich lipoproteins. Cited from Hoeke et al. 2016 (Hoeke et al. 2016).

Endogenous lipoprotein production in the liver begins with the formation of VLDL. VLDL is composed of hepatic cholesterol, TG, and apolipoprotein B, and it is synthesized in the liver to transport fat from the liver to peripheral tissues including AT and skeletal muscle (Feingold and Grunfeld 2000). As muscle and AT remove TG from VLDL, IDL particles are formed, which are cholesterol-rich (Young and Zechner 2013; Feingold and Grunfeld 2000). Apolipoprotein B-100-containing LDL delivers cholesterol to extrahepatic tissues and returns to the liver, whereas LDL is cleared from the liver by LDL-mediated endocytosis (Goldstein and Brown 2009). HDL has the smallest size among those four types of lipoproteins (Feingold and Grunfeld 2000). Apo, mainly Apo A1 and Apo A2, are highly associated with HDL (Gordon et al. 2011; Tailleux et al. 2002; Mahley et al. 1984). Surface-embedded Apo A1 activates lecithin-cholesterol acyltransferase (LCAT) that catalyzes cholesterol esterification. As a result, cholesterol esters move from the surface of HDL to its core, which generates HDL with a core of cholesterol esters (Ossoli et al. 2016). Furthermore, HDL also plays an important role in reverse transporting cholesterol from peripheral tissues to the liver (Tall 1998).

1.1.7 G protein-coupled signaling pathways

G protein-coupled receptors (GPCRs) are the most investigated pharmacological targets, which regulate biological processes in various tissues, including AT (Wettschureck and Offermanns 2005; Hauser et al. 2017). GPCRs are known as 7 transmembrane domain (7TM) receptors, which are responsible for two main signal transduction pathways: the cAMP signal pathway and the phosphatidylinositol 3-kinase pathway (Gilman 1987). The activity of GPCRs is well-regulated (Magalhaes, Dunn, and Ferguson 2012). In general, G proteins are activated by GPCRs upon a stimulus binding; in contrast, β -arrestin desensitizes G protein-mediated signaling via binding to the cytoplasmic side of GPCRs and occluding the binding site for G proteins (Kang et al. 2015; Cahill et al. 2017; Kumari et al. 2016). G proteins belong to a family of enzymes known as GTPases, each heterotrimeric G protein contains three subunits: α -subunit, β -subunit, and γ -subunit (Radhika and Dhanasekaran 2001). When an agonist binds to GPCRs, the activation of GPCRs facilitates guanosine diphosphate (GDP) to replace guanosine triphosphate (GTP) bound to the α -subunit, which causes the conformational change that the α -subunit of G protein detaches from β - and γ -subunits (Wall, Posner, and Sprang 1998). The $G\alpha$ -GTP further activates an effector protein adenylyl cyclase via binding (Simonds 1999). The β - and γ -subunits can also interact with effector proteins (Birnbaumer 1992). In the absence of an agonist, the α -subunit hydrolyzes GTP

to GDP. Subsequently, the α -subunit associates with the β - and γ -subunits again and GPCR becomes inactive (McCudden et al. 2005).

The α -subunit of the G protein can be further assigned into four main classes according to their affinity for different effector proteins: Gs, Gi, Gq, and G_{12/13} (Neves, Ram, and Iyengar 2002). Adenylyl cyclase is the effector protein stimulated by the α -subunit of the Gs protein. Activation of Adenylyl cyclase leads to an increase in cAMP signaling and activation of PKA, while the α -subunit of Gi protein inhibits adenylyl cyclase. In contrast, the α -subunit of the Gq protein activates phospholipase C (PLC), and the α -subunit of the G_{12/13} protein activates GTPase RhoA (Dhanasekaran and Dermott 1996; Chen et al. 2005).

Likewise, the metabolic activities of adipocytes are regulated by GPCR signaling (Eisenstein and Ravid 2014). Gs-coupled receptors including β -adrenergic receptors stimulate cAMP and PKA signaling in adipocytes leading to an increase in the expression of *Ucp1* and lipolysis. Conversely, Gi-coupled signaling inhibits lipolysis in adipocytes via α -adrenergic receptors (Lafontan 1994; Flechtner-Mors et al. 2002; Långberg et al. 2013).

1.1.8 Adrenergic receptors in adipose tissue

As GPCRs, adrenergic receptors are associated with several important signaling pathways in AT (Sheila Collins 2012). There are five subtypes of adrenergic receptors: α 1, α 2, β 1, β 2, and β 3-adrenergic receptors. Catecholamines, including NE released by the SNS, bind to adrenergic receptors (Moura et al. 2006). Nevertheless, the effect of adrenergic receptors is not always the same. Generally, the α 1-adrenergic receptors couple to the Gq protein which causes an increased level of intracellular calcium (Flechtner-Mors et al. 2002). The α 2-adrenergic receptors are Gi-coupled receptors. The activation of α 2-adrenergic receptors can inhibit adenylyl cyclase and reduce cAMP levels (Långberg et al. 2013). A variety of tissues express α 1-adrenergic receptors, including the smooth muscle of the vascular system, cerebral cortex, and the rodent lung (Perez, Piascik, and Graham 1991; Cotecchia et al. 1988; Y et al. 1994). In contrast, β -adrenergic receptors are Gs-coupled receptors. The activation of β -adrenergic receptors increases intracellular cAMP levels (Lafontan 1994). β -adrenergic receptors are also found in several tissues: β 1-adrenergic receptors (ADRB1) are most common in the heart; β 2-adrenergic receptors (ADRB2) are expressed in the lungs, kidneys, and blood vessels as well as the heart; ADRB3 localizes predominantly in urinary bladder smooth muscles and AT (Madamanchi 2007; Xiao 2001; Yamaguchi and Chapple 2007).

The expressions of adrenergic receptors in adipocytes are compared between rodents and humans (Figure 4). In BAT, ADRB3 plays an important role in the regulation of thermogenic signaling (Mund and Frishman 2013). ADRB3 is expressed abundantly on the surface of BA in both rodents and humans (Barbatelli et al. 2010; Cero et al. 2021). By activating ADRB3, G proteins stimulate the activity of adenylyl cyclase, leading to an increase in UCP1 expression and thermogenesis (J. R. Arch and Wilson 1996; Hanoune and Defer 2001). ADRB1 is mainly present in brown pre-adipocytes (pre-BA) (Bronnikov et al. 1999). ADRB2 is expressed in human BA and might also be involved in thermogenesis (Blondin et al. 2020). In WAT, the expression of ADRB3 was also discovered (Revelli et al. 1993). Grujic and Susulic, et al. reported that the activation of ADRB3 on WA was associated with increased energy expenditure and insulin level (Grujic et al. 1997).

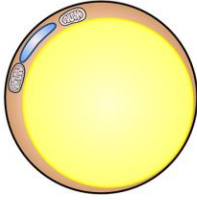
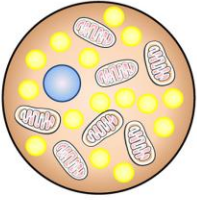
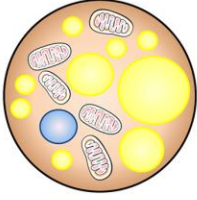
	White adipocyte	Brown adipocyte	Brite adipocyte
			
Visualisation	UCP1 negative Low mitochondrial density Single lipid droplet	UCP1 positive High mitochondrial density Numerous multilocular lipid droplets	UCP1 positive Intermediate mitochondrial density Mixture of small and large lipid droplets
Function	Lipid storage Secretion of adipokines (leptin/adiponectin)	Thermogenesis	Thermogenesis
Adipocyte signature genes	Hoxc9, Fabp4, Adipoq	Ucp1, Prdm16, Cidea, Ppargc1a, Adipoq, Fabp4, Fabp3, Cpt1b	Ucp1, Hoxc9, Prdm16, Cidea, Ppargc1a, Adipoq, Fabp4, Fabp3, Cpt1b
Known AR expression in rodents	β_1 -AR β_2 -AR β_3 -AR	α_{1A} -AR β_1 -AR α_{1D} -AR β_2 -AR α_{2A} -AR β_3 -AR	α_{1A} -AR β_1 -AR α_{1D} -AR β_2 -AR β_3 -AR
Known AR expression in humans	α_{1A} -AR α_{1B} -AR β_1 -AR α_{2A} -AR β_2 -AR α_{2C} -AR	α_{1A} -AR α_{2A} -AR β_1 -AR α_{1B} -AR α_{2B} -AR β_2 -AR α_{2C} -AR β_3 -AR	α_{1A} -AR β_1 -AR β_2 -AR β_3 -AR
Known AR functions in rodents	Adipokine release (β -AR ∇) WA differentiation (β_1 -AR) Lipolysis (β_3 -AR)	Glucose uptake (α_{1A} -AR, β_3 -AR) Mitochondrial uncoupling (β_1 -AR, β_3 -AR) VEGF release (β_3 -AR) BA differentiation (β_1 -AR)	Glucose uptake (α_{1A} -AR, β_3 -AR) Mitochondrial uncoupling (β_3 -AR)
Known AR functions in humans	Lipolysis (β_1 -AR, β_3 -AR) Inhibition of lipolysis (α_2 -AR ∇)	Glucose Uptake (β -AR ∇ , β_3 -AR*)	Mitochondrial uncoupling (β -AR ∇)

Figure 4. Different adrenergic receptor expressions in human and rodent adipose tissue. Cited from Evans et al. 2019 (Evans et al. 2019).

1.1.9 A β 3-adrenergic receptor agonist: Mirabegron

Mirabegron (MIR) is an approved medication intended for the treatment of overactive bladder (OAB) in the United States, Japan, the European Union, and Canada (Leone Roberti Maggiore et al. 2014). The chemical structure of MIR is shown in Figure 5 (Sacco et al. 2014). It is a lipophilic ligand and shows a higher binding affinity to ADRB3 than any other class of β -adrenergic receptors (Takasu et al. 2007). To treat OAB patients, MIR is well tolerated and can effectively relax bladder smooth muscle (Nitti et al. 2013). However, chronic oral administration of MIR at a high dose can induce side effects such as high blood pressure, urinary tract infections, constipation, irregular heart rates, as well as cardiovascular problems (Pouleur et al. 2018; Loh et al. 2019; Bel et al. 2021; Sacco and Bientinesi 2012; Malik et al. 2012).

Several pathways are involved in the biotransformation of MIR, including dealkylation, oxidation, glucuronidation, and amide hydrolysis. Some studies indicated that cytochrome (CYP) P450 including both CYP3A4 and CYP2D6 plays an essential role in MIR oxidation (Takusagawa et al. 2012). In addition to CYPs, butyrylcholinesterase, glucuronosyltransferase (UGT), and alcohol dehydrogenase (ADH) are involved in MIR metabolism as well (Sacco and Bientinesi 2012). The half-life of MIR is approximately 23-25 hours after oral administration in humans (Eltink et al. 2012).

ADRB3 is found in many tissues including the heart, urinary bladder, gastrointestinal tract, prostate, brain, and AT (Berkowitz et al. 1995). Recently, it has been reported that subcutaneous AT of obese patients showed an increased level of *Ucp1* expression and uncoupled respiration after 10-week oral administration of MIR (50 mg/day) (Finlin et al. 2018). Several studies further revealed that individuals treated with 200 mg/day of MIR for 12 weeks had a higher BAT metabolic activity in comparison to those on a placebo (Cypess et al. 2009). Based on these published studies, MIR has the potential to combat obesity by browning WAT and activating BAT. However, MIR remains unapproved for the treatment of obesity due to its poor oral bioavailability (Cypess et al. 2009; J. R. S. Arch 2011). In light of this, the development of novel drug delivery systems that reduce MIR-induced side-effects could make substantial progress toward the treatment of obesity.

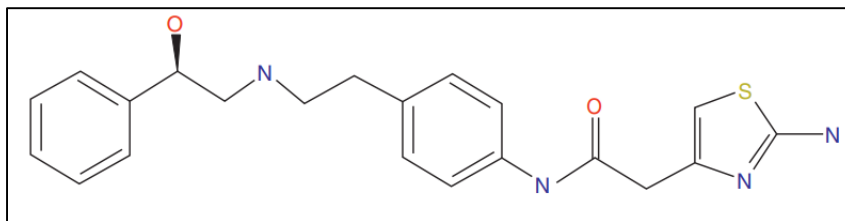


Figure 5. Chemical structure of mirabegron. Cited from Sacco et al. 2014 (Sacco et al. 2014).

1.1.10 A Gq signaling inhibitor: FR900359 (FR)

FR900359 (FR), commercially known as UBO-QIC, is a selective Gq/11 signaling inhibitor (Schrage et al. 2015), which was initially identified from the leaves of the ornamental plant *Ardisia crenata* by Fujioka et al. in 1988 (Fujioka et al. 1988). The chemical structure of FR900359 is shown in Figure 6 (Schrage et al. 2015). Previously, numerous studies have reported that Gq signaling plays an important role in many biological functions, including the development of the heart during embryonic growth, airway smooth muscle contraction, and platelet activation (S Offermanns et al. 1998; Billington and Penn 2003; Stefan Offermanns 2006). Importantly, Klepac et al. recently revealed that the endothelin-1/Gq (ET-1/Gq) signaling can activate the downstream Rho/Rho kinase (ROCK) pathway and inhibit BA differentiation and WA beiging (Klepac et al. 2016). Due to high systolic blood pressure (SBP) causing hypotension with systemic administration of FR, a locally targeted delivery might be more effective for maximizing FR's therapeutic efficacy (A. P. Campbell and Smrcka 2018; Meleka et al. 2019). Thus, inhibition of Gq signaling in adipocytes using an appropriate targeted delivery system might be potentially utilized to treat obesity.

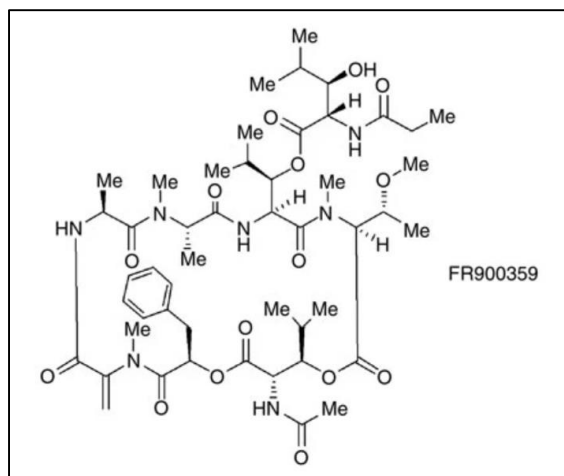


Figure 6. Chemical structure of FR900359. Cited from Schrage et al. 2015 (Schrage et al. 2015).

1.1.11 Thyroid hormones and thyroid hormone activities in adipose tissue

1.1.11.1 Thyroid hormone

Thyroid hormones regulate metabolisms in several tissues including the liver, bone, heart, and AT (A. C. Bianco and Silva 1987a). In general, the hypothalamus releases the thyrotropin-releasing hormone (TRH), which stimulates the pituitary gland to secrete the pituitary glycoprotein thyroid-stimulating hormone (TSH). TSH, in turn, controls thyroid hormone release (Menezes-Ferreira, Petrick, and Weintraub 1986). Increased concentration of thyroid hormone in the bloodstream inhibits the secretion of TSH from the pituitary gland, resulting in a negative feedback mechanism (Snyder and Utiger 1972).

Thyroxine (T₄) and triiodothyronine (T₃) are the two forms of thyroid hormones produced by the thyroid gland. They bind to thyroid hormone receptors (TRs) (Flamant et al. 2006). The affinity of T₃ for TRs in target organs is 10 times greater than T₄, thus, T₃ is known as the active form (Samuels and Tsai 1974). In addition, the plasma elimination $t_{1/2}$ for T₃ is about 1 day, while T₄'s plasma elimination is 7.5 days (Nicoloff et al. 1972). The concentrations of thyroid hormones in tissues are regulated coordinately by type 1 to 3 iodothyronine deiodinases (Dio1, Dio2, and Dio3). Dio1 and Dio2 catalyze T₄ to T₃. In contrast, Dio3 inactivates T₃ to 3,3'-diiodothyronine and protects tissues from excessive T₃ (Wassen et al. 2004). Under normal conditions, *Dio1* is mainly expressed in the liver, thyroid, pituitary, and kidney to produce circulating T₃ (Köhrle 1999). *Dio2*

is expressed in the anterior pituitary, the central nervous system, skin, and murine BAT (Silva, Dick, and Larsen 1978; A. C. Bianco and Silva 1987b). *Dio3* can be found in the brain, skin, pregnant uterus, and placenta, as well as during the early stages of BAT development and BA adipogenesis, but *Dio3* activity can barely be detected in BA (Hall et al. 2010; Tu et al. 1997).

1.1.11.2 Thyroid hormone-related activities in the liver and adipose tissue

Thyroid hormones are essential for the regulation of metabolic processes in the liver such as hepatic FA uptake, hepatic lipogenesis, hepatic lipolysis, β -oxidation, cholesterol homeostasis, bile acid synthesis, and gluconeogenesis (Sinha, Singh, and Yen 2014). As shown in Figure 7, in response to T3, the expressions of several genes involved in the above-mentioned processes are increased. For hepatic lipogenesis, the expressions of acetyl-CoA carboxylase 1 (*ACC1*), malic enzyme 1 (*Me1*), spot14 (*S14*), fatty acid synthase (*FAS*), liver X receptor (*LXR*), and carbohydrate-responsive element-binding protein (*ChREBP*) are upregulated after receiving T3 (Kinlaw et al. 1995; Moustaid and Sul 1991; Sinha, Singh, and Yen 2014). T3 can also positively regulate hepatic genes such as *Cpt1*, sirtuin 1 (*Sirt1*), *Ppargc1 α* , and *Fgf21* (Thakran et al. 2013; Chang and Guarente 2014; Adams et al. 2010). In addition, FA uptake via FA translocase (*CD36*) and cholesterol uptake via low-density lipoprotein receptor (*Ldlr*) both are upregulated by T3 in the liver (Sinha, Singh, and Yen 2014).

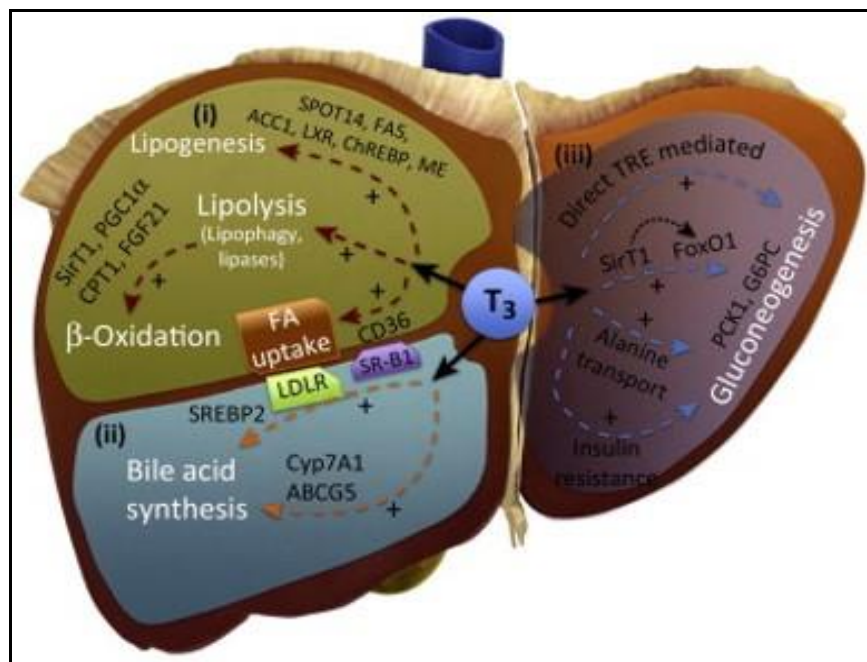


Figure 7. The effects of T3 in the liver. Cited from Sinha, Singh, and Yen, 2014 (Sinha, Singh, and Yen 2014).

In AT, several processes such as adipocyte differentiation, lipogenesis, lipolysis, glucose metabolism, and thermogenesis are significantly affected by T3 (Oppenheimer et al. 1991; Yau et al. 2019). T3 plays an important role in maintaining body temperature and thermogenesis. Bianco and Silva demonstrated that mice with hypothyroid died after a few hours of cold exposure due to hypothermia and insufficient BAT thermogenesis (A. C. Bianco and Silva 1987a). In BAT, the intracellular T3 level is upregulated by the activation of Dio2 (Gereben et al. 2008). As a result, the activation of the thyroid hormone receptors (TRs) by intracellular T3 further upregulates the transcription of *Ucp1* (Cioffi et al. 2018).

Interestingly, there are two isoforms of TR in AT: TR α and TR β (Mishra et al. 2010). The TR β isoform is associated with the transcriptional induction of UCP1 and heat dissipation in BA, while the TR α isoform is required for the synergistic cold-induced β -adrenergic effects (Ribeiro et al. 2001). Moreover, the TR α isoform is known to be responsible for most side effects associated with T3 systemic treatments, including tachycardia, fatigue, and muscle catabolism (Saponaro et al. 2020). Therefore, the systemic administration of T3 is not highly recommended, and several attempts have been made to target the TR β isoform specifically (Johansson, Vennström, and Thorén 1998; Villicev et al. 2007). Recently, a selective TR β agonist GC-1 has been reported and applied in rats showing promising effects on fat mass reduction (Villicev et al. 2007). However,

side effects of GC-1 in other tissues are yet to be investigated and are inevitable (Manzano et al. 2003).

Utilizing a well-studied and marketed drug T3 would be less risky and more beneficial than using a new compound GC-1 in the treatment of obesity as long as the administration of T3 is targeted. The effects of T3 on BA via the TR β isoform are shown in Figure 8. T3 interacts with TR β 1 and forms a TR β 1-RXR (retinoid X receptor) heterodimer, which subsequently binds to DNA in the nucleus and increases transcription of *Ucp1* and *Ucp3*. An increase in UCP3 protein concentration allows more FFA to be transported into mitochondria as fuel, and UCP1 proteins contribute to producing heat (Tsibulnikov et al. 2020).

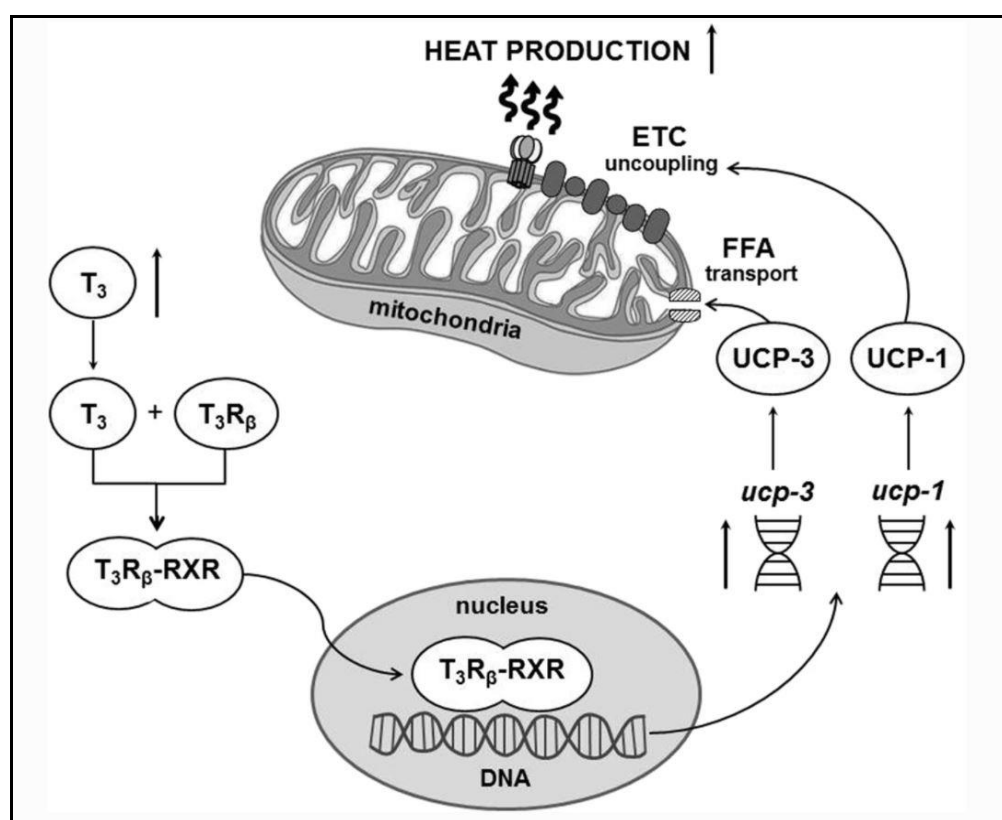


Figure 8. The function of T3 in brown adipocytes. Cited from Tsibulnikov et al. 2020 (Tsibulnikov et al. 2020).

1.2 Poly (lactic-co-glycolic acid) polymer-based delivery system

1.2.1 Intrinsic properties of PLGA copolymers

PLGA was approved by the United States Food and Drug Administration (FDA) in the 1970s as a biodegradable material, which is widely used in drug delivery and nanomedicine due to its excellent biocompatibility, low toxicity, and controlled bio-distribution (Agrahari, Agrahari, and Mitra 2016). Not only proteins and DNA, but a wide range of small molecular drugs (both hydrophilic and hydrophobic) such as paclitaxel, docetaxel, doxorubicin, cisplatin, and curcumin can be encapsulated in PLGA particles (Dinarvand et al. 2011).

PLGA is a linear copolymer composed of both polylactic acid (PLA) and polyglycolic acid (PGA), which is synthesized through direct polycondensation of lactic acids and glycolic acids (H.-R. Lin et al. 2002). Since PLA contains an asymmetric α -carbon, it has two forms in stereochemistry: L-type and D-type (Makadia and Siegel 2011). D-lactic acids and L-lactic acids generate poly D-lactic acids (PDLA) and poly L-lactic acids (PLLA) respectively (Pavlov et al. 2015). In contrast, poly D, L-lactic-co-glycolic acid copolymers possessing an equal ratio of poly D- and L- lactic forms are amorphous, whereas PLGA copolymers synthesized only from L-lactic acids are crystalline (Jain 2000). Additionally, the content of lactic acid also plays an important role in PLGA solubility. Amorphous PLGA copolymers containing less than 70% of lactic acid are ideal for drug delivery applications (Jain 2000).

PLGA is soluble in several solvents, including acetone and ethyl acetate (EA), as well as chlorinated organic solvents such as dichloromethane (DCM) and chloroform (Makadia and Siegel 2011; X. S. Wu and Wang 2001). However, PLGA is insoluble in methanol. The biodegradation rate of PLGA also depends on its content of lactic acid (Casalini et al. 2019). The hydrophobic nature of lactic acid results in PLGA copolymers with a high ratio of lactic acid absorbing less water (Schliecker et al. 2003). Hydrophobicity leads to slower biodegradation of PLGA copolymers (Casalini et al. 2019). PLGA copolymers containing a 50:50 ratio of lactic acid to glycolic acid are the most frequently used type of PLGA in the field of nanomedicine, and it degrades more rapidly (1 - 2 weeks *in vivo* in humans) than other types of PLGA with higher ratios of lactic acid to glycolic acid (Gentile et al. 2014). Additionally, PLGA 50:50 polymer substrates begin to change from a rigid glassy state to a soft state at a temperature in the range of 40 to 60°C, known as a glass transition temperature. PLGA copolymers with high molecular weight and high lactic acid content have a higher PLGA transition temperature (Lü et al. 2009).

1.2.2 Biodegradation mechanism of PLGA microparticles as drug delivery carriers

Microparticles are defined as particles with a diameter smaller than 300 μm , ideally between 50 and 100 μm , which can be used for subcutaneous administration with acceptable pain and discomfort (Kissel et al. 1991; Jain 2000). Except for the intrinsic properties of PLGA copolymers mentioned above (hydrophobicity and crystallinity), the biodegradation of PLGA is affected by several factors, including compound molecular weight, preparation methods, pH, temperature, and application sites (Casalini et al. 2019). Those factors are associated with the mechanism and the rate of drug release (Jain 2000).

As shown in Figure 9, the degradation mechanisms of pharmaceuticals encapsulated in PLGA microparticles include bulk erosion and surface erosion (Panyam et al. 2003). Bulk erosion, the main degradation mechanism for PLGA particles, occurs when ester bonds in the copolymer are hydrolyzed in water by random scission into lactic acids and glycolic acids (X. S. Wu and Wang 2001; Dinarvand et al. 2011). The initial hydrolysis of PLGA leads to a significant decrease in molecular weight. Subsequently, soluble monomers (lactic acids and glycolic acids) are then generated by hydrolysis of the ester linkage (Figure 10). The monomers are eventually metabolized into carbon dioxide and water by the Krebs cycle *in vivo* (Lü et al. 2009; Jain 2000).

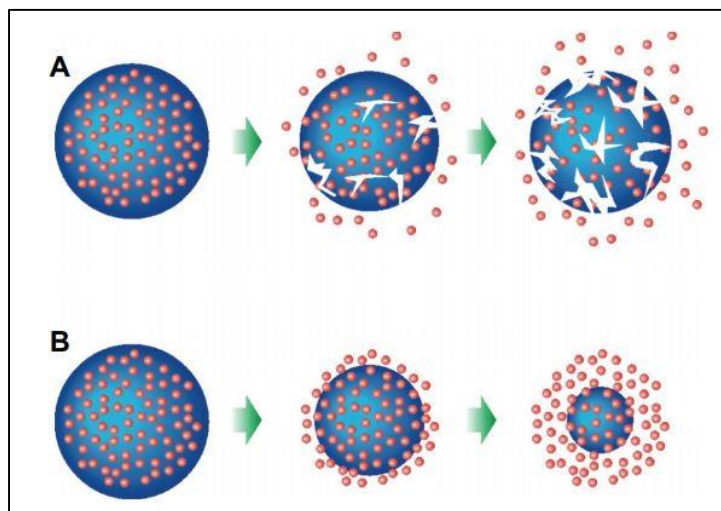


Figure 9. Degradation of drug-loaded PLGA particles. (A) bulk erosion, (B) surface erosion. PLGA: poly (lactic-co-glycolic acid). Cited from Dinarvand et al, 2011 (Dinarvand et al. 2011).

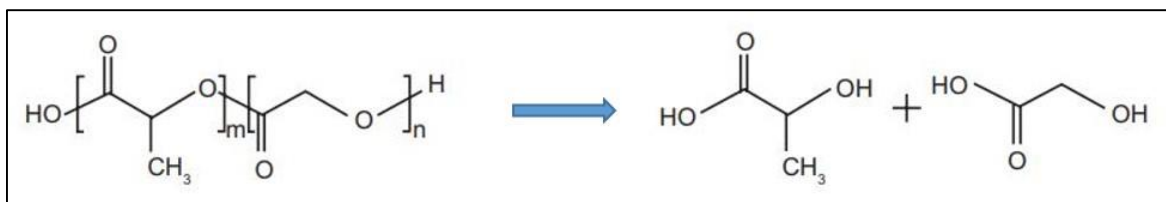


Figure 10. Degradation of PLGA to lactic acid and glycolic acid. PLGA: poly (lactic-co-glycolic acid).

1.3 Artificial triglyceride-rich lipoproteins uptake in adipose tissue

Triglyceride-rich lipoproteins (TRLs), also known as chylomicrons or ultra-low-density lipoproteins (ULDL), play an important role in transporting dietary lipids between the gut and peripheral tissues. TRLs range in diameter from 100 to 1000 nm (Casley-Smith 1962). Recently, TRLs have been used as a tool for investigating nutrient uptake, lipid metabolism, diagnostics, and immunotherapy in several studies (Bartelt et al. 2011; Mulder et al. 2018; Berbée et al. 2015). Lipoprotein lipase at the endothelium mediates the uptake of TRLs into peripheral tissues like muscle tissues and AT, which is followed by the import of FFA (Dominiczak and Caslake 2011; Goudriaan et al. 2005). Additionally, peripheral tissues can take up the whole TRLs by internalization and transcytosis through the endothelium (Bartelt et al. 2011).

Bartelt and Berbee et al. reported that BAT is the main site to clear postprandial TG via local LPL activity after cold exposure (Bartelt et al. 2011; Berbée et al. 2015; Goudriaan et al. 2005). BAT shows an increasing demand for energy substrates such as glucose and FFA during the process of thermogenesis (Carpentier et al. 2018). Interestingly, lipid uptake could potentially be an indicator of BAT activity, thus, using TRLs might be a new method to deliver active pharmaceutical ingredients (APIs) to target tissues (Schilperoort et al. 2016; Hildebrand et al. 2021). Furthermore, it has been shown that artificial chylomicrons (ACM) containing phosphatidylcholine, TG, and cholesterol were prepared as carriers to encapsulate magnetic nanoparticles (MNP) and deliver MNP to AT. Magnetic particle imaging (MPI) has been further used to trace MNP in BAT (Hildebrand et al. 2021).

2 Aim of the thesis

MIR and thyroid hormones are approved medications as standard treatments or guidelines for treating overactive bladder and hypothyroidism, respectively (Nitti et al. 2013; Wiersinga et al. 2012). It is recently discovered that MIR and T3 both have promising therapeutic effects on WA beiging and BA activation as potential anti-obesity agents (O'Mara et al. 2020; Krotkiewski 2000). Paradoxically, chronic conventional oral administration of MIR and T3 at a supra-therapeutic dose can result in undesirable side effects (J. R. S. Arch 2011; Sacco and Bientinesi 2012; Vargas-Uricoechea, Bonelo-Perdomo, and Sierra-Torres 2014). Therefore, this thesis investigates and addresses the following issues:

- How to develop and optimize PLGA-microparticles loaded with MIR as a controlled release system?
- Can MIR-loaded PLGA microparticles (MIR-MPs) induce therapeutic effects against obesity?
- How to develop TRLs as carriers to encapsulate T3 and deliver T3 to the targeted tissue?
- Can T3-TRLs induce therapeutic effects against obesity?

To answer these questions, this thesis is divided into two parts. The first part aims to develop MIR-MPs and investigate the effects of MIR-MPs on stimulating BA/BAT and beiging iWA/iWAT. Additionally, explanted human AT was also included to verify whether the therapeutic effects of MIR-MPs on murine AT can be transferred to human AT. The second part of this thesis is dedicated to establishing and characterizing T3-TRLs, in order to deliver T3 to the targeted tissue BAT. Using such pharmaceutical technologies might provide novel methods to treat obese patients with two promising anti-obesity agents (MIR and T3).

3 Materials and methods

3.1 Common materials and equipment

- Acetic acid (Carl Roth, Cat. No. KK62)
- Autoclave, Varioklav 135 T (Faust)
- Centrifuge (Eppendorf, Cat. No. 5415R)
- Centrifuge (Sigma Aldrich, Cat. No. Z606235)
- Centrifuge, Biofuge Primo, Heraeus (Hanau)
- Chloroform (Carl Roth, Cat. No. Y015)
- Collagenase, Type II (Worthington, Cat. No. CLS2)
- Conical tubes, 15 ml and 50 ml volume (Sarstedt, Cat. No. 62.554.502, 62.547.254)
- Countess Automated Cell Counter (Invitrogen, Cat. No. C10227)
- Cryogenic vials (Sarstedt, Cat. No. 72.379.992)
- EnSpire Multimode Plate Reader (Perkin Elmer)
- Ethanol (EtOH) (Carl Roth, Cat. No. 9065)
- Ethylenediaminetetraacetic acid, EDTA (Carl Roth, Cat. No. 8040)
- Incubator, HeraCell 150, Heraeus, (Hanau)
- Isopropanol (Carl Roth, Cat. No. AE73)
- Laminar air flow, HeraSafe, Heraeus (Hanau)
- Methanol (Cat. No. 0082, Carl Roth)
- Microscope (LEICA DMIL, Leica Microsystems GmbH, Wetzlar)
- NaCl 0.9% saline solution (B. Braun)
- NanoDrop 2000 UV-Vis Spectrophotometer (NanoDrop® Technologies, Thermo Scientific)
- Nylon meshes (Millipore, Cat. No. NY3002500, NY1H00010)
- Oil Red O (Sigma Aldrich, Cat. No. O0625)
- Paraformaldehyde (PFA) (Carl Roth, Cat. No. 0964)
- Potassium hydroxide, KOH (Carl Roth, Cat. No. 7986)
- Reaction tube PP 1.5 mL (Sarstedt, Cat. No. 72706)
- Real-time PCR machine, HT7900 (Applied Biosystems)
- Serological pipettes 5 ml, 10 ml, 25 ml (Sarstedt, Cat. No. 86.1253.001, 86.1254.001, 86.1685.001)
- Sodium chloride, NaCl (Carl Roth, Cat. No. 3953)

- SpeedVac Concentrator, 5301 (Eppendorf)
- Syringe filter 0.22 µm (VWR, Cat. No. 514-0061)
- T175 TC flasks (Sarstedt, Cat. No. 83.3912.002)
- Thermomixer comfort (Eppendorf, Cat. No. 2050-120-04)
- Tris-HCl (Carl Roth, Cat. No. 9090)
- Triton X100 (Carl Roth, Cat. No. 3051)
- Xylol (Carl Roth, Cat. No. 9713)

3.2 Cell culture and isolation of adipocytes

3.2.1 Materials and equipment

- 10 cm TC dishes (Greiner, Cat. No. 664160)
- 10 cm tissue culture (TC) dishes, Standard (Sarstedt, Cat. No. 83.3902)
- 12-well TC plates (Greiner, Cat. No. 662160)
- 12-well TPP plates (TPP Techno Plastic Products AG, Cat. No. 92012)
- 3,3',5-Triiodo-L-thyronine sodium salt (T3; Sigma-Aldrich, Cat. No. T6397)
- 3-Isobutyl-1-methylxanthine (IBMX; Sigma-Aldrich, Cat. No. I5879)
- Dexamethasone (Sigma-Aldrich, Cat. No. D4902)
- Dimethyl sulfoxide (DMSO; Roth, Cat. No. A994)
- DMEM, high glucose, GlutaMAXTM, pyruvate (Gibco, Cat. No. 31966)
- Dulbecco's Modified Eagle Medium (DMEM), high glucose, GlutaMAXTM (Gibco, Cat. No. 31965)
- Fetal Bovine Serum (FBS; Biochrom, Cat. No. S0015)
- Glutamine (Lonza, Cat. No. 17-605E)
- HEPES buffer (1M) in Normal Saline (HEPES; Lonza, Cat. No. BE-17-737E)
- Insulin solution human (Insulin; Sigma-Aldrich, Cat. No. I9278)
- Penicillin/streptomycin (P/S; Merck, Cat. No. A2213)
- Rosiglitazone (Sigma-Aldrich, Cat. No. R2408)
- Trypan Blue Stain (Gibco, Cat. No. 15250)
- Trypsin-ethylenediaminetetraacetic acid (Trypsin-EDTA) (0.05 %), phenol red (Trypsin; Gibco, Cat. No. 25300054)

3.2.2 Isolation and immortalization of BAT-derived mesenchymal stem cells (MSCs)

BAT-derived MSCs were isolated from newborns of wild-type (WT) C57BL/6J mice. Freshly isolated interscapular BAT was chopped into small pieces and digested in BAT digestion medium at 37°C for 30 min in a shaking water bath. The digested tissue was then filtered using a 100 µm nylon mesh and incubated on ice for 30 min. The middle phase containing BAT-derived MSCs was collected using a syringe and filtered again with a 30 µm nylon mesh. MSCs were further centrifuged down at 700 gravity ($\times g$) for 10 min and re-suspended in 2 ml of BA primary cell culture medium. Isolated cells were seeded on a 6-well TC plate and cultured at 37°C, 5% CO₂ for 24h.

After one day of cell culture, each well of preadipocytes was immortalized using lentivirus containing the Simian Virus 40 (SV40) large T-antigen. Each well was filled with 800 µl of BA growth medium containing 200 ng of the virus. The BA growth medium was filled up to 2 ml the next day. The BA growth medium was replenished every other day.

BAT digestion medium

CaCl₂	1.3 mM
Glucose	5 mM
HEPES	100 mM
KCl	5 mM
NaCl	123 mM
BSA	1.5% (w/v)
Collagenase II	2 mg/ml

All substances were dissolved in H₂O. The pH of the medium was adjusted to 7.4 and sterile-filtered. BSA and Collagenase II were added freshly and sterile filtered before use.

BA primary cell culture medium

FBS	10%
HEPES	10 mM
Insulin	4 nM
P/S	1%
Sodium ascorbate	25 µg/ml
Triiodothyronine	4 nM

All substances were dissolved in DMEM, high glucose, and GlutaMAX^(TM) (Gibco, Cat. No. 61965)

BA growth medium

FBS	10%
P/S	1%

All substances were added in DMEM, high glucose, and GlutaMAX (TM) (Gibco, Cat. No. 61965).

3.2.3 Isolation of WAT-derived mesenchymal stem cells (MSCs)

WAT-derived MSCs were isolated from iWAT of 8-to-12-week-old WT C57BL/6J mice. Freshly isolated iWAT was chopped into small pieces and digested in the WAT digestion medium at 37°C for 30 min. Samples were shaken vigorously every 5 min during the digestion period. Cells were stood for 10 min at room temperature. The upper layer of fat was aspirated carefully, and cells were then filtered through a 100 µm nylon mesh. After filtration, cells were centrifuged at 1000 revolutions per minute (RPM) for 10 min. The pellet was re-suspended in 1 ml of WA growth medium. Isolated cells were seeded and cultured in a T175 TC flask at 37°C and 5% CO₂ for expansion.

WAT digestion medium

BSA (fatty acid free)	0.625% (w/v)
Collagenase II	0.4% (w/v)

All substances were dissolved in DMEM, high glucose, GlutaMAX(TM), and pyruvate (Gibco, Cat. No. 31966). WAT digestion medium should be prepared freshly and sterile filtered before use.

WA growth medium

FBS	10%
P/S	1%

All substances were added to DMEM, high glucose, GlutaMAX(TM), and pyruvate (Gibco, Cat. No. 31966). iWA growth medium was stored at 4°C.

3.2.4 Differentiation of adipocytes**3.2.4.1 Differentiation of brown adipocytes**

Pre-adipocytes were seeded (day -4) in a density of 1 million cells per plate on a 6-well plate or a 12-well plate in BA growth medium and incubated at 37°C, 5% CO₂. Two days after seeding the cells (day -2), the BA growth medium was replaced with the BA differentiation medium. Following

incubation in BA differentiation medium for 2 days, BA adipogenesis was induced by induction medium at day 0. As of day 2, cells were maintained in the BA differentiation medium, which was replenished every other day until day 7.

BA differentiation medium

FBS	10%
P/S	1%
Insulin	1 nM
Triiodothyronine	20 nM

All substances were added in DMEM, high glucose, and GlutaMAX (TM) (Gibco, Cat. No. 61965).

BA induction medium

FBS	10%
P/S	1%
Insulin	1 nM
T3	20 nM
Dexamethasone	1 μ M
IBMX	0.5 mM

All substances were added in DMEM, high glucose, and GlutaMAX (TM) (Gibco, Cat. No. 61965).

3.2.4.2 Differentiation of white adipocytes

Cells were seeded in WA growth medium, which was replenished every other day until confluence was achieved. After reaching confluence (day 0), cells were induced with the WA induction medium. After 2 days of induction, cells were maintained in the WA maintenance medium for the next 10 days (from day 2 to day 12). The maintenance medium was replenished every other day.

WA induction medium

FBS	5%
P/S	1%
Insulin	0.172 μ M
Dexamethasone	1 μ M
IBMX	0.5 mM
T3	1 nM
D-biotin	1 mM
Pantothenate	17 mM
L-ascorbate	50 mg/ml
Rosiglitazone	1 μ M

All substances were added to DMEM, high glucose, GlutaMAX (TM), and pyruvate (Gibco, Cat. No. 31966). WA induction medium was freshly prepared before use.

WA maintenance medium

FBS	5%
P/S	1%
Insulin	0.172 μ M
T3	1 nM
D-biotin	1 mM
Pantothenate	17 mM
L-ascorbate	50 mg/ml

All substances were added to DMEM, high glucose, GlutaMAX (TM), and pyruvate (Gibco, Cat. No. 31966). WA maintenance medium was freshly prepared before use.

3.3 Nucleic acid methods

3.3.1 Materials and equipment

- Diethyl pyrocarbonate, DEPC (Carl Roth, Cat. No. K028.1)
- InnusOLV RNA Reagent (Analytik Jena AG, Cat. No. 845-SB-2090100)
- ProtoScript II First Strand cDNA Synthesis Kit (New England Biolabs, Cat. No. E6560S)
- SYBR-Green PCR master mix (Applied Biosystems, Cat. No. 4309155)

3.3.2 RNA isolation

RNA isolation from cells and tissues in this thesis was performed following the acid guanidinium thiocyanate-phenol-chloroform extraction protocol using InnusOLV RNA Reagent. To isolate mRNA from cell samples, 1 ml of pre-cooled InnusOLV RNA Reagent was added to the cells

followed by adding 200 µl of chloroform. A vigorous shake was performed on the samples, and samples were kept at room temperature for 5 min. Following centrifugation at 13000 RPM for 25 min at 4°C, the upper aqueous phase was transferred to new RNAase-free reaction tubes. The samples were added 500 µl of isopropanol and then centrifuged at 13000 RPM for 10 min at 4°C to precipitate RNA. After centrifugation, the supernatant was discarded, and RNA pellets were washed three times with 1 ml of pre-cold 75% EtOH (in diethylpyrocarbonate-water, DEPC-H₂O). RNA samples were collected by centrifugation at 13000 RPM at 4°C for 5 min during each washing step. After drying, the RNA pellets were then incubated at 55°C for 10 min with agitation in nuclease-free water and stored at -80°C for further use.

The RNA isolation method for tissues with high lipid content was optimized. 80 - 90 mg of tissue was homogenized in 1 ml pre-cold InnuSOLV RNA Reagent. The homogenized samples were kept at room temperature for 5 min before being centrifuged at 13000 RPM for 10 min at 4°C. The InnuSOLV RNA Reagent from each sample was carefully transferred to a new RNAase-free reaction tube without transferring the lipid monolayer. For each sample, 300 µl of chloroform was added to InnuSOLV RNA Reagent. The samples were vigorously shaken and kept at room temperature for 3 min. After centrifuging the samples at 13000 RPM for 15 min at 4°C, the upper aqueous phase was transferred to new RNAase-free reaction tubes. The purified aqueous phase that contains RNA was obtained by repeating those steps twice. For RNA precipitation, each sample was subsequently added 500 µl isopropanol and centrifuged at 13000 RPM for 10 min at 4°C. Following centrifugation, the supernatant was discarded, and the RNA pellets were washed three times in 1 ml of pre-cold 75% EtOH (DEPC-H₂O). During each washing step, RNA samples were collected by centrifugation at 13000 RPM for 5 min at 4°C. The RNA pellets were then incubated at 55°C for 10 min with agitation in nuclease-free water after drying and stored at -80°C for further use. The concentration and quality of RNA samples were measured using NanoDrop 2000 UV-Vis Spectrophotometer.

3.3.3 Complementary DNA (cDNA) synthesis

According to the manufacturer's instructions, up to 1 µg of RNA was used to synthesize cDNA using a First Strand cDNA Synthesis Kit. The PCR program for cDNA synthesis was designed as followed: 5 min incubation at 25°C before the incubation at 42°C for 1h. By incubating samples at 80°C for 5 min, the enzyme was inactivated. cDNA samples were stored at -20°C.

3.3.4 Real-time quantitative PCR (RT-qPCR)

The quantitative polymerase chain reaction (qPCR) was performed using the HT7900 instrument (Applied Biosystems) or Step One Plus Thermocycler instrument. Fluorescent dyes SYBR-Green PCT master mix (Applied Biosystems) and qPCR program (Table 1) were utilized in this study. mRNA quantification was performed according to the crossing point values of the amplification curves using the comparative C_T method ($2^{-\Delta\Delta C_T}$ method) (Schmittgen and Livak 2008). The expression of murine *Hprt* (Hypoxanthine-guanine phosphoribosyltransferase) or human *Rpl13a* was used as an internal control for murine samples and human samples, respectively. Primer sequences for target genes are listed in Table 2.

Table 1. qPCR Program

Step	Temperature (°C)	Time (s)
1	95	600
2	95	15
3	60	60
Step 2 and step 3 were cycled 40 times.		
Melting curve:		
4	95	1
5	65	15
6	95	N/A

Table 2. qPCR primer sequences

Name	Species		Primer sequence (5' - 3')
<i>Ucp1</i>	Murine	Forward	TAAGCCGGCTGAGATCTTGT
		Reverse	GGCCTCTACGACTCAGTC
<i>Ucp2</i>	Murine	Forward	CGGTCCGGACACAATAGTATGA
		Reverse	GAAAATGGCTGGGAGACGAA
<i>Ucp3</i>	Murine	Forward	CCTGTTTACTGACAACCTTCCCC
		Reverse	AGCGTTCATGTATCGGGTCT
<i>Ppary</i>	Murine	Forward	AGCCTCATGAAGAGCCTTCCA
		Reverse	TCCGGAAGAAACCCTTGCA
<i>Fabp4</i>	Murine	Forward	TGTGCAGAAATGGGATGGAAA
		Reverse	CAACGTCCCTTGGCTTATGCT
<i>Ppargc1α</i>	Murine	Forward	CCCTGCCATTGTTAAGAC
		Reverse	GCTGCTGTTCTGTTTTC
<i>Dio2</i>	Murine	Forward	GCGATGGCAAAGATAGGTGA
		Reverse	GAATGGAGCTGGGTGTAGCA
<i>Cidea</i>	Murine	Forward	GTCAAAGCCACGATGTACGAGAT
		Reverse	CGTCATCTGTGCAGCATAGGA

Prdm16	Murine	<i>Forward</i>	TGTGCGAAGGTGTCCAAACT
		<i>Reverse</i>	CAACGTCACCGTCACTTTTGG
Cpt1a	Murine	<i>Forward</i>	GGACTCCGCTCGCTCATT
		<i>Reverse</i>	TCAGGGGTGACTGTGAACTG
Dgat	Murine	<i>Forward</i>	CGACGGCTACTGGGATCTG
		<i>Reverse</i>	CTCAGGATCAGAATCACCACA
Lipc	Murine	<i>Forward</i>	ACTGACCTGCACTCAGAGAA
		<i>Reverse</i>	TGTCTAGAAGGTAAAGGCTGC
Ldlr	Murine	<i>Forward</i>	AATCGACTCACGGGTTCAGA
		<i>Reverse</i>	CAGTGTGCGACTTCTCTAGGCT
Spot14	Murine	<i>Forward</i>	TTCTGAAGATCGCTTTACACG
		<i>Reverse</i>	GATGCACTCAGAGGGAGACG
Me1	Murine	<i>Forward</i>	ACCCGCATCTCAACAAGGA
		<i>Reverse</i>	GGCGGCAACAATCCATGA
Dio1	Murine	<i>Forward</i>	GCAGGATCTGCTACAAGGGTA
		<i>Reverse</i>	CTTTTCCAGGACAGCTCGGA
Srebp2	Murine	<i>Forward</i>	CAAGCTGGGCGATGGATG
		<i>Reverse</i>	CTGTAGCATCTCGTCGATGTC
Cyp7a1	Murine	<i>Forward</i>	TACCTGCAAACCTGATGGGGA
		<i>Reverse</i>	CCAAATGCCTTCGCAGAAGTA
Dio2	Murine	<i>Forward</i>	CAAACAGGTTAAACTGGGTGA
		<i>Reverse</i>	GTCAAGAAGGTGGCATTTCGG
Lipc	Murine	<i>Forward</i>	TGCAAGCTCAAAGCAGGGAT
		<i>Reverse</i>	TCTAGAAGGTAAAGGCTGCTG
Scarb1	Murine	<i>Forward</i>	TCCCAGGATAAGGAGGCCAT
		<i>Reverse</i>	TGTCTTCAGGACCCTATA
Ppara	Murine	<i>Forward</i>	CATTTGGGCGTATCTCACCG
		<i>Reverse</i>	ACTTCAACTTGGCTCTCCTCT
Pdk4	Murine	<i>Forward</i>	AGCAGTAGTCCAAGATGCCT
		<i>Reverse</i>	AATGTGGATTGGTTGGCCTG
Adrb3	Murine	<i>Forward</i>	CAGAGTCCACCGCTCAACAG
		<i>Reverse</i>	AGGGGACTCACTAGCTTCCT
Adrb2	Murine	<i>Forward</i>	AATAGCAACGGCAGAACGGA
		<i>Reverse</i>	TCAACGCTAAGGCTAGGCAC
Hprt	Murine	<i>Forward</i>	GTCCCAGCGTCGTGATTAGC
		<i>Reverse</i>	TCATGACATCTCGAGCAAGTCTTT
UCP1	Human	<i>Forward</i>	TGCCCAACTGTGCAATGAA
		<i>Reverse</i>	CCAGGATCCAAGTCGCAAGA
PPARGC1a	Human	<i>Forward</i>	CTGTGTCACCACCCAAATCCTTAT
		<i>Reverse</i>	TGTGTCGAGAAAAGGACCTTGA
DIO2	Human	<i>Forward</i>	GTCAGTGGTCAGCGTGGTTTT
		<i>Reverse</i>	TTCTTCACATCCCCCAATCCT
TNFa	Human	<i>Forward</i>	GCCCATGTTGTAGCAAACCCT
		<i>Reverse</i>	ATGAGGTACAGGCCCTCTGAT
CIDEA	Human	<i>Forward</i>	GGGTCTCCAACCATGACAGG
		<i>Reverse</i>	GAGGGCATCCAGAGTCTTGC
PRDM16	Human	<i>Forward</i>	CGAGGCCCTGTCTACATTC
		<i>Reverse</i>	GCTCCCATCCGAAGTCTGTC

TMEM26	Human	<i>Forward</i>	ATGGAGGGACTGGTCTTCCTT
		<i>Reverse</i>	CTTCACCTCGGTCACTCGC
ADRB3	Human	<i>Forward</i>	GCTCGACGGGGCTTCTT
		<i>Reverse</i>	TCTGAACAGAGGCCAGAGGT
ADRB2	Human	<i>Forward</i>	ATGCCAATGAGACCTGCTGT
		<i>Reverse</i>	GCTCCACCTGGCTAAGGTTC
RPL13A	Human	<i>Forward</i>	GGACCGTGCGAGGTATGCT
		<i>Reverse</i>	ATGCCGTCAAACACCTTGAGA

3.4 Protein analysis

3.4.1 Materials and equipment

- BioPhotometer D30 (Eppendorf)
- Bovine Serum Albumin (Sigma-Aldrich, Cat. No. A7030)
- Bromophenol blue (Carl Roth, Cat. No. 6558)
- Cell scraper (Labomedic, Cat. No. 2015217)
- Chemiluminescence films, Amersham Hyperfilm® (GE Healthcare Life Sciences, Cat. No. 28906837)
- Complete protease inhibitor cocktail (Roche, Cat. No. 04693116001)
- Coomassie brilliant blue G-250 (Merck, Cat. No. 1.15444.0025)
- Enhanced chemiluminescence (ECL) Western Blotting Detection Reagent (Amersham Biosciences, Cat. No. RPN2106)
- Ethylene glycol-bis(β -aminoethyl ether)-*N,N,N',N'*-tetraacetic acid, EGTA (Sigma Aldrich, E4378)
- Glycerol (Sigma Aldrich, Cat. No. G5516)
- Glycine (Carl Roth, Cat. No. 3908)
- Image Quant LAS 4000 mini (Life sciences, Cat. No. 28-9558-10)
- Mini-PROTEAN Tetra Cell electrophoresis system (BioRad)
- *N,N,N',N'*-Tetramethylethylenediamine, TEMED (Sigma Aldrich, T9281)
- Nitrocellulose membrane, Amersham Protran 0.45 NC (GE Healthcare Life Sciences, Cat. No. 10600002)
- Nonidet P 40 Substitute, NP-40 (Sigma Aldrich, Cat. No. 74385)
- PageRuler Prestained Protein Ladder (Thermo Scientific, Cat. No. 26616)

- Phosphoric acid (Carl Roth, Cat. No. 9076)
- Power supply, Consort EV 202 (Sigma-Aldrich, Cat. No. Z654418)
- Primary and secondary antibodies (Cell Signalling, Dianova, LSBio, Santa Cruz, Sigma-Aldrich, Thermo Fisher Scientific)
- Secondary antibody HRP-conjugated anti-mouse (Dianova, Cat. No. 115-035-146)
- Secondary antibody HRP-conjugated anti-rabbit (Cell Signaling, Cat. No. 7074)
- Sodium deoxycholate (Sigma Aldrich, Cat. No. D6750)
- Sodium fluoride, NaF (Carl Roth, Cat. No. 4530)
- Sodium orthovanadate, Na₃VO₄ (Carl Roth, Cat. No. 0735)
- Sonoplus HD 2070 (Bandelin, Germany)
- Tween 20 (Carl Roth, Cat. No. 9127)
- Ultra-Turrax®, T8, IKA, Staufen
- β-Mercaptoethanol (Sigma Aldrich, Cat. No. M6250)

3.4.2 Protein lysates from cells and tissues

During cell lysates, cells were placed on ice and washed with pre-cold phosphate-buffered saline (PBS) before adding radioimmunoprecipitation assay (RIPA) buffer. Cells were scraped off and incubated in lysis buffer on ice for 30 min. Samples were further centrifuged at 13000 RMP at 4°C for 10 min. The supernatant was collected and quantified in concentrations using the Bradford method. For tissue lysates, tissues were placed in ice-cold supplement lysis buffer (RIPA+) and homogenized using Ultra-Turrax®. The NaF, Na₃VO₄, and complete cocktail were additionally added to the RIPA buffer, which was respectively Serine/Threonine and acidic phosphatase inhibitors, Tyrosine and alkaline phosphatase inhibitors, and protease inhibitors. Samples were centrifuged at 13000 RPM at 4°C for 10 min and quantified using the Bradford method.

Phosphate-buffered saline (PBS) pH 7.4

NaCl	137 mM
Na₂HPO₄	8 mM
KH₂PO₄	1.4 mM
KCl	2.7 mM

Substances were dissolved in H₂O. PBS was autoclaved and stored at room temperature.

Lysis buffer (RIPA buffer)

Tris-HCl (pH 7.5)	50 mM
NaCl	150 mM
NP-40	1%
Sodium deoxycholate	0.5%
Sodium dodecyl sulfate (SDS)	1 mM
EDTA	0.1 mM
EGTA	0.1 mM

The Lysis buffer was sterile-filtered and stored at 4°C.

Supplement lysis buffer (RIPA+)

Complete® EDTA free (25x)	40 µl/ml
NaF	10 mM
Na₃VO₄	1 mM

Substances were added freshly to the RIPA buffer before use.

3.4.3 Protein quantification using the Bradford method

Using the Eppendorf BioPhotometer D30, protein samples were quantified at the absorbance of 595 nm, which was calibrated with the range of 1 µg/ml to 30 µg/ml using BSA standard dilutions. Each protein sample was 1:50 diluted in 0.15 M NaCl solution. The protein samples were mixed with Coomassie solution before being measured with the BioPhotometer. Quantified protein samples were subsequently added to Laemmli solution 3x containing 10% β-mercaptoethanol and incubated at 98°C for 5 min. For further use, the prepared protein samples were stored at -20°C.

Coomassie solution

Coomassie brilliant blue G-250	0.01%
EtOH	5%
Phosphoric acid	8.5%

Substances were dissolved in H₂O. Coomassie solution was stored at 4°C.

Laemmli solution 3x

Tris-HCl (pH 6.8)	125 mM
Glycerol	20%
SDS	17%

Substances were dissolved in H₂O. Laemmli solution 3x was stored at -20°C. 10% β-mercaptoethanol was added to Laemmli solution 3x before use.

3.4.4 Western Blot

3.4.4.1 One-dimensional SDS-polyacrylamide electrophoresis (SDS-PAGE)

An SDS-PAGE gel consisting of stacking gel and resolving gel was used to separate proteins. Protein samples were loaded into stacking gel and then separated by resolving gel (12% acrylamide) according to their electrophoretic mobility. The Mini-PROTEAN Tetra Cell electrophoresis system (BioRad) was used for electrophoresis at 100 V in SDS-PAGE running buffer at room temperature.

Stacking gel

H ₂ O	3.4 ml
Acrylamide	830 µl
1.0 M Tris-HCl (pH 6.8)	630 µl
20% ammonium peroxodisulfate (APS)	25 µl
Tetramethylethylenediamine (TEMED)	5 µl

Resolving gel

	12%	15%
H ₂ O	3.3 ml	2.3 ml
Acrylamide	4 ml	5 ml
1.5 M Tris-HCl (pH 8.8)	2.5 ml	2.5 ml
20% APS	50 µl	50 µl
TEMED	4 µl	4 µl

Electrophoresis buffer 10x

Tris	250 mM
Glycine	2 M
SDS	0.1%

Substances were dissolved in H₂O. The pH of the electrophoresis buffer 10x was adjusted to 8.3. Electrophoresis buffer 10x was diluted to 1x in H₂O before use. The electrophoresis buffer 10x was stored at room temperature.

3.4.4.2 Blotting and immunodetection

Proteins separated by an SDS-PAGE gel were electrically transferred from the SDS-PAGE gel to a nitrocellulose membrane at 4°C for 1.5h (300 mA) in the transfer buffer. Subsequently, the nitrocellulose membrane was blocked in the blocking solution for 1h at room temperature. Following blocking, the membrane was washed three times in the Tris-buffered saline with 0.1% Tween® 20 detergent (TBST), each wash lasting 5 min, and then incubated in primary antibody overnight at 4°C. Primary antibodies were diluted 1:1000 in antibody solution. The incubation with the primary antibody was followed by three TBST washes of the membrane and one hour of incubation with the secondary antibody (dilution factor: anti-mouse, 1:10000; anti-rabbit, 1:5000). The membrane was washed three more times after the second antibody incubation. Proteins were visualized using Amersham ECL Western Blotting detection reagent according to the manufacturer's instructions. Quantification was performed using Image J software after the detection of proteins using ImageQuant LAS 4000 mini.

Transfer buffer

H₂O	70%
Methanol	20%
Electrophoresis buffer 10x	10%

Transfer buffer was prepared freshly before use.

Tris-buffered saline (TBS) 10x

Tris-HCl	100 mM
NaCl	1.4 M
SDS	0.1%

Substances were dissolved in H₂O. The pH of TBS buffer 10x was adjusted to 8.0.

TBST

TBS 10x	10%
Tween-20	0.1%

Substances were dissolved in H₂O. TBST solution was stored at room temperature and protected from light.

Blocking solution

Milk powder	5%
--------------------	----

Milk powder was freshly dissolved in TBST before use.

Antibody solution

Milk powder	1%
--------------------	----

Milk powder was freshly dissolved in TBST before use.

Primary antibodies

-
- Tubulin (Dianova, Cat. No. MS-719-P0)
 - Calnexin (Cell Signaling, Cat. No. 3704241)
 - UCP1 (Sigma Aldrich, Cat. No. sc-6529)

Secondary antibodies

-
- Anti-rabbit (Cell Signaling, Cat. No. 7074)
 - Anti-mouse (Dianova, Cat. No. 115-035-146)

3.5 Oil Red O staining

The cells were washed twice in PBS and fixed in 4% PFA for 15 min at room temperature. PFA was removed and the fixed cells were washed twice with PBS. Subsequently, cells were incubated in the Oil Red O working solution for 1 hour at room temperature. Following Oil Red O staining, cells were washed with distilled water and dry plates at room temperature for further visualization and analysis.

Oil Red O solution (5 mg/ml)

Oil Red O	0.5 g
Isopropyl alcohol (99%)	100 ml

Oil Red O was well dissolved in isopropyl alcohol using a magnetic stir overnight and stored at room temperature.

Oil Red O working solution (3 mg/ml)

Oil Red O solution (5 mg/ml)	6 ml
H₂O	4 ml

Oil Red O working solution was freshly prepared and filtered twice with a paper filter before use.

3.6 Lipolysis

3.6.1 Materials and equipment

- 24-well plates (Sarstedt, Cat. No. 83.3921)
- 96-well plates (Sarstedt, Cat. No. 83.3924)
- Bovine serum albumin, fatty acids free (Sigma Aldrich, Cat. No. A7030)
- Dulbecco's Modified Eagle Medium (DMEM) (Gibco, Cat. No. 21063)
- EnSpire Multimode Plate Reader (Perkin Elmer)
- Free glycerol reagent (Sigma Aldrich, Cat. No. F6428)
- Glycerol standard (Sigma Aldrich, Cat. No. G7793)

3.6.2 *In vitro* lipolysis

First, cells were washed twice with the pre-warmed lipolysis medium. Treatments were freshly prepared in 400 μ l lipolysis medium and added to each condition. Next, cells were further incubated in the lipolysis medium at 37°C, 5% CO₂ for 3h. After the incubation, 20 μ l of lipolysis medium from each condition was mixed with 80 μ l of Free glycerol reagent and transferred to a 96-well plate. The glycerol standards were prepared as follows: The positive glycerol standard contained 5 μ l of Glycerol plus 95 μ l of free glycerol, while the negative standard contained 5 μ l of lipolysis medium mixed with 95 μ l of free glycerol. Samples and glycerol standards were incubated for 5 min in duplicates at 37°C, with 5% CO₂. The absorption of each sample was measured at 540 nm wavelength using EnSpire Multimode Plate Reader (Perkin Elmer). The concentration of glycerol released from each sample was determined and normalized to its protein content.

Lipolysis medium

BSA	2% (w/v)
------------	----------

BSA was prepared freshly in DMEM (Gibco, Cat. No. 21063) before use.

3.6.3 *Ex vivo* lipolysis

AT was isolated freshly from WT mice to perform *ex vivo* lipolysis. Freshly isolated BAT was cut into pieces of 4 - 5 mg each. iWAT and gonadal WAT (gWAT) were cut into pieces of 15 to 20 mg each. Human scWAT was cut into pieces of 40 to 50 mg each. Samples were incubated in 400 μ l lipolysis medium for 3 hours, 6 hours, or 1 day at 37°C, with 5% CO₂. After the incubation, 20 μ l of lipolysis medium from each sample was mixed with 80 μ l free glycerol reagent and transferred to a 96-well plate. In addition, to prepare samples for the direct injection treatment, samples of human scWAT were cut into pieces of 150 - 200 mg each and further incubated in 400 μ l lipolysis for 1 day at 37°C, 5% CO₂. Following the incubation, 10 μ l of lipolysis medium from each sample was mixed with 90 μ l free glycerol reagent and transferred to a 96-well plate. The glycerol standards were prepared as follows: The positive glycerol standard contained 5 μ l of Glycerol plus 95 μ l of free glycerol, while the negative standard contained 5 μ l of lipolysis medium mixed with 95 μ l of free glycerol. Samples and glycerol standards were incubated for 5 min in duplicates at 37°C, with 5% CO₂. The absorption of each sample was measured at 540 nm wavelength using EnSpire Multimode Plate Reader (Perkin Elmer). The concentration of glycerol released from each sample was determined and normalized to its tissue weight.

3.7 Immunohistochemistry

3.7.1 Materials and equipment

- DAB peroxidase HRP-substrate kit (Vector Laboratories, Cat. No. SK-4100)
- Eosin Y-solution (Merck, Cat. No. 1.09844)
- EVOS® FL Color Imaging System (Thermo-Fischer Scientific)
- Mayer's hemalum solution (Merck, Cat. No. 1.09249)
- Microtome HM315 (Microm)
- Roti-Histokitt (Carl Roth, Cat. No. 6640)
- Secondary antibody HRP-conjugated anti-rabbit (Cell Signaling, Cat. No. 7074)
- UCP1 primary antibody (Sigma Aldrich, Cat. No. sc-6529)

3.7.2 Tissue preparation for staining

The freshly isolated tissues were fixed for no more than 16h in PBS containing 4% paraformaldehyde (PFA) and washed twice for 5 min each with ice-cold PBS. Following washing, the samples were dehydrated in ethanol with increasing concentrations: 50 %, 70 %, 95 %, and 100 % (3 times, 20 min for each concentration). Tissues were incubated and defatted three times in Xylol, each for 10 min. Samples were further incubated twice in paraffin at 60°C for 1h, followed by overnight incubation at 60°C. The processed tissues were embedded in a warmed liquid paraffin solution using cassettes and subsequently solidified and stored at room temperature. A microtome (Microm) was used to cut incorporated tissue into 5 µm thick sections for each staining, and the stained sections were then dried on histological slides for 24h at 40°C.

4% PFA

PFA	4% (w/v)
------------	----------

PFA was dissolved at stirred in PBS at 60°C and stored at 4°C.

3.7.3 Hematoxylin/Eosin (H&E) staining

Three xylol washes, 5 min for each, were required to remove paraffin from histology slides. Samples were incubated in ethanol with decreasing concentrations: 100%, 95%, 90%, 75%, and 50% (for each concentration, wash twice for 2 min), followed by two more washes in H₂O (each wash for 5 min). After two seconds of incubation in hematoxylin, the slides were rinsed under running water for 10 min. In the next step, slides were stained with eosin for 2 min and washed in distilled water with agitation for 4 min. Tissues were dehydrated using increasing concentrations of ethanol: 50%, 75%, 95%, and 100% (for each concentration, tissues were washed twice for 2 min) and followed by two more times wash in xylol, each for 2 min. In the end, slides were mounted using Roti-Histokitt.

3.7.4 Immunohistochemistry for UCP1 detection

To remove paraffin from histological slides, AT sections were washed 3 times in xylol, five minutes for each. Samples were incubated in ethanol with decreasing concentrations: 100%, 95%, 90%, 75%, and 50% (for each concentration, tissues were washed twice for 2 min), followed by two

more washes in H₂O (each wash for 5 min). Following the incubation in 20 mM sodium citrate (pH 6.0) for 5 min, samples were incubated in 10 mM sodium citrate (pH 6.0) for 5 min at 75 - 80°C. To neutralize the function of endogenous peroxidases, samples were washed 3 times (each wash for 10 min) in 3% hydrogen peroxide and once in H₂O for 5 min. Tissues were blocked with 2.5% goat serum in PBST solution at room temperature for 1h to reduce unspecific binding and then incubated with UCP1 antibody (1:75 in PBST) at 4°C overnight. On the following day, slides were washed 3 times in PBST (each time for 5 min) and incubated with the secondary antibody (1:200 in TBST) for 1h at room temperature. Before visualization, slides were washed 3 times in PBST (each wash for 5 min). Final development and visualization were performed by using 3,3'-Diaminobenzidine (DAB). Slides were mounted using Roti-Histokitt and dried. The microscope EVOS® FL Color Imaging System was used to visualize at magnifications of 20x and 40x.

3.8 Mitochondrial Stress Assay

Mitochondrial respiration of iWA was measured by Seahorse XF24 Analyzer (Agilent Seahorse Bioscience, Santa Clara, CA, USA). The Seahorse XF24 Analyzer can measure the oxygen consumption rate (OCR) and glycolysis of living cells in real-time by automatically adding and mixing compounds (Plitzko and Loesgen 2018). Mitochondrial respiration can be represented by several parameters including basal respiration, spare respiratory capacity, ATP production, and proton leak (Smolina et al. 2017). In a Seahorse 24-well XF Cell Culture microplate, pre-WA were seeded; the number of cells and the volume of WA growth medium were calculated (20000 cells per 100 µl per well). The microplate was incubated in the incubator for 1h at 37°C and 5% CO₂. Gently, each well was filled up to 250 µl WA growth medium, then the microplate was incubated overnight in the incubator. On the next day (day -2), each well was filled up to 500 µl of WA growth medium by adding an extra 250 µl of WA growth medium. On day 0, when cells reached confluence, the WA growth medium was replaced with 500 µl of high WA induction medium in each well and incubated in the incubator for 2 days at 37°C and 5% CO₂. From day 2, each well was replaced with fresh 500 µl of WA maintenance medium every other day till day 7. On the day before the XF assay, a Seahorse XF Sensor Cartridge hydrated overnight with 1 ml Seahorse XF Calibrant Solution was placed in each well of the XF Utility Plates. Bubbles attached to the column should be carefully removed. The XF Utility Plate was incubated in a non-CO₂ incubator for 1 day at 37°C.

On the day of the XF assay, WA were treated with MIR or MIR-MPs in 500 μ l buffered Seahorse Medium for 3h before the seahorse measurement. The mitochondrial respiration of cells was measured by sequentially injecting modulators into each well (final concentration of each compound and modulator injection volume): 1. Buffered seahorse medium (56 μ l); 2. Oligomycin (2 μ M, 62 μ l); 3. Carbonyl-cyanide-4-(trifluoromethoxy) phenylhydrazine (FCCP) (1 μ M, 69 μ l); 4. A mix of rotenone (0.5 μ l) and antimycin A (0.5 μ M, 75 μ l). Opiomycin inhibits ATP synthase and reduces OCR. FCCP increases mitochondrial proton permeability as a protonophore and maximizes OCR. Antimycin A and rotenone inhibit complexes I and III and minimize OCR (Smolina et al. 2017; Plitzko and Loesgen 2018). The compounds mentioned above were dissolved in a warmed buffered seahorse medium. Each XF assay measurement cycle contains 4 min of mixing, 2 min of waiting, and 2 min of measurement. The XF assay protocol is listed above. Programmed measurement cycles were performed after adding each compound.

XF assay protocol

	Cycles
Basal rate	4
Acute injection (1)	3 to 4
Oligomycin (2)	3
FCCP (3)	3 to 4
A mix of rotenone and antimycin (4)	3

High WA induction medium

	Volume	Final concentration
WA maintenance medium	50 ml	-
Dexamethasone	20 μ l	1 μ M
IBMX (5.67 mg in 500 μl 0.5 M KOH)	500 μ l	500 μ M
Rosiglitazone (10 mM)	5 μ l	1 μ M

Buffered Seahorse Medium

	Volume	Final concentration
Seahorse medium	200 ml	-
Glucose (2.5 M in H₂O)	2 ml	25 mM
Glutamine (200 mM in H₂O)	2 ml	2 mM
Sodium Pyruvate (44.02 mg)	-	2 mM

The buffered Seahorse Medium was adjusted to pH 7.4 before use.

3.9 Toxicity assays

3.9.1 MTT assay

Pre-brown adipocytes or pre-white adipocytes were seeded in the growth medium. The treatments were administrated when pre-adipocytes reached confluence. The differentiation of both iWA and mature BA was accomplished by following the differentiation protocols described above in **3.2.4**. This study used Mosmann's MTT test protocol with modifications (Mosmann 1983). After 1 day of treatments, 100 μ l of a 5 mg/ml MTT solution (MERCK, Germany) was added to each well of a 12-well plate. The plate was further incubated for 3h at 37°C. The solution from each well was aspirated and cells were washed with PBS (pH 7.4) twice. To dissolve the formazan salt and lyse cells, 500 μ l of DMSO was then added to each well and the plate was shaken for 1h. The absorbance of each sample was measured duplicate at 540/600 nm using EnSpire Multimode Plate Reader (Perkin Elmer).

3.9.2 ATP-based assay

Pre-brown adipocytes and pre-white adipocytes were seeded in the growth medium. The treatments were administrated when pre-adipocytes reached confluence. The differentiation of both mature iWAs and mature BAs was accomplished by following the differentiation protocols described above in **3.2.4**. After 1 day of treatments, the supernatant was discarded and cells were washed with PBS (pH 7.4) twice. Each well then received 600 μ l of cell lysis medium. The plate was shortly shaken to detach cells. Cell lysis medium with all detached cells was transferred from each well to individual 1.5 ml reaction tubes and each sample was incubated for 5 min at 65°C to lyse cells completely and release ATP. Forty microliters of lysis medium from each sample were mixed with 40 μ l of reagent. The plate was incubated for 10 min in the dark and luminescence signals were further measured using EnSpire Multimode Plate Reader (Perkin Elmer).

3.10 MIR-loaded PLGA MPs synthesis method

3.10.1 Materials and equipment

- 0.2 μ m Polytetrafluoroethylene (PTFE) membrane syringe filter (VWR, USA)
- Acetone (SupraSolv®, 67-64-1, Merck)

- Acetonitrile (BDH®, 75-05-8, VWR Chemicals)
- Dichloromethane (DCM) (SupraSolv®, 75-09-2, Merck)
- Hitachi S-2460N scanning electron microscope (Hitachi High Tech. Crop., JP-Tokyo)
- ICI 118,551 hydrochloride (Cat. No. 0821, Tocris)
- Mirabegron (Swapnroop Drugs & Pharmaceuticals, Aurangabad, India)
- Poly lactide-co-glycolide acid (PLGA) (Resomer RG 502H, EVONIK, Darmstadt, Germany)
- Polyvinyl alcohol (PVA) (Mw: 31,000, Aldrich)
- Salbutamol Hemisulfate (S0531, OMAHK-MB, Tokyo Chemical Industry, Japan)
- Steris Lyovac GT₂ freeze dryer (Mentor, OH, USA)
- Vacuum concentrator (5800-101-03, Eppendorf®)

3.10.2 Microparticles preparation

The MIR-MPs were prepared by adding 96 mg MIR to 12 ml of DCM and stirring at 750 RPM for 30 min, followed by adding 2 ml of DMSO to dissolve the MIR in DCM completely. One hundred milligrams of PLGA were further added into DCM and stirred for 1h at 750 RPM room temperature. To generate an emulsion, 5 ml of the mixture was added to 25 ml 0.1% polyvinyl alcohol (PVA) and stirred for 6 min at 750 RPM. After transferring the emulsion to 250 ml MilliQ H₂O (pH 8.0), it was stirred for 4h at 400 RPM to evaporate DCM and harden microparticles. Microparticles were filtered through a 0.2 µm filter and washed with 100 ml MilliQ H₂O (pH 8.0). Next, microparticles were resuspended in 5 ml MilliQ H₂O and frozen immediately for use in the freeze dryer. Samples were placed in the freeze dryer overnight to evaporate ice and collect microparticles.

To characterize the drug loading (Equation 1) of MIR-MPs, 1 mg microparticles were dissolved in 1 ml acetone. Acetone was further evaporated using a vacuum concentrator. PLGA was precipitated and removed by adding 1 ml of methanol (99%). The MIR pellet was dissolved in acetonitrile (60%) and analyzed using high-performance liquid chromatography (HPLC). The encapsulation efficiency of MIR-MPs was calculated following equation 2 below.

$$\text{Drug loading (\%)} = \frac{\text{Weight of the drug in microparticles}}{\text{Weight of the microparticles}} \times 100 \quad (1)$$

$$\text{Encapsulation efficiency (\%)} = \frac{\text{Weight of the drug in microparticles}}{\text{Weight of the adding drug}} \times 100 \quad (2)$$

3.10.3 Drug releasing condition

Drug release was carried out in a water bath with constant shaking. One milligram of MIR-MPs was freely suspended in 20 ml of PBS (pH 7.4) at 37°C or in 20 ml of lipolysis medium at 37°C. Samples were collected according to different time points (1h, 3h, 5h, 12h, 1d, 2d, 3d, 4d, 5d, 6d, 7d, 8d, 9d, and 15d). Before HPLC measurements, all samples were filtered using a 0.2 µm PTFE membrane syringe filter.

3.10.4 Human subcutaneous white adipose tissue

Human subcutaneous adipose tissue involved in section 4.5 were all contributed by healthy obese volunteers from the Plastic surgery department of Dreifaltigkeits-Krankenhaus Wesseling, Bonner Str. 84, 50389 Wesseling, Germany. Applied by Prof. Dr. Alf Lamprecht, the research is entitled “Charakterisierung der Wirk- und Hilfsstoff Penetration und Permeation in Abhängigkeit der Körperstelle und des Hautzustandes” and issued by the Ethik-Kommission of Rheinische Friedrich-Wilhelms-Universität Bonn in 2020. The ethical approval number is Lfd. Nr. 082/20.

3.11 HPLC system and Liquid Chromatography-Mass Spectrometry (LC/MS) analysis

3.11.1 Materials and equipment

- 1290 Infinity Liquid Chromatography System (Agilent, Waldbronn)
- 996 photodiode array detector (Waters, Milford, MA, USA)
- Ammonium acetate (CAS No.631-61-8, Roth)
- C-18 column 100RP 18-5µ EC (CS-Chromatographie, Merck)
- Formic acid (CAS No.64-18-6, Sigma Aldrich)
- Methanol (Cat. No. 0082, Carl Roth)
- Ortho-phosphoric acid (85%, Art.: 1172.1000, TH. GEYER)
- QTRAP 6500+ LC/MS System (Sciex, Darmstadt)
- Synergi™ 4 µm Fusion-RP, LC Column 50 x 2 mm (Synergi, Phenomenex)
- Trifluoroacetic acid (Uvasol®, CAS 76-05-1, Merck)
- Waters Alliance 2695 HPLC (Waters, Milford, MA, USA)

3.11.2 HPLC methods

HPLC measurements were performed using a Waters Alliance HPLC 2695 (Waters, Milford, MA, USA) equipped with the Waters 996 Photodiode Array Detector. 50 µl of each sample was injected into a C-18 100RP 18-5 EC analytical column for liquid chromatography separation.

T3 HPLC analysis used the mobile phase of 60% H₂O (0.1% Trifluoroacetic acid): 40% acetonitrile (v/v). The column was eluted at a flow of 1ml/min before samples were injected. T3 was detected in the ultraviolet (UV) at 225 nm.

HPLC analysis of MIR, the mobile phase consisted of 50% potassium dihydrogen phosphate (1.36 g/ml in MilliQ water, pH 4.0 adjusted with orthophosphoric acid) and 50% acetonitrile (v/v). The column was eluted at a flow of 1 ml/min before 50 µl of each sample was injected. MIR was detected in the ultraviolet (UV) at 249 nm.

3.11.3 LC/MS method

FR was measured using the liquid chromatography-mass spectrometry (LC/MS) system. During measurements, the Synergi™ 4 µm Fusion-RP column was kept at 60°C. The HPLC system was initially run with an eluent consisting of 60% H₂O (2 mM ammonium acetate and 0.1% formic acid) and 40% methanol (v/v) for 1 min. The gradient changed to 100% methanol containing 2 mM ammonium acetate and 0.1% formic acid for the next 6 min. A three-minute equilibration with 100% methanol (2 mM ammonium acetate and 0.1% formic acid) was followed before a new sample was injected. The flow rate of the column was 0.6 ml/min and 1 µl of each sample was injected. A positive multiple reaction monitoring (MRM) 1002.4/799.4 was used for quantification.

3.11.4 Scanning Electron Microscope (SEM) analysis

The SEM (Hitachi S-2460N, Hitachi Tech. Corp., Tokyo, Japan) was used to obtain SEM pictures of all microparticle samples in this study. Samples of dry microparticles were attached to aluminum stubs and subsequently sputter-coated with gold for 4 min using a Polaron SC76040 Sputter Coater (Quorum Technologies Ltd., Newhaven, UK). SEM images were acquired at an acceleration voltage of 10 kV.

3.12 The API-loaded triglyceride-rich lipoproteins synthesis method

3.12.1 Materials and equipment

- 1 μ m polyethersulfone (PES) syringe filter (GE Healthcare Life Sciences, Chicago, USA)
- 10 kD Dialysis Membrane (Pre-wetted RC Tubing, Cat. No. 132570, Spectra/Por 6)
- Centrifugal concentrator (MWCO 100 kDa, 0.2 μ m, PES, Vivaspin 20, Sartorius, UK)
- Chloroform (Sigma Aldrich, St. Louis, USA)
- Cholesterol (Sigma Aldrich, St. Louis, USA)
- Dynamic light scattering (ZetaSizer 90S, Malvern Panalytical, Malvern, UK)
- Egg phosphatidylcholine (Avanti polar lipids, Alabaster, USA)
- Rotary evaporator (VWR, USA)
- Sephadex-G25 PD-10 column (GE Healthcare, UK)
- T3 Enzyme-linked Immunosorbent Assay (ELISA) Kit (Cat. NO. KA4010, Abnova, Taiwan)
- Triglycerides (Soybean Oil, St. Louis, USA)

3.12.1 API-loaded TRLs preparation

To prepare high-concentrated T3-loaded TRLs, 3 mg cholesterol, 3 mg phosphatidylcholine, 48 mg TG, and 15 μ g T3 were mixed in chloroform. Low-concentrated T3-TRLs were prepared using 1 mg cholesterol, 1 mg phosphatidylcholine, 16 mg TG, and 8.3 μ g T3. FR-loaded TRLs were prepared using 1 mg cholesterol, 1 mg phosphatidylcholine, 16 mg TG, and 15 μ g FR900359. The mixture was dissolved in 1 ml of chloroform. The chloroform was then evaporated in a heated water bath (60°C) at 75 mbar using a rotary evaporator. Using a Probe Sonicator, the mixed lipid film was sonicated twice with 1 ml of PBS (pH 7.4) (each sonication lasting 5 minutes). Between each sonication procedure, samples were cooled on ice. The samples were stabilized overnight at 4°C. The next day, API-loaded TRLs were filtered twice with Sephadex-G25 PD-10 columns to remove nonencapsulated API in the samples and a final time with a 1 μ m polyethersulfone (PES) syringe filter before use. Dynamic light scattering (ZetaSizer 90S) was used to characterize samples. Vehicle-TRLs were prepared in the same procedures as described above but did not load T3 or FR. To determine the concentration of free T3 in the purified sample, purified T3-TRLs were centrifuged in a Vivaspin 20 centrifugal concentrator with a PES membrane 100000 molecular weight cut-off (MWCO) for 10 min at 2000 x g. The filtrates were collected and

measured using a T3 ELISA kit. The concentration of free FR in the purified FR-TRLs was determined using an LC/MS system.

Original samples were loaded into a dialysis membrane to determine the encapsulation efficiency of API-loaded TRLs. The dialysis membranes were completely immersed in 50 ml PBS for 2 days with magnetic stirring at 400 RPM at room temperature. Following dialysis, samples in dialysis membranes and dialysis medium were analyzed using an HPLC system or an LC/MS system.

The encapsulation efficiency of API-loaded TRLs was calculated following equation 3 below:

Encapsulation efficiency (%) of API loaded TRLs

$$= \frac{\text{Amount of API in dialysis membrane}}{\text{Amount of API used for formulation}} \times 100 \text{ (3)}$$

3.13 Animal experiments

Animal experiments in this thesis were approved by Landesamt für Natur, Umwelt und Verbraucherschutz (LANUV), Nordrhein-Westfalen, Germany. The approval number is 84-02.04.2016.A171. WT male C57B1/6J mice at 8 weeks old were purchased from Charles River, Sulzfeld, Deutschland. Animals involved in this thesis were housed at the Haus für experimentelle Therapie (HET), Universitätsklinikum Bonn (UKB), and the Institut für Pharmakologie und Toxikologie, UKB.

3.13.1 Materials and equipment

- Omnifix® 100 Solo 1 ml syringe (B. Braun, Cat. No. 9161708V)
- Phenomaster (TSE Systems)
- Sterican® 27G needle (B. Braun, Cat. No. 4665406)

3.13.2 Targeted delivery T3-TRLs to BAT

Mice at the age of 8 weeks were housed in single cages with bedding and free access to water and chow diets. The light cycle consisted of a 12-hour light (06:00 - 18:00) and a 12-hour dark (18:00 - 06:00). Animals were acclimatized at 16°C for 3 days and transferred to single metabolic

cages (Phenomaster, TSE System) at 4°C on day 4. The T3-TRLs or Vehicle-TRLs treatments were administered every second day from day 4 till day 10 (on day 4, day 6, and day 8) to the treated and control group, respectively. The injection volume was 5ml/kg body weight. Before sacrifice, the animals were kept at 23°C from day 10 to day 12. During cold exposure, animals' body weights were recorded daily. Tissues from mice were isolated for further analysis.

3.14 Statistics

All data are represented as mean \pm standard error of the mean (s.e.m). In this thesis, a student's t-test was performed to compare the means of two experimental groups. Analysis of variance (ANOVA) with a Dunnett's test was used to compare the means of more than two experimental groups. *p* values below 0.05 were considered statistically significant. “*n*” indicates the number of independent cell-culture experiments for *in vitro* studies or the number of mice per group for *ex vivo* and *in vivo* studies. The analyses were all performed using GraphPad Prism 6 software.

4 Results of Project I: MIR-loaded PLGA microparticles

4.1 Characterization of MIR-loaded microparticles

4.1.1 Characteristics and morphology of MIR-loaded microparticles

PLGA is an FDA-approved biodegradable polymer, it has been utilized as a drug delivery carrier because of its controllable degradation characteristics, high biocompatibility, and long clinical experience (Makadia and Siegel 2011; Mohamed and van der Walle 2008). PLGA particles have been investigated for their ability to deliver various drugs, such as the antitumor drug Paclitaxel and the antidiabetic drug Exenatide (Wang et al. 2003; Qi et al. 2013). To load the hydrophobic drug, MIR, into PLGA microparticles, DCM was chosen for dissolving MIR and PLGA copolymers and forming the oil phase due to its high evaporation rate and high miscibility. The oil-in-water (o/w) emulsion technique was used to prepare MIR-loaded PLGA microparticles (MIR-MPs). As illustrated in Table 3, four formulations of MIR-MPs were prepared. Since MIR has limited solubility in DCM, a small amount of DMSO was added to DCM to achieve a high concentration of MIR in the oil phase. Formulation 1 (F1) was the initial formulation, which was prepared with 5 mg/ml MIR in DCM, 2% PLGA, and 14% DMSO. Since the amount of MIR and PLGA affect the encapsulation efficiency and drug loading of MIR-MPs (Soomherun et al. 2017; Fan et al. 2017), and the drug release profile might be related to the concentration of DMSO (Xu et al. 2017), three additional formulations were prepared: formulation 2 (F2) with reduced DMSO, formulation 3 (F3) with reduced PLGA, and formulation 4 (F4) with increased MIR.

To evaluate the morphology of MIR-MPs, scanning electron microscopy (SEM) was used. The SEM images revealed that MIR-MPs exhibited a spherical morphology for all four formulations with slight differences in surface, as formulation F2 with reduced DMSO appeared less porous surface than the other three formulations (Figures 11A to D). The porous structure on the surface of microparticles can be caused by several factors, including the concentration of PLGA used during preparation, the slow removal of DCM during evaporation, DMSO diffusion, and the time to harden the microparticles (Amoyav and Benny 2019; Xu et al. 2017). It is assumed that MIR-MPs might harden slowly due to the diffusion of MIR in DMSO during evaporation, resulting in porous structures on their surfaces.

The diameter of MIR-MPs was quantified using Image J according to SEM images. Each formulation of MIR-MPs exhibited similarities in size distribution pattern (Figures 11D to H). The frequency distributions illustrate that the majority of MIR-MPs were in a range from 20 μm to 40

μm in diameter, and this population comprises almost 70% in each formulation. As shown in Figure 11I, MIR-MPs in F1 to F4 displayed an average size of $33.76 \pm 1.25 \mu\text{m}$, $32.29 \pm 0.89 \mu\text{m}$, $29.55 \pm 1.17 \mu\text{m}$, and $33.83 \pm 1.25 \mu\text{m}$, respectively. Only F3, with reduced PLGA concentration, showed a significantly reduced mean diameter compared to other formulations (Figure 11I).

Table 3. Four formulations of MIR-loaded microparticles

Formulation	MIR concentration (in DCM)	PLGA (50:50) concentration (w/v)	DMSO (v/v)	PVA
1	5 mg/ml	2%	14%	0.1%
2	5 mg/ml	2%	7%	0.1%
3	5 mg/ml	1.5%	14%	0.1%
4	8 mg/ml	2%	14%	0.1%

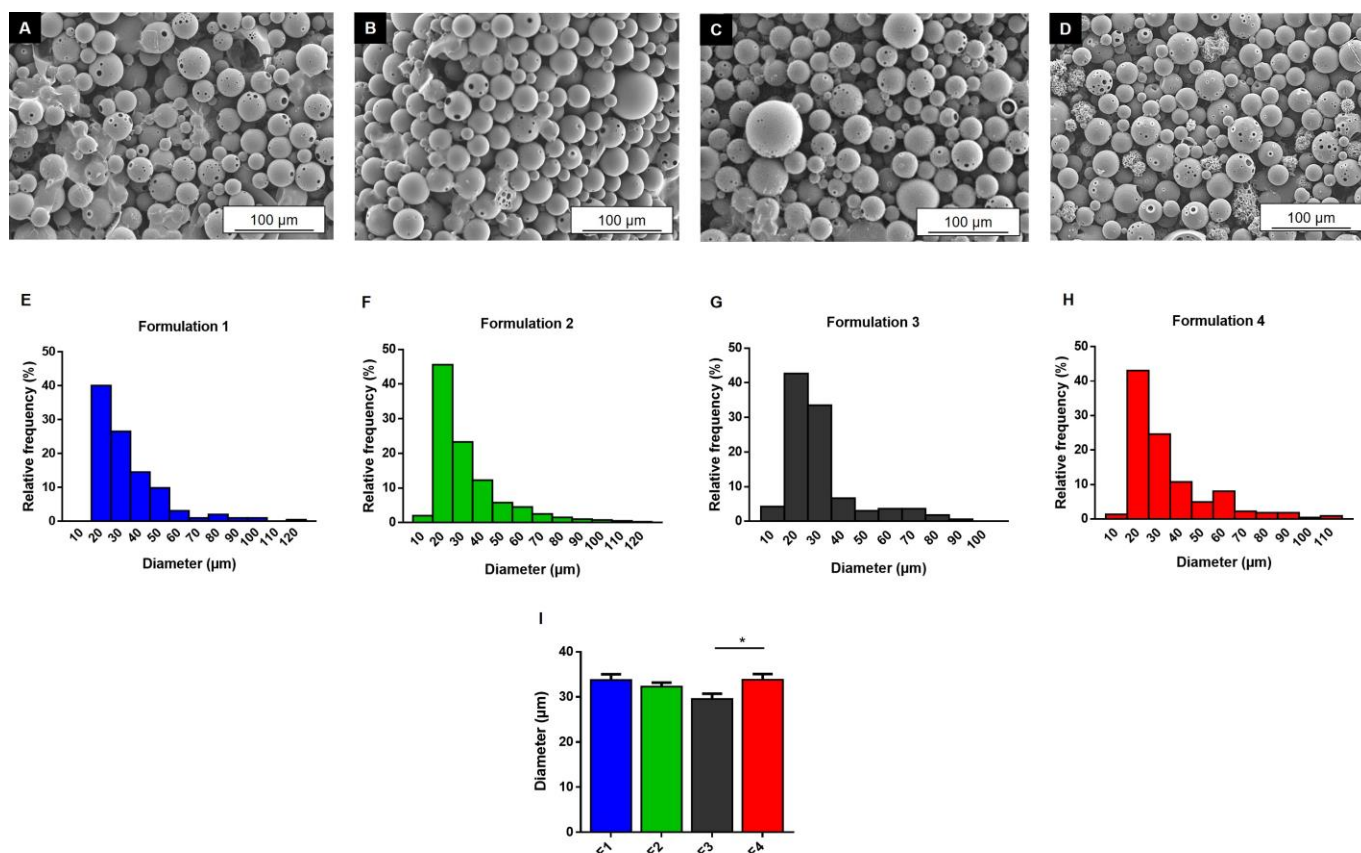


Figure 11. Assembly and characterization of MIR-loaded microparticles. (A) Scanning electron microscopic image of formulation 1 (F1) MIR-MPs, (B) Scanning electron microscopic image of formulation 2 (F2) MIR-MPs, (C) Scanning electron microscopic image of formulation 3 (F3) MIR-MPs, (D) Scanning electron microscopic image of formulation 4 (F4) MIR-MPs, (E) Microparticle size distribution histogram of F1 MIR-MPs, (F) Microparticle size distribution histogram of F2 MIR-MPs, (G) Microparticle size distribution histogram of F3 MIR-MPs, (H) Microparticle size distribution histogram of F4 MIR-MPs, (I) Average diameter of four formulations of MIR-MPs. Data were presented as means \pm s.e.m and analyzed using ANOVA. * $p < 0.05$.

4.1.2 Encapsulation efficiency and drug loading of MIR-loaded microparticles

The encapsulation efficiency and drug loading of all four formulations of MIR-MPs were measured and calculated following the equations mentioned in 3.10.2. The encapsulation efficiency and drug loading of PLGA microparticles are determined by several factors, including the concentration of PLGA, lactide to glycolide residue ratio (L/G ratio), molecular weight (MW), and end-group capping (Lagrec et al. 2020). Since only one type of PLGA polymer (Resomer RG 502H, 50:50 L/G ratio) was used to prepare MIR-MPs, the difference in encapsulation efficiency

between four formulations was primarily affected by additional three parameters: the initial amount of drug, the concentration of PLGA, and the amount of DMSO.

Figure 12A shows that both formulations F3 and F4 showed reduced encapsulation efficiency compared to the original formulation F1 ($25.5 \pm 0.7\%$ and $25.3 \pm 1.0\%$, respectively, compared to $31.2 \pm 1.3\%$ for F1). It suggests that the encapsulation efficiency decreased with decreasing PLGA concentration from 2% to 1.5%. Moreover, when the same concentration of PLGA was used to prepare MIR-MPs in F1 and F4, a lower initial amount of the drug resulted in a higher encapsulation efficiency, indicating that an increased amount of MIR could cause a decrease in encapsulation efficiency due to the capacity of PLGA.

To determine the drug loading of each formulation, MIR-MPs were dissolved in acetone, and PLGA was further precipitated in methanol to extract MIR from MIR-MPs. The drug loading of each formulation of MIR-MPs was then measured by HPLC. In Figure 12B, the drug loading of the F1 to F3 MIR-MPs ($5.5 \pm 0.2\%$, $5.4 \pm 0.1\%$, and $5.7 \pm 0.1\%$) showed no dependency on either DMSO or PLGA concentration. Compared to the other three formulations, F4 showed a spike in drug loading ($6.5 \pm 0.2\%$). Due to the addition of an excessive amount of MIR beyond the capacity of PLGA, the encapsulation efficiency decreased, but drug loading elevated. Considering the high drug loading, F4 of MIR-MPs was chosen for further experiments. These data indicate that a reduction in the amount of PLGA or an increase in MIR impacts the encapsulation efficiency and the drug loading of MIR-MPs.

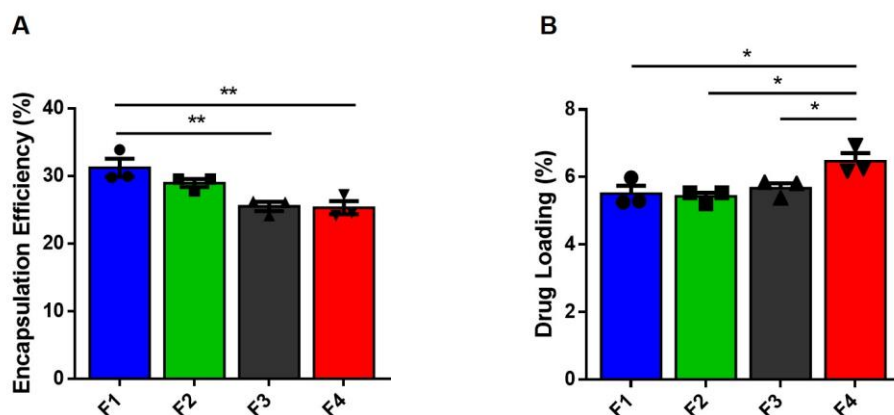


Figure 12. Encapsulation efficiency and Drug loading of four formulations of MIR-loaded PLGA microparticles. (A) Encapsulation efficiency of four formulations of MIR-MPs ($n = 3$). (B) Drug loading of four formulations of MIR-MPs ($n = 3$). Data were presented as means \pm s.e.m and were analyzed using ANOVA. * $p < 0.05$, ** $p < 0.01$.

4.1.3 *In vitro* release profile of MIR-loaded microparticles

MIR was released *in vitro* from MIR-MPs in PBS buffer (pH 7.4) at 37°C under constant shaking. Using the F4 of MIR-MPs and control microparticles (Ctrl-MPs), a 15-day *in vitro* release profile was conducted. MIR-MPs and Ctrl-MPs differed only in MIR loading. Figure 13A shows that the kinetic release profile of MIR-MPs contained an initial burst release and a sustained release. The initial release exhibited 10.9%, 20.8%, and 48.2% of MIR release over the first 1h, 5h, and 12h. The kinetic release profile of MIR revealed a release of 80% in the first 3 days followed by a sustained release till day 15. As of day 15, a total of 93% to 100% of loaded MIR were released. In contrast, pure MIR dissolved in the buffer within 5 hours, indicating PLGA microparticles effectively controlled MIR release. Ctrl-MPs with no MIR loaded served as a negative control, and no release of MIR was detected (Figure 13B). The *in vitro* release profile of MIR-MPs can be used as a reference for the concentration of MIR reached in an aqueous medium after a certain period.

The morphology of PLGA microparticles during the release in PBS was further checked (Figure 14). SEM images showed that the initial spherical morphology of Ctrl-MPs and MIR-MPs became swollen and porous after 9 days of release in PBS (Figures 14B and E). PLGA is a degradable biopolymer that degrades in bulk erosion where water permeates into the matrix and forms pores (Varde and Pack 2004; Y. Li et al. 2021). After 15 days of release, the initial spherical shape of Ctrl-MPs and MIR-MPs cannot remain. Instead, a collapsed and shapeless structure of the polymer was observed in both Ctrl-MPs and MIR-MPs (Figures 14C and F). These data confirm that MIR release from MIR-MPs in PBS is correlated with the degradation of PLGA microparticles.

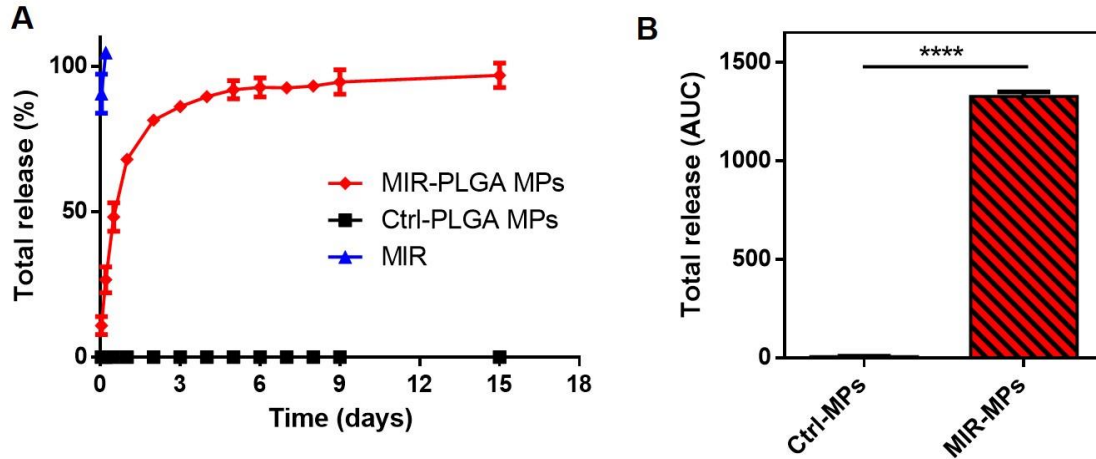


Figure 13. *In vitro* release profiles of MIR-loaded PLGA microparticles. (A) *In vitro* release profiles of MIR-MPs and Ctrl-MPs after 15 days of release ($n = 3$), (B) AUC of MIR release from PLGA microparticles after 15 days of *in vitro* release ($n = 3$). Data were presented as means \pm s.e.m and were analyzed using a t-test. **** $p < 0.0001$.

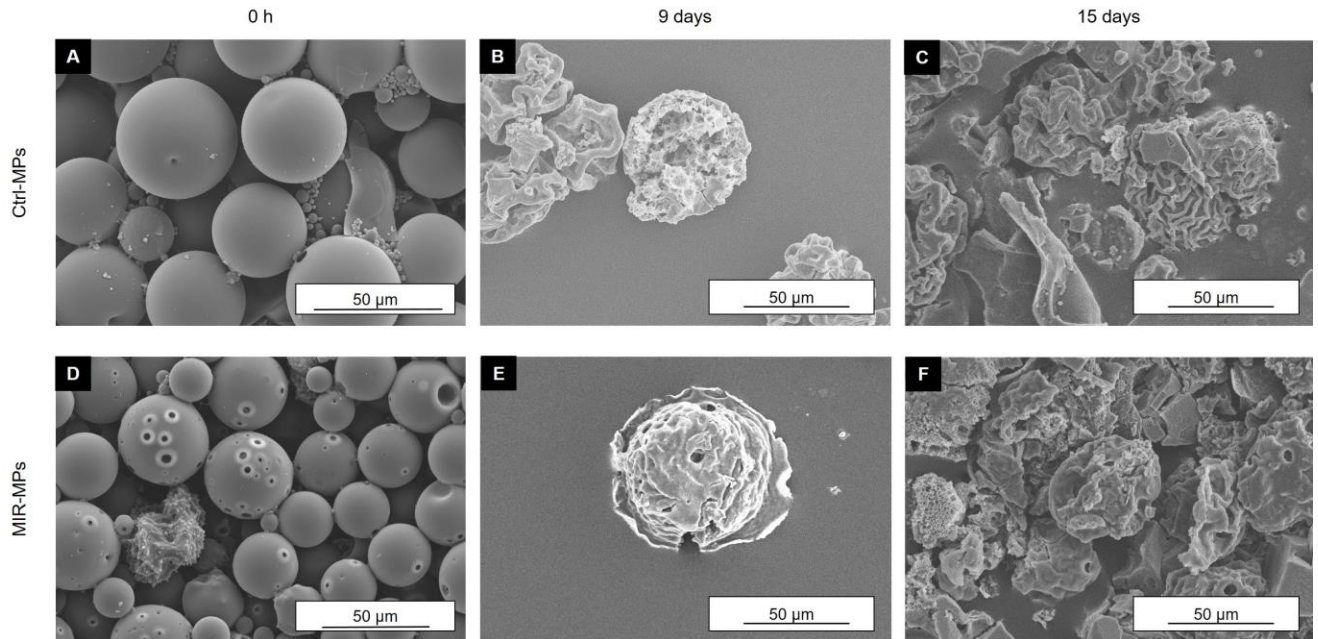


Figure 14. Morphological images of MIR-loaded microparticles after release. (A) Scanning electron microscopic image of Control microparticles (Ctrl-MPs) before release, (B) Scanning electron microscopic image of Ctrl-MPs after 9 days of release, (C) Scanning electron microscopic image of Ctrl-MPs after 15 days of release, (D) Scanning electron microscopic image of MIR-loaded microparticles (MIR-MPs) before release, (E) Scanning electron microscopic image of MIR-MPs after 9 days of release, (F) Scanning electron microscopic image of MIR-MPs after 15 days of release. $n = 3$.

4.1.4 Stability of MIR-loaded microparticles

The morphology of both Ctrl-MPs and MIR-MPs was examined eight months after preparation to explore whether microparticles can retain their original morphology after a longer period of storage. SEM images showed that the morphology of freshly prepared Ctrl-MPs and MIR-MPs (Figures 15A and B) did not alter after 8 months of storage (Figures 15C and D). Neither structural collapses nor abnormalities were observed in SEM images. Accordingly, PLGA-based microparticles can be stored in a dry environment for at least 8 months.

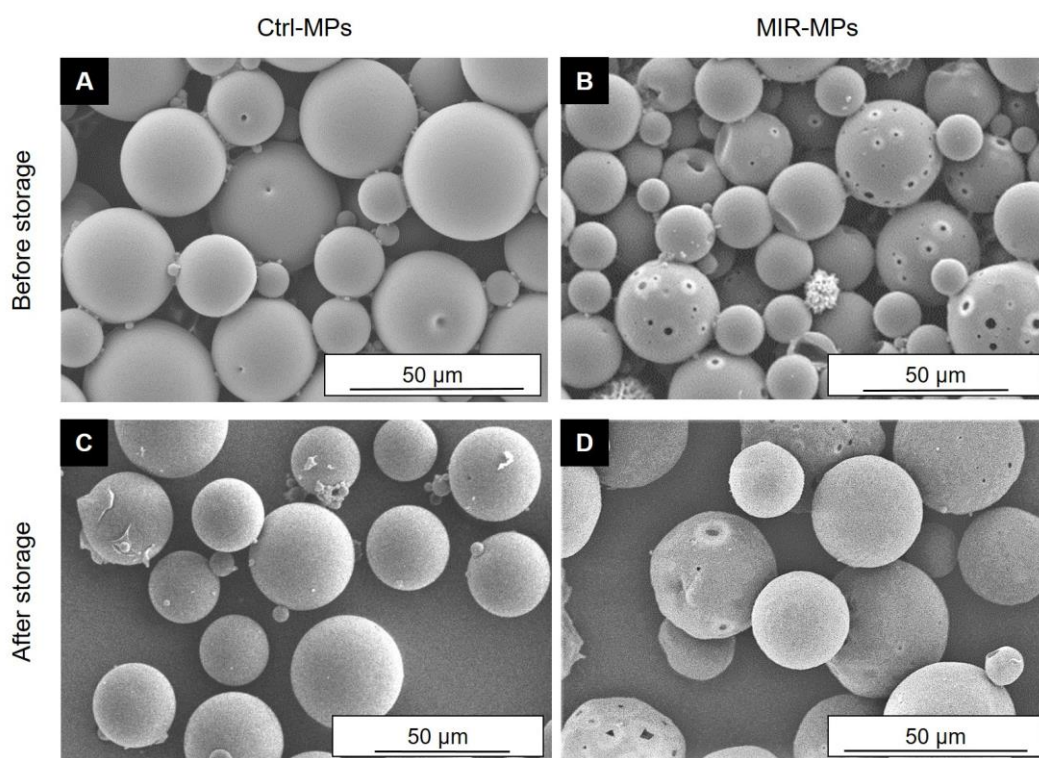


Figure 15. Scanning electron microscopic pictures of microparticles before and after 8 months of storage. (A) Scanning electron microscopic image of freshly prepared Ctrl-MPs, (B) Scanning electron microscopic image of freshly prepared MIR-MPs, (C) Scanning electron microscopic image of Ctrl-MPs after 8 months of storage, (D) Scanning electron microscopic image of MIR-MPs after 8 months of storage. $n = 3$.

4.2 Effects of MIR-loaded microparticles on adipocytes

4.2.1 *In vitro* lipolysis induced by MIR-loaded microparticles

The activation of BA is primarily stimulated by the SNS that secretes NE resulting in an increased level of intracellular cAMP via ADRB3 signaling. (Cannon and Nedergaard 2004; Zhao et al. 1994). By activating PKA, cAMP further stimulates BA cytosolic lipid droplet lipolysis, which provides FFA for BA to generate heat (Honnor, Dhillon, and Londos 1985). To verify the effects of MIR-MPs on BA, BA were treated with MIR-MPs for 3h and glycerol release was analyzed after treatment. According to Figure 16A, treatment with MIR upregulated glycerol release in BA compared to the non-treated group (1.9 ± 0.2 -fold). Importantly, BA treated with MIR-MPs showed a significantly higher level of glycerol release (1.6 ± 0.1 -fold) than the group treated with Ctrl-MPs. The group treated with Ctrl-MPs showed no difference in glycerol release compared to the non-treated group.

To further investigate the effect of MIR and MIR-MPs on iWA, iWA were given the same treatment. As shown in Figure 16B, glycerol release level increased 3.1 ± 0.4 -fold in the MIR-treated group. Notably, iWA treated with MIR-MPs showed a significant increase in lipolysis (4.4 ± 1.0 -fold) compared to iWA treated with Ctrl-MPs. Importantly, Ctrl-MPs did not alter the lipolysis level in iWA compared to the non-treated group. These data indicate that treatments with MIR and MIR-MPs could induce a pronounced effect of lipolysis on both iWA and BA.

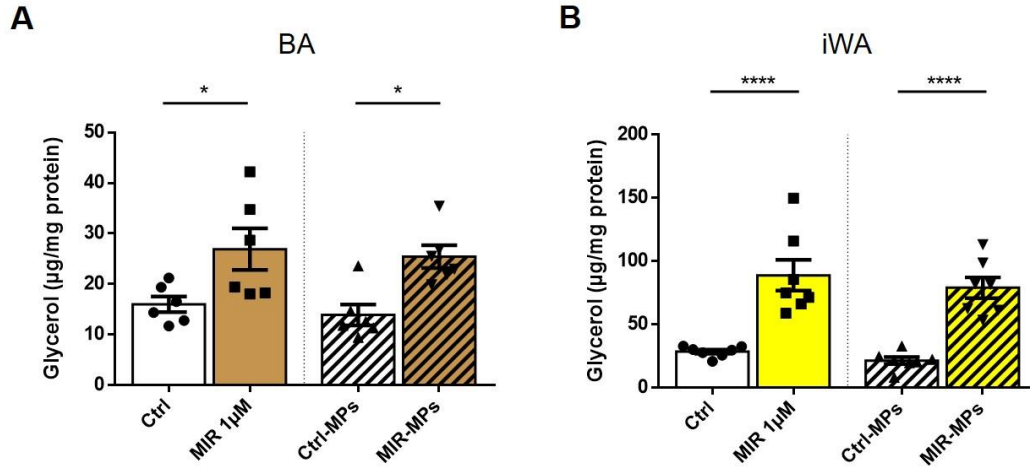


Figure 16. Lipolysis of adipocytes after treatments. (A) Lipolysis of BA treated with Ctrl-MPs, MIR-MPs, and MIR for 3 hours ($n = 6$), (B) Lipolysis of iWA treated with Ctrl-MPs, MIR-MPs, and MIR for 3 hours ($n = 7$). Data were presented as means \pm s.e.m and were analyzed using ANOVA. * $p < 0.05$, **** $p < 0.0001$.

4.2.2 MIR-loaded microparticles induced BA thermogenesis

To validate the effect of MIR-MPs on BA thermogenesis, the expression of the thermogenic marker (*Ucp1*) and two adipogenic markers (*Ppar γ* and *Fabp4*) were analyzed after 3-hour treatments with MIR and MIR-MPs. As shown in Figure 17A, both treatments with MIR and MIR-MPs induced an increased level of *Ucp1* expression in BA by 23.7 ± 3.2 -fold and 31.9 ± 9.9 -fold, respectively, compared to the respective control group. Figure 17B shows that the increase was not only observed in mRNA expression levels but also UCP1 protein levels. The group treated with MIR showed an upregulation of UCP1 protein level (6.1 ± 2.0 -fold), while BA treated with MIR-MPs exhibited a 4.7 ± 0.7 -fold increase in UCP1 protein level. These results suggest that treatment with MIR-MPs can effectively stimulate BA activation. The adipogenic markers, *Ppar γ* and *Fabp4*, were not statistically significant changes in both the MIR-treated group and the MIR-MPs-treated group.

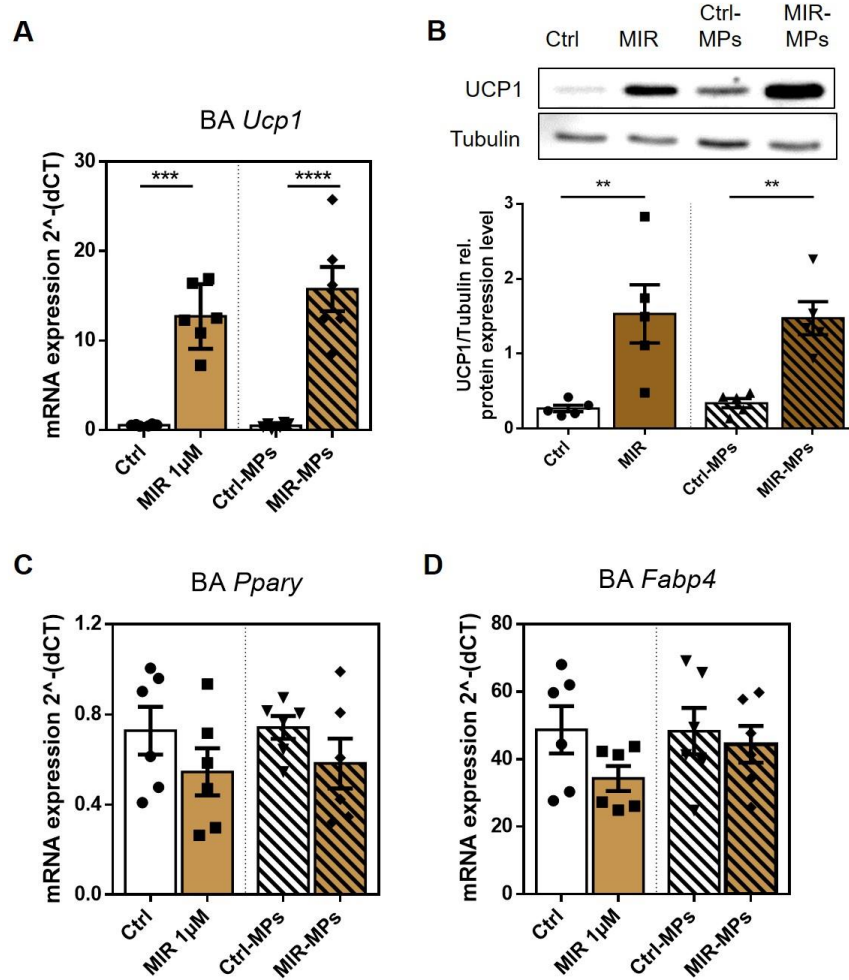


Figure 17. Gene expression of *Ucp1*, *Pparγ*, and *Fabp4* in BA after treatments. (A) *Ucp1* expression in BA after 3-hour treatments with Ctrl-MPs, MIR-MPs, and MIR ($n = 6$), (B) UCP1 protein expression immunoblots after 1-day treatments ($n = 5$), (C) *Pparγ* expression in BA after 3-hour treatments with Ctrl-MPs, MIR-MPs, and MIR ($n = 6$), (D) *Fabp4* expression in BA after 3-hour treatments with Ctrl-MPs, MIR-MPs, or MIR ($n = 6$). Data were presented as means \pm s.e.m and analyzed using ANOVA. *** $p < 0.001$, **** $p < 0.0001$.

4.2.3 MIR-loaded microparticles induced iWA beiging and morphological changes

One origin of beige adipocytes has been suggested to be the trans-differentiation of WA into beige adipocytes via cold exposure or treatment with ADRB3 agonists (Barbatelli et al. 2010; Rosenwald et al. 2013). To investigate the effect of MIR-MPs on iWA beiging, the expression of beiging-related genes (*Ucp1*, *Ppargc1α*, *Dio2*, *Cidea*, and *Prdm16*) was analyzed (Ferrannini et al. 2016). As shown in Figure 18A, *Ucp1*, the most important browning marker, was upregulated significantly in the MIR-treated iWA (50.8 ± 14.0 -fold) compared to the non-treated group. Importantly, the

Ucp1 expression exhibited a more pronounced increase in iWA after treatment with MIR-MPs (17.0 ± 9.4 -fold) than the group treated with Ctrl-MPs. Treatment with Ctrl-MPs did not change the expression of *Ucp1* in iWA as compared to the non-treated group. Similarly, treatment with MIR and MIR-MPs also induced an upregulation of UCP1 protein level in iWA. As shown in Figure 18B, UCP1 protein levels increased by 1.8 ± 0.1 -fold and 2.4 ± 0.3 -fold in iWA treated with MIR and MIR-MPs, respectively. Additionally, MIR-MPs upregulated not only the expression of *Ucp1* but also the expressions of *Ppargc1a* and *Dio2* (Figures 18C and D). The mean expression of *Cidea* and *Prdm16* in the MIR-MPs treated group also increased (1.6 ± 0.6 -fold and 1.8 ± 0.3 -fold respectively) compared to the Ctrl-MPs treated group, albeit not significantly (Figures 18E and F). These data indicate that treatment of MIR-MPs can induce beiging in iWA.

Furthermore, iWA treated with MIR-MPs exhibited less intensity of Oil Red O staining than the Ctrl-MPs treated group, indicating that treatment with MIR-MPs decreased the lipid content in iWA (Figure 18G). By comparing the morphology of iWA treated with MIR-MPs and Ctrl-MPs, a reduction in the size of lipid droplets was observed in iWA treated with MIR-MPs by 0.8 ± 0.1 -fold, while iWA treated with Ctrl-MPs showed no change in the size of lipid droplets (Figures 18H and I). Altogether, these results suggest that treatment with MIR-MPs can effectively induce the beiging of iWA and decrease lipid content in iWA.

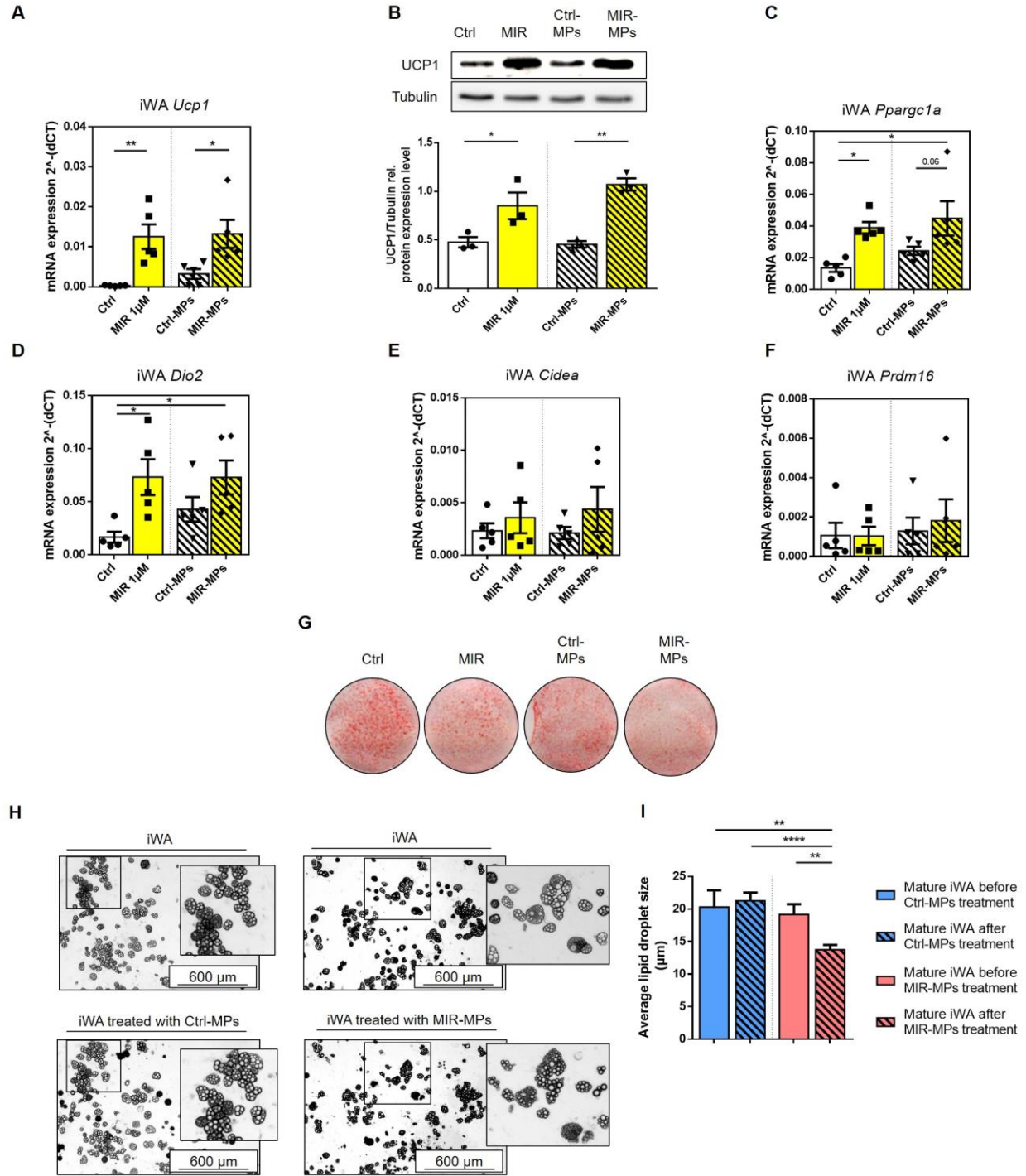


Figure 18. Changes in iWA after treatments. (A) *Ucp1* expression in iWA after 3-hour treatments with Ctrl-MPs, MIR-MPs, and MIR ($n = 6$), (B) UCP1 protein expression immunoblots after 1-day treatments Ctrl-MPs, MIR-MPs, and MIR ($n = 3$), (C) *Pparg1a* expression in iWA after 3-hour treatments ($n = 6$), (D) *Dio2* expression in iWA after 3-hour treatments ($n = 6$), (E) *Cidea* expression in iWA after 3-hour treatments ($n = 6$), (F) *Prdm16* expression in iWA after 3-hour treatments ($n = 6$), (G) Oil Red-O stain of iWA after 1-day treatments with Ctrl-MPs, MIR-MPs, and MIR ($n = 3$), (H) Representative microscope pictures of the morphology of iWA before and after 1-day treatments with Ctrl-MPs and MIR-MPs ($n = 3$), (I) Average lipid droplet size of iWA before and after treatments. Data were presented as means \pm s.e.m and analyzed using ANOVA or a t-test. * $p < 0.05$, ** $p < 0.01$, **** $p < 0.0001$.

4.2.4 Mitochondrial stress assay on adipocytes

In cellular respiration, oxygen consumption is coupled with ATP synthesis during oxidative phosphorylation, which is used to evaluate cellular metabolism (Divakaruni et al. 2014). As it is demonstrated above in 4.2.3, treatments with MIR and MIR-MPs can significantly upregulate the expression of beiging and thermogenic markers and induce *in vitro* lipolysis in iWA. To further verify the effects of MIR and MIR-MPs on mitochondrial respiration in iWA, the OCR of iWA was measured by the Seahorse XF24 Analyzer. The OCR of iWA was upregulated following treatment with MIR and MIR-MPs, whereas the Ctrl-MPs treated group exhibited no difference in OCR compared to the non-treated group (Figure 19A). The basal respiration was significantly upregulated in the MIR-treated group by 3.1 ± 1.1 -fold, and the mean of basal respiration increased in the MIR-MPs treated group (2.2 ± 0.5 -fold) compared to the Ctrl-MPs treated group (Figure 19B). This indicates that the respiration required for endogenous ATP demand in MIR-treated iWA was upregulated (Divakaruni et al. 2014). The FCCP-stimulated maximal respiratory capacity is characterized as an indicator of mitochondrial function (Brand and Nicholls 2011). Notably, treatments with MIR and MIR-MPs increased the maximal respiration (following FCCP treatment) significantly in iWA by 3.7 ± 1.8 -fold and 1.5 ± 0.3 -fold, respectively (Figure 19C). Additionally, iWA treated with MIR-MPs exhibited an increasing mean of ATP production (1.8 ± 0.4 -fold) and proton leakage (3.0 ± 1.1 -fold), but not statistically significant (Figures 19D to F). These data suggest that treatment with MIR and MIR-MPs can effectively upregulate oxygen consumption and maximal respiration in iWA.

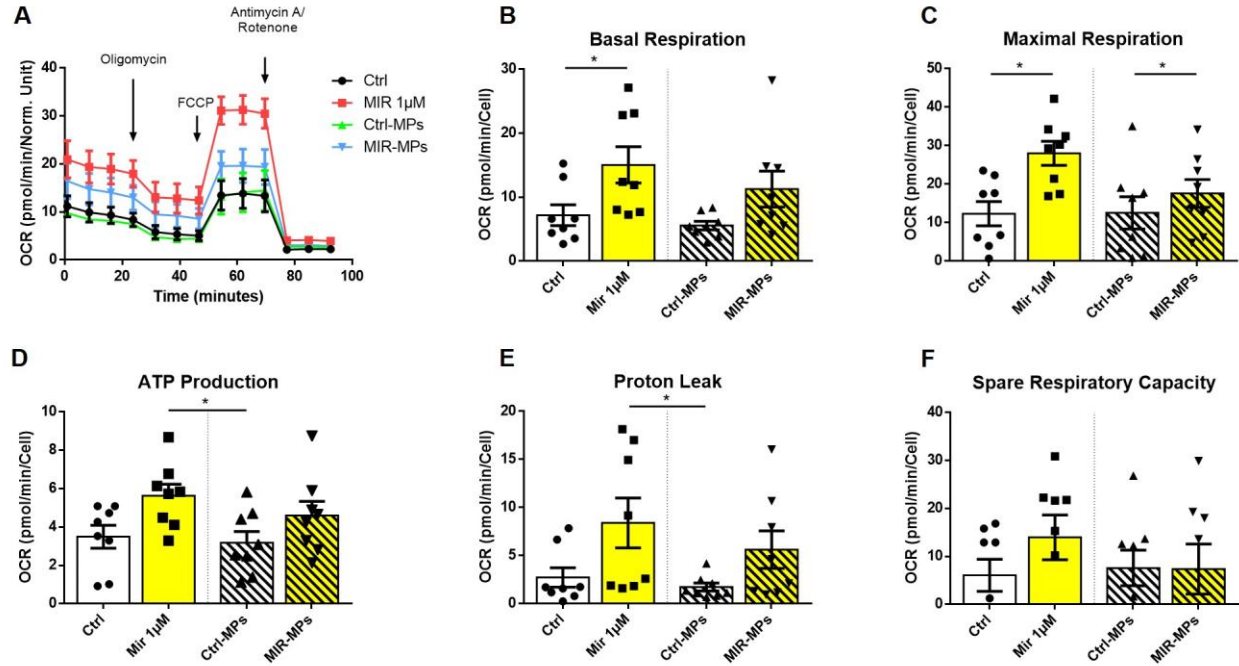


Figure 19. MIR-loaded microparticles induced effects on mitochondrial respiration of iWA. (A) Mitochondrial profile (Normalized OCR) after 3-hour treatments with Ctrl-MPs, MIR-MPs, and MIR, (B) Basal Respiration, (C) Maximal Respiration, (D) ATP Production, (E) Proton Leak, (F) Spare Respiratory Capacity. $n = 4$. The mitochondrial profile was normalized to the cell number of each well. Data were presented as means \pm s.e.m and analyzed using ANOVA. * $p < 0.05$, ** $p < 0.01$.

4.3 Toxicity tests of MIR-loaded microparticles on adipocytes

MTT assay was conducted to investigate whether MIR-MPs cause cytotoxicity in murine adipocytes, including pre-BA, BA, inguinal white pre-adipocytes (pre-iWA), and iWA. A nonionic surfactant, Triton X100 (v/v 2%), was used as a negative control to induce significant cytotoxicity by lysing cells (Koley and Bard 2010). Figure 20 illustrates that Ctrl-MPs did not induce a decrease in adipocyte viability compared to the non-treated group. Moreover, MIR, at the concentration of 1 μ M and 10 μ M, did not alter the viability in adipocytes except for BA (Figures 20A, C, and D). Interestingly, as compared to the controls, the viability of BA decreased by 0.9 ± 0.1 -fold and 0.8 ± 0.1 -fold following treatments with MIR and MIR-MPs, respectively (Figure 20B). Moreover, a higher MTT optical density (OD) value was observed in BA than in other adipocytes, indicating that BA has a higher basal metabolic activity than other adipocytes (pre-BA, pre-iWA, and iWA). It has been reported that the reduction of tetrazolium dye is dependent on nicotinamide adenine dinucleotide phosphate (NADPH) enzymes, suggesting that the MTT assay is highly dependent on cellular metabolic activity (Berridge, Herst, and Tan 2005). Therefore, to verify that the

decrease of MTT OD value in BA was not caused by treatment with MIR and MIR-MPs, ATP assay was additionally performed.

The ATP assay was based on the detection of ATP by the luciferin-luciferase reaction (Andreotti et al. 1995). In the ATP assay, the same treatments were given to adipocytes as in the MTT assay. Cells treated with Triton X100 (v/v 2%) served as a negative control. As shown in Figure 21B, the ATP assay revealed that the cell viability of MIR-treated BA did not reduce compared to the non-treated group. Moreover, BA treated with MIR-MPs showed no significant differences in cell viability (Figure 21B). Treatment with MIR and MIR-MPs did not alter the viability of pre-BA, pre-iWA, and iWA and exhibited a similar pattern to the MTT assay (Figures 21A, C, and D). Taken together, these data indicate that treatment with MIR, Ctrl-MPs, and MIR-MPs did not lead to toxicity in adipocytes.

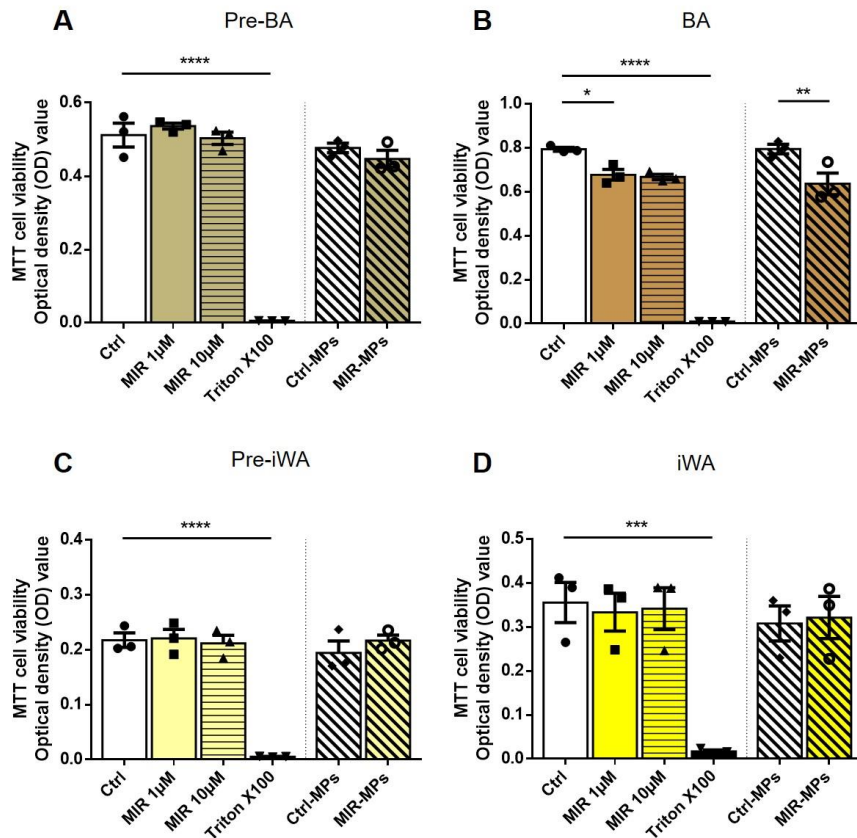


Figure 20. MTT assay for adipocytes after treatments. (A) MTT assay for pre-BA after 1-day treatments with Ctrl-MPs, MIR-MPs, MIR, and Triton X100, (B) MTT assay for BA after 1-day treatments, (C) MTT assay for pre-iWA after 1-day treatments, (D) MTT assay for iWA after 1-day treatments. $n = 3$. Data were presented as means \pm s.e.m and analyzed using ANOVA. * $p < 0.05$, ** $p < 0.01$, **** $p < 0.0001$.

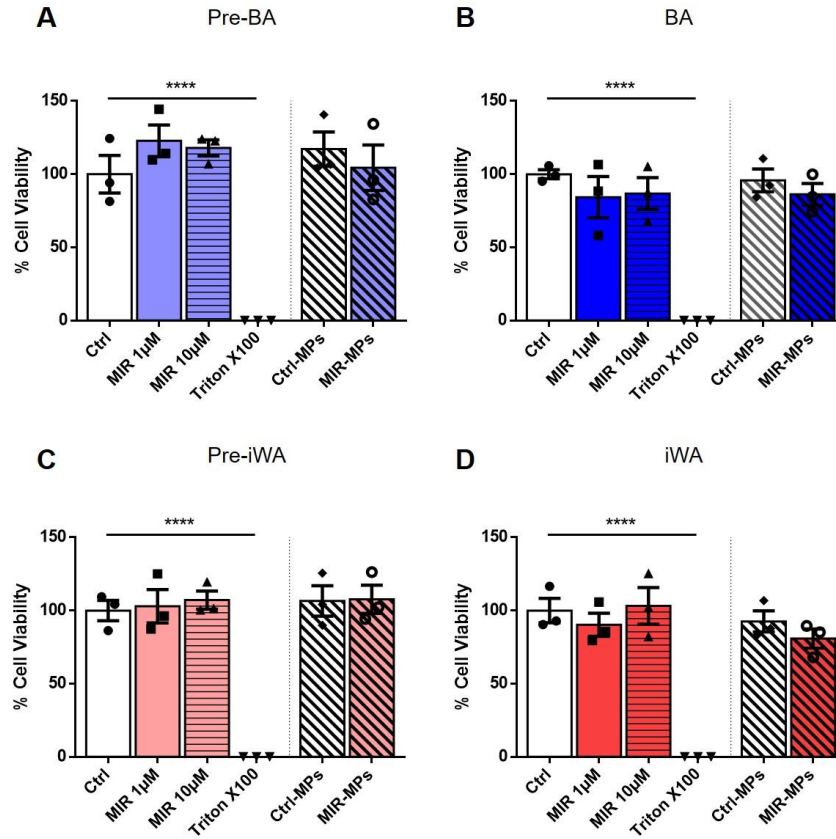


Figure 21. ATP assay for adipocytes after treatments. (A) ATP assay for pre-BA after 1-day treatments with Ctrl-MPs, MIR-MPs, MIR, and Triton X100 ($n = 3$), (B) ATP assay for BA after 1-day treatments, (C) ATP assay for pre-iWA after 1-day treatments, (D) ATP for iWA after 1-day treatments. $n = 3$. Data were presented as means \pm s.e.m and analyzed using ANOVA. **** $p < 0.0001$.

4.4 *Ex vivo* lipolysis induced by MIR-loaded microparticles

Treatment with MIR-MPs can effectively induce lipolysis in adipocytes. To investigate the *ex vivo* lipolytic effects of MIR-MPs on murine AT, murine BAT, iWAT, and gWAT were included. AT were freshly isolated from 8-week-old WT mice, and the *ex vivo* lipolysis assay was performed subsequently. The weight of each piece of AT was recorded for normalization. The explanted AT was incubated with MIR-MPs in the lipolysis medium for 3h. As shown in Figure 22, treatment with MIR and MIR-MPs can lead to an upregulation of glycerol release in all types of AT. The BAT generally exhibited a higher level of glycerol release than iWAT and gWAT (Figure 22). Despite the high lipolysis level of BAT, treatment with MIR-MPs can further increase glycerol release in BAT compared to the Ctrl-MPs treated group (1.3 ± 0.1 -fold) (Figure 22A). Notably, the upregulation of lipolysis induced by treatment with MIR and MIR-MPs showed a higher fold change in iWAT and gWAT, and the glycerol release did not change following treatment with Ctrl-

MPs (Figures 22B and C). As shown in Figure 22B, treatment with MIR and MIR-MPs considerably increased the lipolysis level in iWAT by 4.1 ± 0.7 -fold and 2.5 ± 0.3 -fold, respectively, as compared to the control groups. In gWAT, the mean of glycerol release in the non-treated group and the Ctrl-MPs treated group was lower than in iWAT. The fold changes of lipolysis induced by MIR and MIR-MPs were 6.6 ± 1.1 -fold and 5.8 ± 1.8 -fold, respectively (Figure 22C). These data indicate that treatment with MIR and MIR-MPs can strongly upregulate lipolysis levels in BAT, iWAT, and gWAT.

To further verify the increased lipolysis in iWAT treated with MIR and MIR-MPs was mediated via ADRB3 rather than other β -adrenergic receptors, a selective ADRB1 antagonist CGP 20712A (CGP, concentration: 100 nM) and a selective ADRB2 antagonist ICI 118,551 (ICI, concentration: 50 nM) were applied (Kannabiran et al. 2020). Figure 22D shows that treatment with ICI and CGP individually or together did not attenuate the glycerol release in iWAT induced by MIR and MIR-MPs, suggesting that treatment with MIR and MIR-MPs increased lipolysis in iWAT via ADRB3.

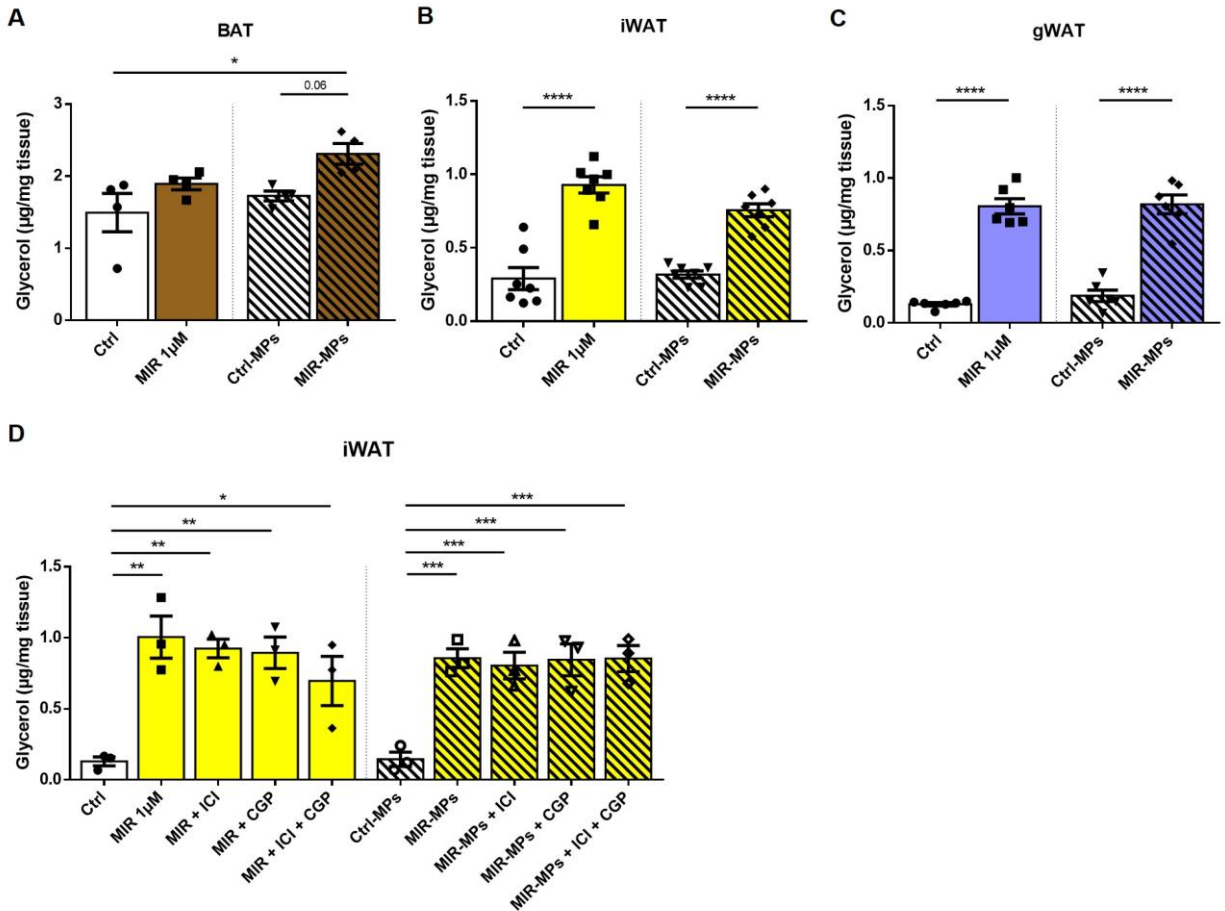


Figure 22. Lipolysis of adipose tissue after treatments. (A) Lipolysis of BAT after 3-hour treatments with Ctrl-MPs, MIR-MPs, and MIR ($n = 4$), (B) Lipolysis of iWAT after 3-hour treatments ($n = 7$), (C) Lipolysis of gWAT after 3-hour

treatments ($n = 6$), (D) Lipolysis of iWAT after 3-hour treatments with Ctrl-MPs, MIR-MPs, MIR (1 μM), ICI (50 nM), and CGP (100 nM) ($n = 3$). Data were presented as means \pm s.e.m and analyzed using ANOVA. * $p < 0.05$, ** $p < 0.01$, *** $p < 0.001$, **** $p < 0.0001$.

Next, to evaluate whether MIR-MPs can release MIR inside WAT and induce lipolysis, MIR-MPs were injected into iWAT and gWAT, and *ex vivo* lipolysis was subsequently performed. MIR-MPs were suspended in PBS (pH 7.4) and injected directly into WAT. As shown in Figure 23A, each sample of WAT was injected with 50 μl of PBS containing the same amount of microparticles. In every single injection of MIR-MPs, MIR can reach a concentration of 50 μM , as MIR was completely released from the microparticles. Following injection, PBS diffused out of the tissue, but the MIR-MPs remained inside of AT and release MIR (Figure 23A). Figure 23B and C show that the lipolysis of control groups in iWAT and gWAT both remained at a low level after 3 hours of incubation. Interestingly, 3-hour treatment with MIR-MPs via direct injection elicited an increase of lipolysis in both iWAT and gWAT (Figure 23), which was consistent with the increased level of lipolysis in WAT that co-cultured with MIR-MPs (Figure 22). These results suggest that MIR can release from MIR-MPs in AT following direct injection and induce lipolysis in iWAT and gWAT.

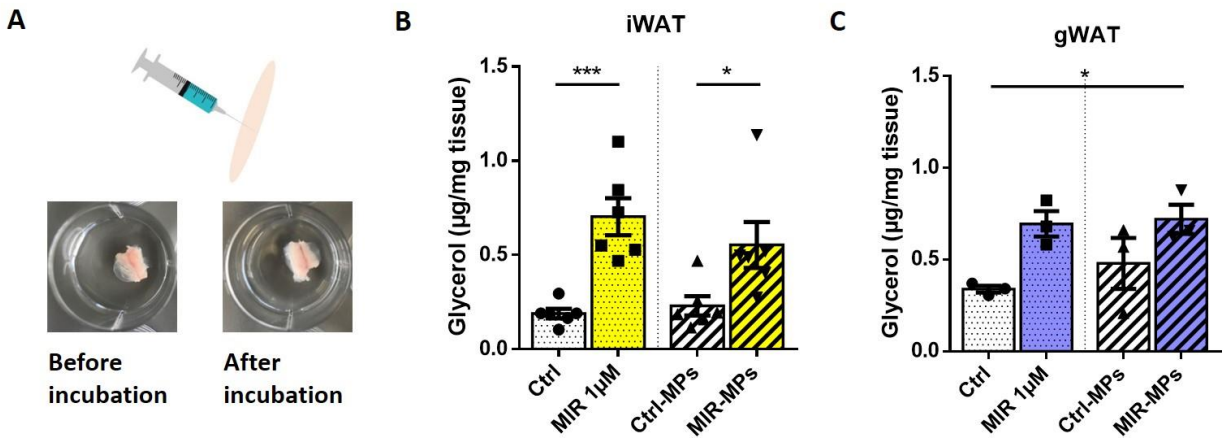


Figure 23. Lipolysis of white adipose tissue after treatments via direct injection. (A) iWAT treated with MIR-MPs via direct injection, (B) Lipolysis of iWAT after 3-hour treatments with Ctrl-MPs, MIR-MPs, and MIR via direct injection ($n = 6$), (C) Lipolysis of gWAT after 3-hour treatments via direction injection ($n = 3$). Data were presented as means \pm s.e.m and analyzed using ANOVA. * $p < 0.05$; *** $p < 0.0005$.

As illustrated in 4.1.5, MIR-MPs can release sustainably MIR in the aqueous medium for 2 weeks. Prolonging the incubation of *ex vivo* lipolysis allows more MIR to release from MIR-MPs and achieve a higher concentration of MIR in the medium, which might result in a higher lipolysis level in WAT. To evaluate whether prolonged incubation or a higher concentration of MIR further facilitates *ex vivo* lipolysis in WAT, the prolonged *ex vivo* lipolysis (6 hours of incubation) was

compared to the normal *ex vivo* lipolysis with 3-hour incubation. As shown in Figure 24A, glycerol release of iWAT in control groups did not change by prolonging incubation from 3 hours to 6 hours. Notably, iWAT treated with MIR and MIR-MPs with 6 hours of incubation showed a significant increase in glycerol release by 5.4 ± 1.6 -fold and 4.7 ± 1.0 -fold respectively compared to the control groups. The fold change of glycerol release was higher than the normal *ex vivo* lipolysis (4.4 ± 0.6 -fold and 4.0 ± 0.7 -fold, respectively). However, prolonged treatment with MIR-MPs did not exhibit a further increase in lipolysis compared to the group treated with MIR at a concentration of $1 \mu\text{M}$ (Figure 24A). Similar results were also observed in gWAT (Figure 24B). These data illustrate that prolonged incubation, rather than a higher concentration of MIR, can lead to a further increase in *ex vivo* lipolysis of iWAT and gWAT after treatment with MIR and MIR-MPs.

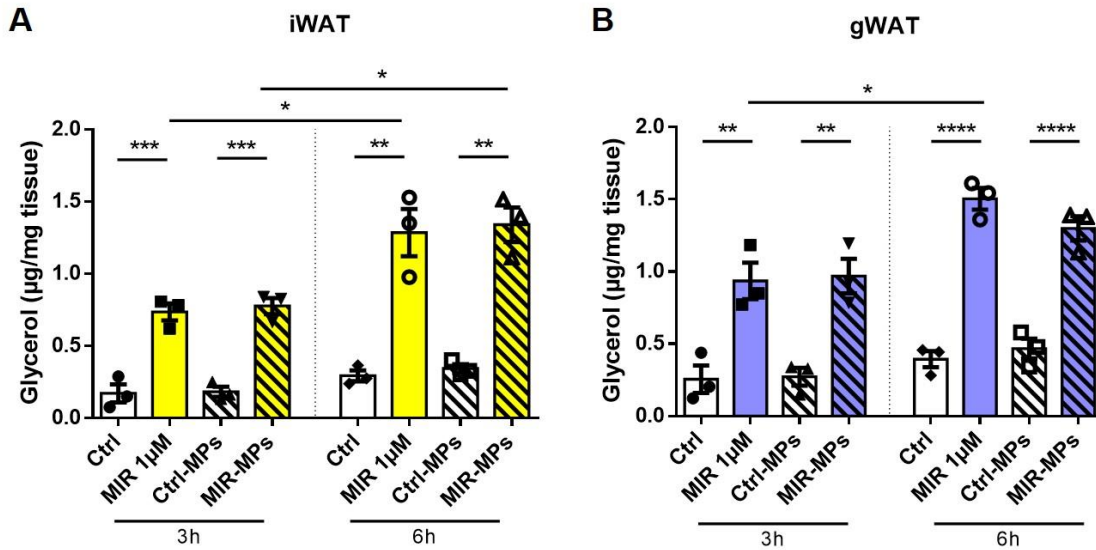


Figure 24. Prolonged lipolysis of white adipose tissue after treatments. (A) Prolonged lipolysis of iWAT after treatments with Ctrl-MPs, MIR-MPs, and MIR ($n = 3$), (B) Prolonged lipolysis of gWAT after treatments ($n = 3$). *Ex vivo* lipolysis data were presented as means \pm s.e.m. and were analyzed using ANOVA. * $p < 0.05$; ** $p < 0.005$; *** $p < 0.0005$; **** $p < 0.0001$.

Taken together, these results indicate:

1. MIR-MPs can induce lipolysis not only *in vitro* but also *ex vivo* via ADRB3 in explanted BAT, iWAT, and gWAT;
2. MIR-MPs released MIR inside of WAT after direct injection and increased *ex vivo* lipolysis levels in both iWAT and gWAT;
3. By prolonging the incubation time, *ex vivo* lipolysis levels can be further enhanced in iWAT and gWAT after treatment with MIR and MIR-MPs.

4.5 MIR-loaded microparticles induce lipolysis in human subcutaneous white adipose tissue

Considering the significant effects of MIR-MPs on upregulating lipolysis in murine adipocytes and AT, it is necessary to examine whether these effects of MIR-MPs can be transferred to human subcutaneous white adipose tissue (scWAT). Some previous studies have demonstrated that the expression pattern of β -adrenergic receptors is different in murine WAT and human WAT: murine WAT expresses mostly *ADRB3* whereas human WAT expresses *ADRB2* (Evans et al. 2019; S. Collins et al. 1994). The expression of *ADRB2* and *ADRB3* in human WA and human WAT were investigated in this thesis and compared with the expression of *Adrb2* and *Adrb3* in murine iWA and iWAT. Figures 25A to D show that the expression level of *Adrb2* and *Adrb3* in rodents was generally higher than in humans. *ADRB2* was expressed more dominantly than *ADRB3* in human WA, whereas the expression of *Adrb2* and *Adrb3* showed no significant difference in murine iWA (Figures 26A and B). Importantly, the expression of *ADRB3* was detected in both human scWAT and murine iWAT. In human scWAT, *ADRB2* was expressed at a higher level (36.9 ± 18.6 -fold) than *ADRB3*, while the expression of *Adrb3* in murine iWAT was 6.6 ± 0.9 -fold higher than *Adrb2* (Figures 25C and D).

Next, to investigate the effects of MIR and MIR-MPs on human scWAT, *ex vivo* lipolysis was conducted following treatment with MIR and MIR-MPs. As shown in Figure 25B, after 3 hours of incubation, the lipolysis level in the MIR-treated group and the MIR-MPs-treated group did not differ from the control groups. When prolonged the incubation from 3 hours to 24 hours, the glycerol release in the non-treated group and the Ctrl-MPs treated group did not change. Notably, the *ex vivo* lipolysis level in human scWAT treated with MIR and MIR-MPs was upregulated by 3.1 ± 0.8 -fold and 4.3 ± 1.3 -fold, respectively, compared to the control groups, suggesting that treatment with MIR and MIR-MPs can increase lipolysis in human scWAT after 1-day incubation (Figure 25F).

Additionally, Blondin et al. reported that *ADRB2* has an important role in human BA thermogenesis (Blondin et al. 2020). To verify that the increased lipolysis in human scWAT treated with MIR and MIR-MPs was mediated via *ADRB3* rather than via potential cross-talk via *ADRB2*, a selective *ADRB2* agonist, salbutamol (SAL, concentration 2 μ M), was used individually or together with ICI (concentration: 1 μ M). As shown in Figure 25G, treatment with SAL can effectively elevate the lipolysis level in human scWAT. Moreover, adding an *ADRB2* antagonist ICI reduced the mean of SAL-induced glycerol release by 0.7 ± 0.1 -fold. Notably, the addition of

ICI did not decrease the lipolysis level either in the MIR-treated group or in the MIR-MPs treated group (Figure 25H), suggesting that the increase of lipolysis in human scWAT treated with MIR and MIR-MPs was induced via ADRB3.

Summarizing the results from **4.4** and **4.5**, these data indicate that MIR-MPs elevated *ex vivo* lipolysis levels both in murine iWAT and human scWAT via ADRB3.

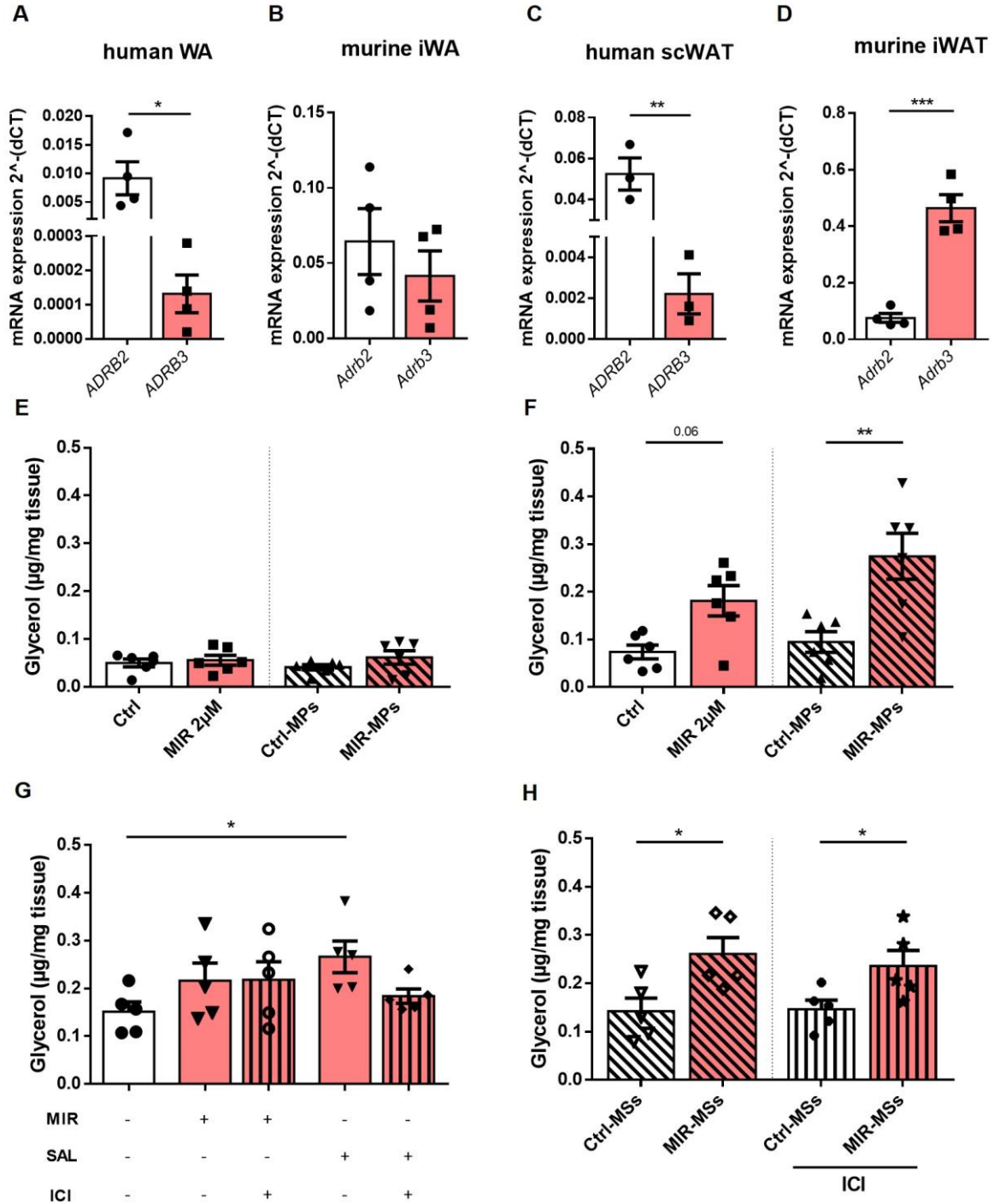


Figure 25. β -adrenergic receptor expression in human/murine WA and WAT and ex vivo lipolysis of human scWAT after treatments. (A) Gene expression of *ADRB2* and *ADRB3* in human WA ($n = 3$), (B) Gene expression of *Adrb2* and *Adrb3* in murine iWA ($n = 4$), (C) Gene expression of *ADRB2* and *ADRB3* in human scWAT ($n = 3$), (D) Gene expression of *Adrb2* and *Adrb3* in murine iWAT ($n = 4$), (E) Lipolysis of human scWAT after treatments with MIR (2 μ M), Ctrl-MPs, and MIR-MPs for 3 hours ($n = 3$), (F) Lipolysis of human scWAT after treatments with MIR (2 μ M), Ctrl-MPs, and MIR-MPs for 1 day ($n = 3$), (G) Lipolysis of human scWAT after treatments with MIR (2 μ M), SAL (2 μ M), and ICI (1 μ M) for 1 day ($n = 5$), (H) Lipolysis of human scWAT after treatments with Ctrl-MPs, and MIR-MPs, and ICI (1 μ M) for 1 day ($n = 5$). Data were presented as means \pm s.e.m and analyzed using a t-test or ANOVA. * $p < 0.05$, ** $p < 0.01$, *** $p < 0.001$.

4.6 *Ex vivo* lipolysis and gene expressions in explanted human subcutaneous white adipose tissue after direct injection of MIR-loaded microparticles

Subcutaneous WAT beneath rodent skin is separated by a striated muscle layer known as the panniculus carnosus. Unlike rodents, humans lack the panniculus carnosus, and human scWAT is located in the hypodermis, the innermost layer of human skin (Driskell et al. 2014). Moreover, Kohane et al. illustrated that local subcutaneous implantation might be the most suitable and potential clinical application for PLGA microparticles according to its characteristics (Kohane 2007). Due to these anatomical differences between human skin and rodent skin as well as the characteristics of PLGA microparticles, injecting MIR-MPs directly into human scWAT would be a feasible method to apply MIR-MPs in humans.

Therefore, MIR-MPs were suspended in PBS and directly injected into explanted human scWAT to further examine their effect on human scWAT. The *ex vivo* lipolysis level and expression of beiging markers were further analyzed. As shown in Figure 26A, treatment with MIR via direct injection significantly increased the lipolysis level in human scWAT compared to the control group (1.8 ± 0.3 -fold). Importantly, direct injection with MIR-MPs also significantly upregulated glycerol release by 1.9 ± 0.4 -fold, indicating that MIR can also release from MIR-MPs in human scWAT after direct injection and increase human scWAT lipolysis. Notably, Figure 26B shows that human scWAT treated with MIR-MPs via direct injection exhibited a significant upregulation of *UCP1* expression (2.7 ± 0.4 -fold). The mean expression of *CIDEA*, *PPARGC1 α* , *DIO2*, *TMEM26*, and *PRDM16* was higher after the treatment with MIR-MPs than those groups treated with Ctrl-MPs, albeit not significantly (Figure 26C to G). These results suggest that direct injection of MIR-MPs can upregulate human scWAT lipolysis and induce the expression of beiging markers.

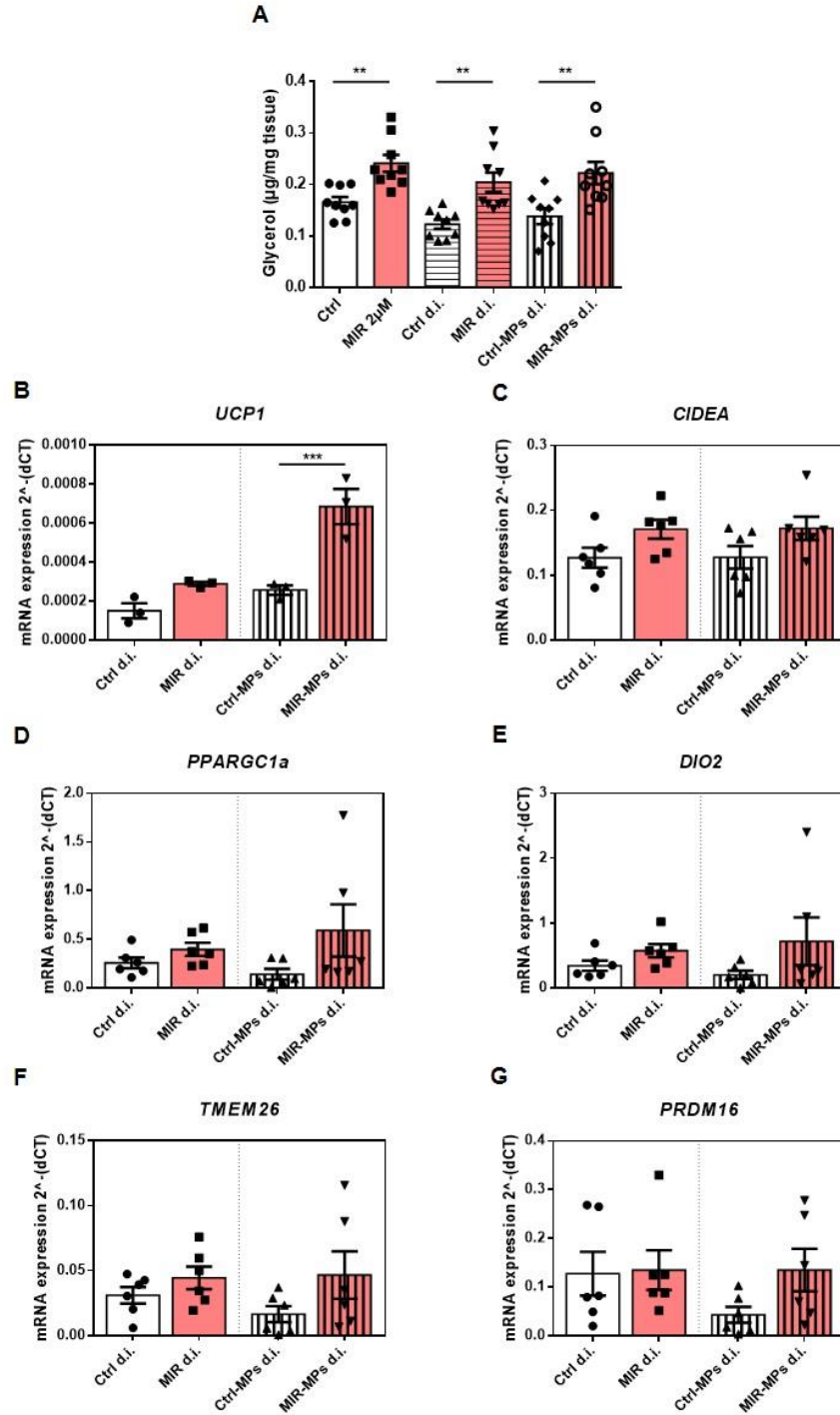


Figure 26. Ex vivo lipolysis and gene expressions in human scWAT after treatment with MIR-MPs via direct injection. (A) human scWAT lipolysis after 1-day treatments via direct injections. ($n = 3$), (B) *UCP1* expression in human scWAT after 1-day treatments with Ctrl-MPs, MIR-MPs, and MIR via direct injections ($n = 3$), (C) *CIDEA* expression in human scWAT after 1-day treatments via direct injections ($n = 4$), (D) *PPARGC1 α* expression in human scWAT after 1-day treatments via direct injections ($n = 4$), (E) *DIO2* expression in human scWAT after 1-day treatments via direct injections ($n = 4$), (F) *TMEM26* expression in human scWAT after 1-day treatments via direct injections ($n = 4$), (G) *PRDM16* expression in human scWAT after 1-day treatments via direct injections ($n = 4$). The data were presented as means \pm s.e.m and analyzed using ANOVA. ** $p < 0.01$, *** $p < 0.001$. d.i: direct injection.

5 Results of Project II: API-loaded TRLs

5.1 Characterization of API-loaded TRLs

Two different drugs were used in this study to prepare API-loaded TRLs: T3-loaded TRLs (T3-TRLs) and FR-loaded TRLs (FR-TRLs). Figure 27A illustrates a basic structure of API-loaded TRLs: a monolayer of phospholipids surrounds a lipid core encasing T3 or FR molecules, TG, and cholesterol. The particle size, polydispersity index (PDI), and zeta potential of the formulated TRLs diluted 1:100 in PBS were measured by dynamic light scattering (DLS) at an angle of light incidence of 90° using ZetaSizer 90S (Malvern Panalytical, Malvern, UK). Electrophoretic mobility was determined using laser Doppler Velocimetry. According to the electrophoretic mobility, the zeta potential was calculated using the Smoluchowski equation (Sze et al. 2003). The encapsulation efficiency of each formulation was measured and calculated as mentioned previously in 3.12.1.

As shown in Table 4, two formulations of T3-TRLs and one formulation of FR-TRLs were prepared. Formulation 1 was the initial formulation for T3 TRLs, which was prepared with 1 mg cholesterol, 1 mg phosphatidylcholine, 16 mg TG, and 8.3 µg T3. Formulation 2 of T3-TRLs was additionally prepared with the same weight ratio of cholesterol, phosphatidylcholine, and TG, but a reduced ratio of T3. Formulations 3 and 4 were Vehicle-TRLs, which differed only in T3 loading from formulations 1 and 2. FR-TRLs (formulation 5) were prepared using the same weight ratio of cholesterol, phosphatidylcholine, and TG, but an increased amount of FR. The diameter of TRLs in formulations 1 to 4 fluctuated within a limited spectrum and remained at the same level in the range of 270 nm to 320 nm (Table 4). Zeta potential is an important parameter for particle stability, and it shows an essential effect on the *in vivo* fate of particles (Torchilin 2005; R. Singh and Lillard 2009). Formulations 2 and 4 showed a higher absolute value of zeta potential (-10.8 ± 0.4 mv and -17.3 ± 0.3 mv, respectively) than formulations 1 and 3 (-6.7 ± 0.2 mv and -6.6 ± 0.3 mv), indicating that formulation 2 and 4 showed better stability than formulation 1 and 3. The polydispersity index (PDI) represents the homogeneity of particles. Formulations 1 and 3 exhibited a lower PDI (0.14 ± 0.01 and 0.20 ± 0.01 , respectively) compared to formulations 2 and 4. Notably, the encapsulation efficiency of formulation 2 ($40.8 \pm 1.8\%$) was doubled compared to formulation 1 ($17.7 \pm 1.9\%$), suggesting that reducing the weight ratio of T3 can improve encapsulation efficiency. Alternatively, the encapsulation efficiency and zeta potential of FR-TRLs (formulation 5) were similar to formulation 1, but with a lower PDI (0.38 ± 0.02) and a larger size (385.8 ± 6.8 nm) most likely due to the different chemical properties of FR compared to T3. Due to the high

absolute value of zeta potential and high encapsulation efficiency, formulation 2 of T3-TRLs was chosen and further used in the following study.

Table 4. Characteristics of TRLs

Formulation	TRLs description	Particle size (Z-average) (nm)	Polydispersity index (PDI)	Zeta potential (mv)	Encapsulation Efficiency (%)
1.	Low-concentrated T3-loaded TRLs	283.4 ± 4.4	0.14 ± 0.01	-6.7 ± 0.2	17.7 ± 1.9
2.	High-concentrated T3-loaded TRLs	275.1 ± 7.8	0.22 ± 0.02	-10.8 ± 0.4	40.8 ± 1.8
3.	Low-concentrated Vehicle-TRLs	315.6 ± 16.5	0.16 ± 0.01	-6.6 ± 0.3	N/A
4.	High-concentrated Vehicle-TRLs	298.4 ± 15.4	0.21 ± 0.01	-17.3 ± 0.3	N/A
5.	FR-loaded TRLs	385.8 ± 6.8	0.38 ± 0.02	-8.7 ± 0.4	17.7 ± 1.0
6.	Vehicle-TRLs	443.4 ± 4.0	0.37 ± 0.02	-8.9 ± 0.7	N/A

5.2 Optimization of API-loaded TRLs

Despite the importance of T3 in activating thermogenesis in BAT, excessive injection of T3 can lead to adverse effects such as hyperthyroidism, arrhythmia, and cardiac arrest. (Yau et al. 2019; Biondi et al. 2002). To minimize side effects induced by nonencapsulated T3, PD-10 desalting columns packed with Sephadex G-25 resin were used to remove nonencapsulated T3 and FR from drug-loaded TRLs. Since the size of TRLs is larger than nonencapsulated small molecules, TRLs were first eluted out of the column. In contrast, nonencapsulated T3 and FR penetrated pores in the Sephadex matrix and it took longer for them to be eluted out of the column than TRLs (Ó'Fágáin, Cummins, and O'Connor 2010). Sephadex G25 filtration was performed twice to remove nonencapsulated drugs, followed by 1 µm polyethersulfone (PES) syringe filtration once for removal of aggregated TRLs. Before injections, the remaining free drug was further separated using a centrifugal Vivaspın 20 ultrafiltration unit and quantified using LC/MS following Sephadex G25 filtration (Figure 27B).

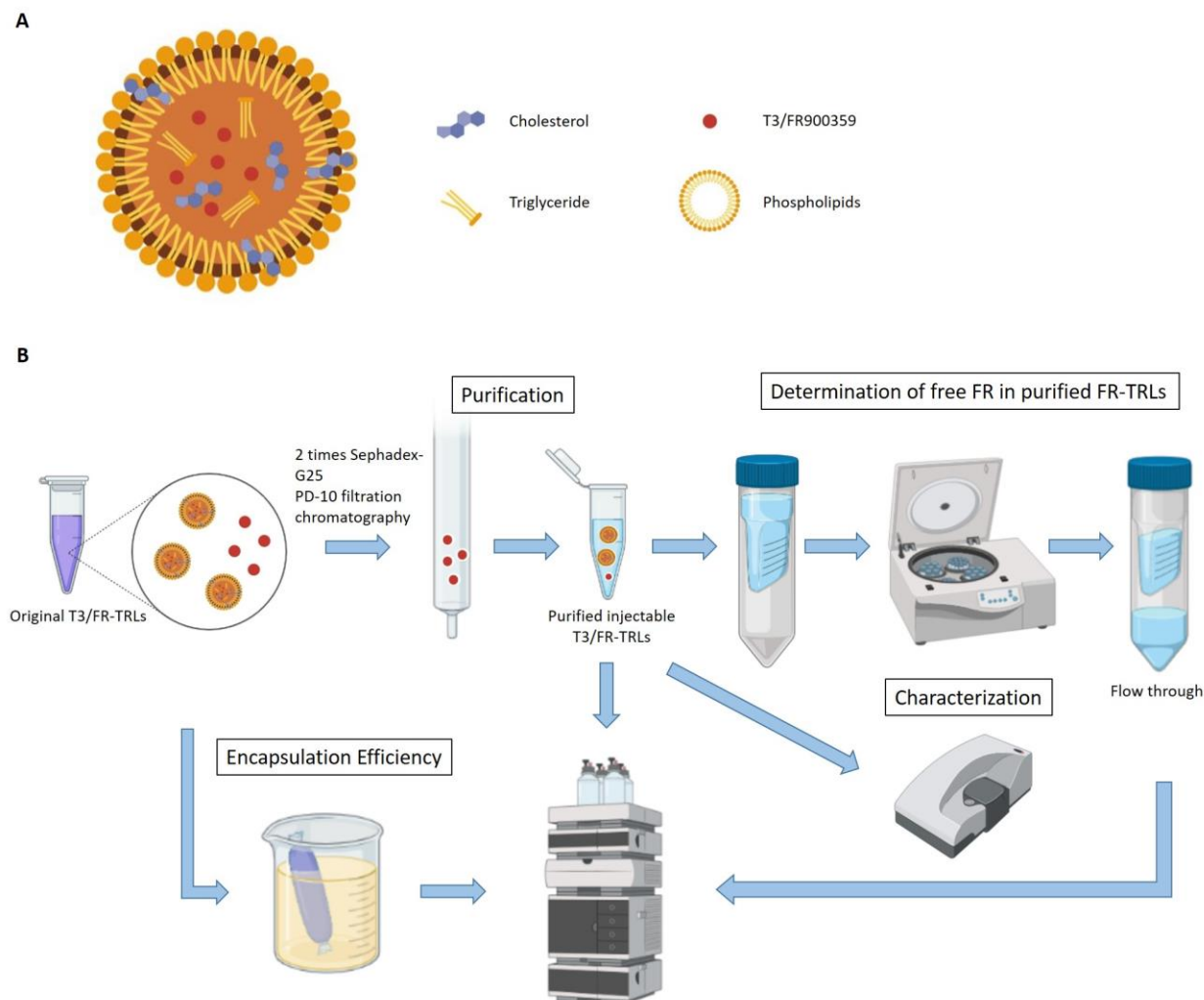


Figure 27. Schematic overview of API-loaded TRLs and API-loaded TRLs preparation protocol. (A) Schematic illustration of T3/FR-TRLs. (B) Schematic representation of T3/FR-TRLs preparation protocol. Filtration twice with Sephadex G25 PD-10 chromatography removed nonencapsulated API from the original API-loaded TRLs. The purified injectable FR-TRLs subsequently were characterized by Zetasizer. Simultaneously, a centrifugal concentrator of Vivaspın 20 was used to separate the remaining nonencapsulated API in purified API-loaded TRLs. The Encapsulation efficiency of original API-loaded TRLs was evaluated using dialysis tubes. The amount of API in each step was quantified by HPLC or liquid chromatography/mass spectrometry (LC/MS). The scheme is generated using Bio render. TRLs: triglyceride-rich lipoproteins, HPLC: high-performance liquid chromatography.

It was obvious that the scavenger role of Sephadex G25 in removing nonencapsulated T3 was obvious (Figure 28A). The total concentration of T3 in the purified T3-TRLs (114.0 ± 13.7 ng/ml) was significantly reduced compared to the total T3 concentration in the original T3-TRLs (14314.0 ± 665.4 ng/ml). In Figure 28B, T3-TRLs showed a single sharp peak in the size distribution (275.1 ± 7.8 nm) after optimization. Importantly, Figure 28C exhibits that the nonencapsulated T3 after Sephadex G25 filtration remained at an extremely low level (1.8 ± 0.3 ng/ml), which was

significantly lower than the T3 level in an 8-week-old C57BL/6L WT mouse serum (3.2 ± 0.1 ng/ml). Moreover, the same optimization was also conducted for FR-TRLs. As shown in Figure 29, the size of purified FR-TRLs was 385.8 ± 6.8 nm in diameter. The total concentration of FR reduced from 10794.0 ± 477.4 ng/ml to 190.4 ± 2.3 ng/ml after Sephadex G25 filtrations. Purified FR-TRLs contained a very low level of nonencapsulated FR (1.4 ± 0.6 ng/ml), while a lethal dose 50% (LD_{50}) of FR for subcutaneous injection in mice was reported by Onken et al. to be 0.6 mg/kg (Onken et al. 2021). These results suggest that the nonencapsulated T3 and FR remained at a low level in T3-TRLs and FR-TRLs respectively after optimization procedures.

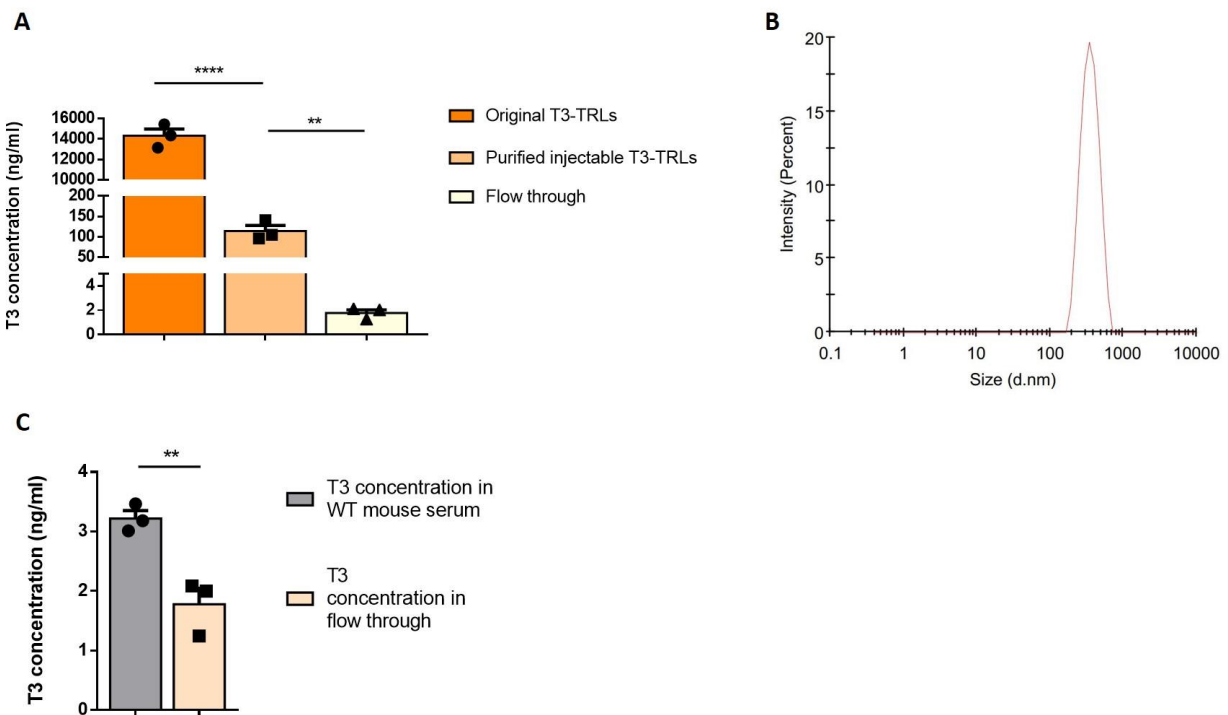


Figure 28. Optimization of T3-loaded TRLs. (A) Optimization of T3-TRLs, (B) Size distribution of purified T3-TRLs, (C) Concentration of free T3 in purified T3-TRLs compared with the T3 level in 8-week-old WT mouse serum. $n = 3$. The data were presented as means \pm s.e.m and analyzed using t-test or ANOVA. ** $p < 0.005$; **** $p < 0.0001$.

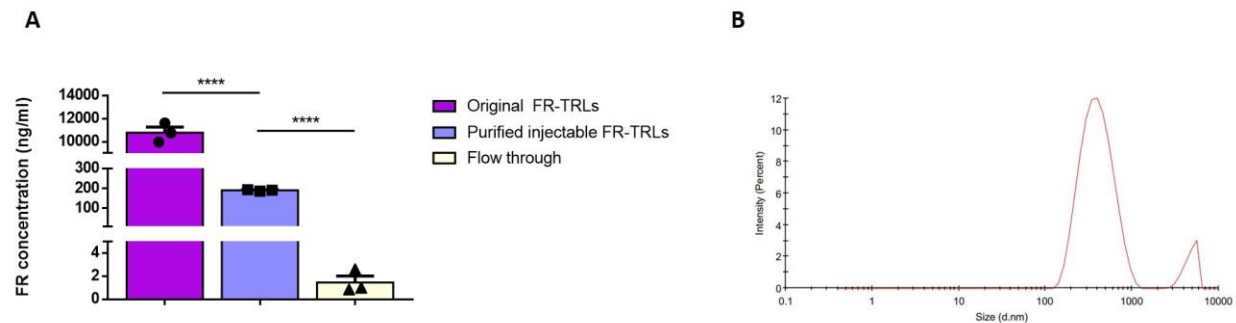


Figure 29. Optimization of FR-loaded TRLs. (A) Optimization of FR-TRLs, (B) Size distribution of purified FR-TRLs. $n = 3$. The data were presented as means \pm s.e.m and analyzed using t-test or ANOVA. **** $p < 0.0001$.

5.3 *In vivo* effects of T3-TRLs

5.3.1 Metabolic changes in mice treated with T3-TRLs

To activate BAT and trigger TRLs uptake in BAT, animals were acclimatized at 18°C for 7 days and subsequently exposed to cold (4°C) for 1 day before being treated with T3-TRLs or Vehicle-TRLs. Treatments with T3-TRLs and Vehicle-TRLs were administered every second day via i.v. injection (Figure 30A). Using metabolic cages, the oxygen consumption of two treated groups was measured after treatments at 4°C. Figures 30B to D show that the mean oxygen consumption in the T3-TRLs treated group was slightly higher (1.03 ± 0.01 -fold) than in the Vehicle-TRLs treated group during 24h of cold exposure, but not statistically significant. The body weight and food intake were recorded daily. As shown in Figure 30E, the body weight of the two treated groups was similar before treatment. All mice in the two groups lost body weight within the first day of cold exposure; interestingly, mice treated with Vehicle-TRLs lost more body weight than mice treated with T3-TRLs, albeit not significantly. From day 1 to day 4, the body weight of the T3-TRLs treated group remained relatively stable but showed a slight reduction on day 4. In contrast, the body weight of mice treated with Vehicle-TRLs showed a drop in the first 2 days of cold exposure, indicating that Vehicle-TRLs-treated mice might take longer to adapt to cold than mice treated with T3-TRLs. Interestingly, after 2 days of cold exposure, the body weight of Vehicle-TRLs treated mice began to recover and reached the same level as mice treated with T3-TRLs on day 5 of cold exposure. Figure 30F further shows that mice treated with T3-TRLs had a higher food intake than mice in the Vehicle-TRLs treated group, but not significantly. Moreover, the weight of BAT and iWAT in the group treated with T3-TRLs exhibited a decreasing tendency (0.7

± 0.1 -fold and 0.8 ± 0.2 -fold, respectively) compared to the Vehicle-TRLs treated group, while the weight of heart and gWAT had no difference between both groups (Figure 30G).

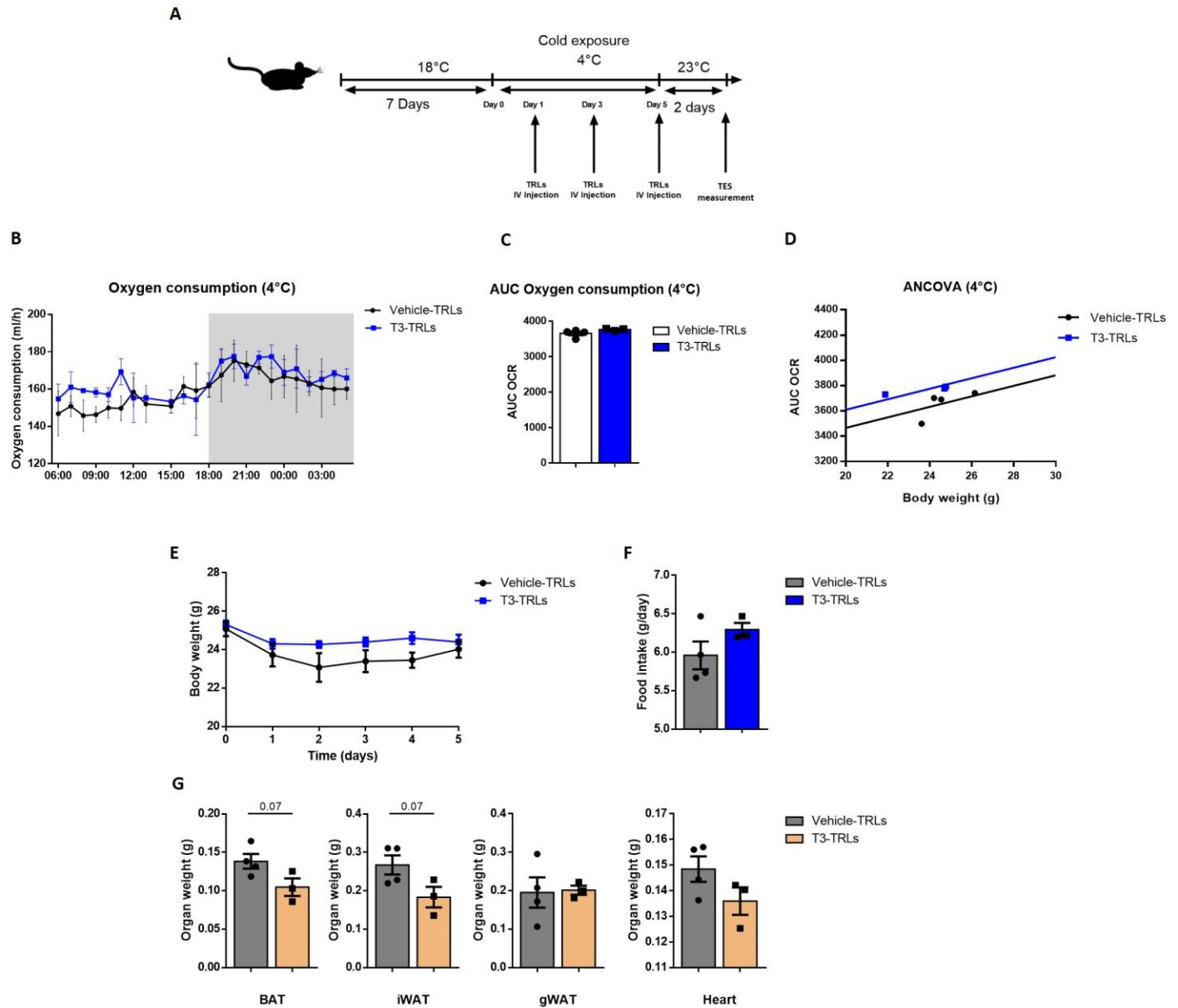


Figure 30. Assembly and physiological changes of mice after treatment with Vehicle-TRLs/T3-TRLs. (A) The treatment plan for two groups, (B) Oxygen consumption of mice treated with Vehicle TRLs and T3-TRLs during 24 hours of cold exposure, (C) Area under the curve (AUC) of the oxygen consumption in two groups during 24 hours of cold exposure, (D) ANCOVA analysis of oxygen consumption/body weight, (E) Change of body weight after treatments, (F) Food intake, (G) Organ weight of BAT, iWAT, and gWAT of Vehicle-TRLs treated mice and T3-TRLs treated mice. $n = 3 - 4$. The data were presented as means \pm s.e.m and analyzed using a t-test. * $p < 0.05$.

5.3.2 T3-TRLs induced effects in brown adipose tissue

Bartelt et al. first illustrated that radiolabeled TRLs can be detected in several organs including the liver, spleen, BAT, WAT, muscle, and heart after administration, but not in the brain (Bartelt et al. 2011). Recently, Hildebrand et al. further reported the distribution and *in vivo* uptake of Iron-oxide-nanoparticle-loaded TRLs (IRON-TRLs) via i.v. injection. IRON-TRLs have iron oxide nanoparticles (IONPs) embedded in the lipid core, which provided a novel method to quantify and trace *in vivo* uptake of TRLs (Hildebrand et al. 2021). Bartelt et al. and Hildebrand et al. both demonstrated that TRLs can be taken up by mice in BAT after cold exposure and the liver (Bartelt et al. 2011; Hildebrand et al. 2021). Using the same method, Vehicle-TRLs and T3-TRLs were prepared with the same structure and at the same size as IONP-TRLs. According to Bartelt's and Hildebrand's findings, the *in vivo* uptake pattern of Vehicle-TRLs and T3-TRLs manifest a similar *in vivo* uptake pattern of radiolabeled TRLs or IRON-TRLs (Bartelt et al. 2011; Hildebrand et al. 2021).

T3-TRLs and Vehicle-TRLs were administrated every two days at a volume of 5 ml/kg (100 μ l/ 20 g) for 1 week. To assess the effects of T3 delivered by T3-TRLs on BAT, the expression of thermogenic genes and proteins was analyzed. Figures 31A and B exhibit that the expression of thermogenic markers (*Ucp1* and *Dio2*) in the BAT of mice treated with T3-TRLs was significantly increased by 3.35 ± 0.93 -fold and 4.70 ± 1.24 -fold, respectively. Figures 31C and D further show that treatment with T3-TRLs could lead to an increase in the mean expression of adipogenic markers (*Fabp4* and *Ppar γ*) compared to the Vehicle-TRLs treated group. Additionally, an apparent increase in the mean protein level of thermogenic and adipogenic markers (*Ucp1* and *Fabp4*) in BAT could also be observed following treatment with T3-TRLs (1.4 ± 0.3 -fold and 1.3 ± 0.2 -fold, respectively), albeit not significantly (Figures 31E to F). These data suggest that the expression of thermogenic markers in BAT was effectively upregulated following treatment with T3-TRLs.

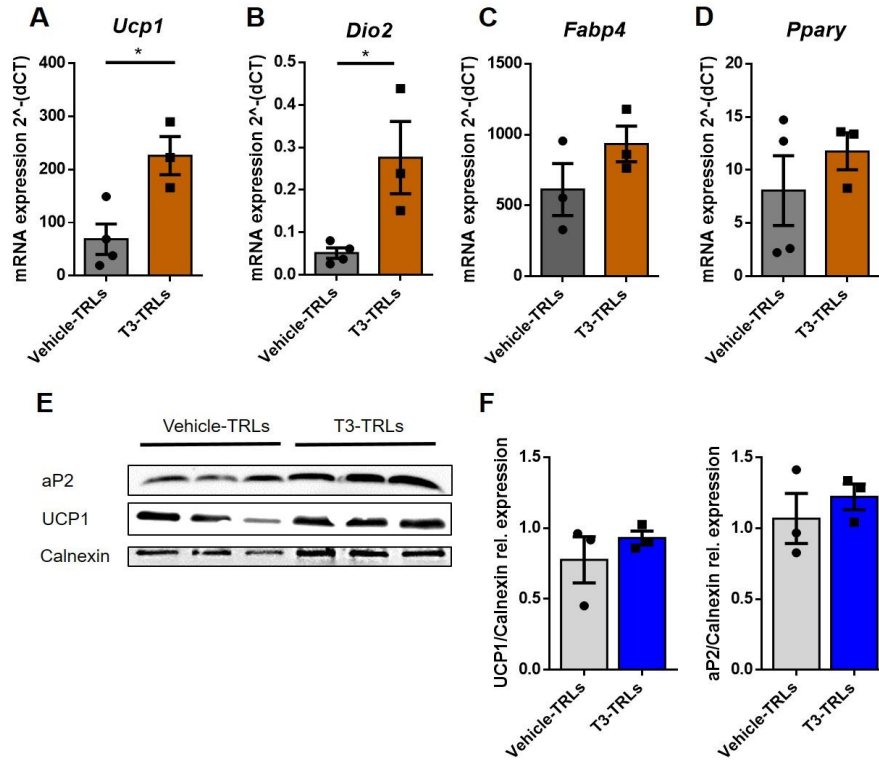


Figure 31. Gene and protein expression in BAT after treatment with Vehicle-TRLs/T3-TRLs. (A - D) *Ucp1*, *Dio2*, *Fabp4*, and *Pparg* expression in BAT after treatments with Vehicle-TRLs and T3-TRLs, (E - F) UCP1 and FABP4 (aP2) protein expression levels in BAT after treatments. $n = 3 - 4$. The data were presented as means \pm s.e.m and analyzed using a t-test. * $p < 0.05$.

5.3.3 T3-TRLs-induced gene expressions

The liver is metabolically benefited from T3, as T3 promotes FA oxidation and hepatic lipogenesis (Mendoza et al. 2021). In turn, the liver synthesizes several plasma proteins that can bind thyroid hormones and provide a large and exchangeable pool of circulating hormones (Antonio C. Bianco et al. 2002). To investigate the effects of treatment with T3-TRLs on regulating hepatic metabolism, the expression of hepatic genes was analyzed. Several T3-related hepatic genes, associated with hepatic lipogenesis, hepatic lipase activity, and lipoprotein receptors, were analyzed in this study, including *Dio1*, Cytochrome P450 Family 7 Subfamily A Member 1 (*Cyp7a1*), Low-Density Lipoprotein Receptor (*Ldlr*), peroxisome proliferator-activated receptor- α (*Ppara*), Carnitine Palmitoyltransferase 1A (*Cpt1a*), Malic enzyme 1 (*Me1*), Scavenger Receptor Class B Member 1 (*Scarb1*), Sterol Regulatory Element Binding Transcription Factor 2 (*Srebp2*), *Dio2*, Diacylglycerol O-Acyltransferase 1 (*Dgat*), Lipase C (*Lipc*), and Pyruvate Dehydrogenase Kinase 4 (*Pdk4*) (Kinlaw et al. 1995; Moustaid and Sul 1991; Sinha, Singh, and Yen 2014; 2014).

Figures 32A to E show that the expression of *Dio1* (5.3 ± 0.7 -fold), *Cyp7a1* (4.6 ± 1.0 -fold), *Ldlr* (6.7 ± 0.6 -fold), *Ppara* (2.6 ± 0.9 -fold), and *Cpt1a* (2.9 ± 0.6 -fold) was significantly upregulated in the liver after treatment with T3-TRLs. An increase in the mean expression of other T3-related hepatic genes could also be observed after treatment with T3-TRLs, such as *Me1* (1.4 ± 0.1 -fold), *Scarb1* (3.9 ± 0.8 -fold), *Srebp2* (2.7 ± 1.1 -fold), *Dio2* (1.9 ± 0.5 -fold), *Dgat* (1.8 ± 0.5 -fold), *Lipc* (3.6 ± 1.4 -fold), and *Pdk4* (1.4 ± 0.3 -fold), albeit not significantly (Figures 33F to L). These results indicate that T3 encapsulated in TRLs successfully achieved in the liver and effectively induced the expression of T3-related hepatic genes.

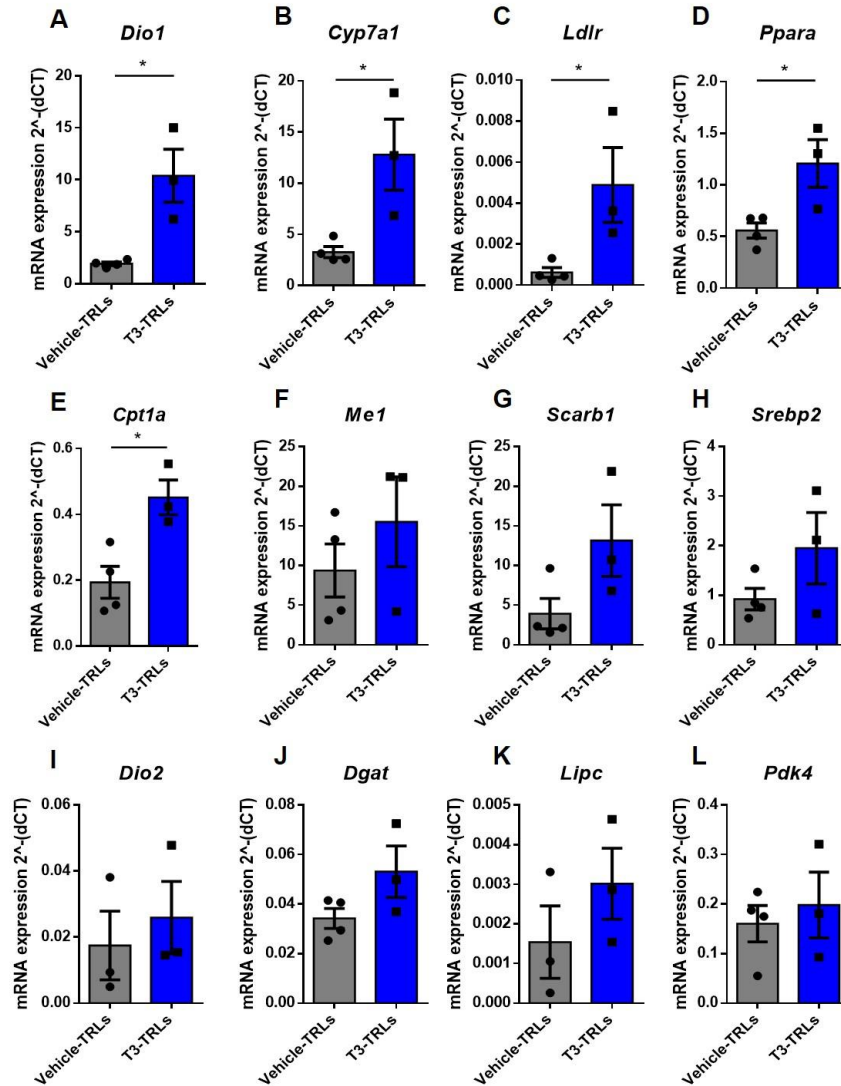


Figure 32. Hepatic gene expression in mice treated with Vehicle-TRLs and T3-TRLs. (A - E) *Dio1*, *Cyp7a1*, *Ldlr*, *Ppara*, and *Cpt1a* expression in the liver, (F - L) *Me1*, *Scarb1*, *Srebp2*, *Dio2*, *Dgat*, *Lipc*, and *Pdk4* expression in the liver. $n = 3 - 4$. The data were presented as means \pm s.e.m and analyzed using a t-test. * $p < 0.05$.

Next, to assess whether treatment with T3-TLRs could have cardiac effects, the expression of four thyroid hormone-related genes in the heart (*Dio2*, *Pdk4*, *Ucp2*, and *Ucp3*) was examined in the Vehicle-TRLs treated group and the T3-TRLs treated group. *Dio2* has a high affinity for T4 and it converts T4 to T3 (Escobar-Morreale et al. 1999). As shown in Figure 33A, following treatment with T3-TRLs, the mean expression of cardiac *Dio2* was down-regulated by 0.8 ± 0.3 -fold, but not significantly. Moreover, the expression of *Pdk4* is regulated by T3. It has been reported that hyperthyroidism can strongly result in high expression of *Pdk4* in the heart (Sugden

et al. 2000; Attia et al. 2010). Figure 33B shows that the expression of *Pdk4* had no significant changes after treatment with T3-TRLs compared to the Vehicle-TRLs treated group. Several previous studies have illustrated that an increasing level of T3 in serum enhances the expression of *Ucp2* and *Ucp3* in the heart (Lanni et al. 1997; Queiroz, Shao, and Ismail-Beigi 2004). Interestingly, Figures 33C to D exhibit that treatment with T3-TRLs did not induce an increase in the expression of *Ucp2* or *Ucp3*. These data indicate that treatment with T3-TRLs did not affect the gene expression in the heart compared to mice treated with Vehicle-TRLs.

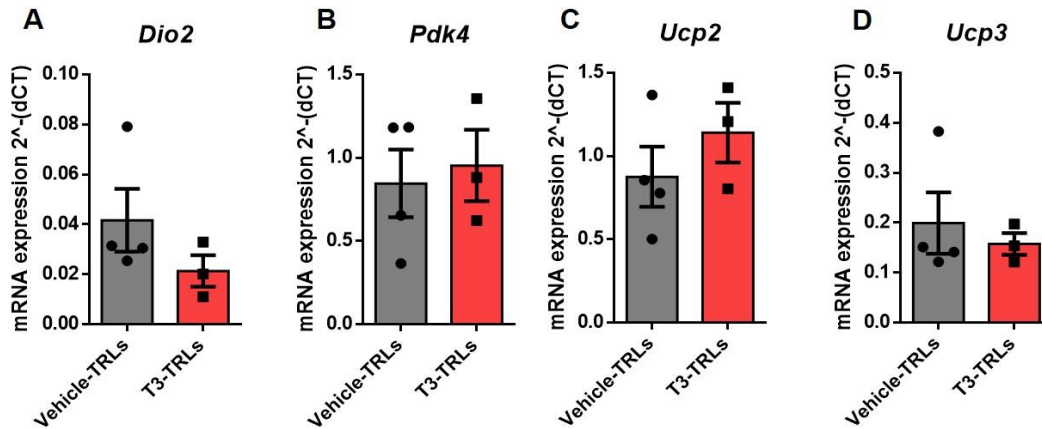


Figure 33. T3 regulated gene expression in the heart after treatment with Vehicle-TRLs and T3-TRLs. (A) the expression of *Dio2* in the heart after treatments with Vehicle-TRLs and T3-TRLs, (B) the expression of *Pdk4* in the heart after treatments, (C) the expression of *Ucp2* in the heart after treatments, (D) the expression of *Ucp3* in the heart after treatments. $n = 3 - 4$. The data were presented as means \pm s.e.m.

5.3.4 Histological changes in mice treated with T3-TRLs

Since treatment with T3-TRLs upregulated the expression of the thermogenic gene in BAT and T3-related hepatic genes in the liver, it is necessary to verify histological changes in BAT and the liver after treatments. First, BAT from T3-TRLs treated mice and Vehicle-TRLs treated mice was analyzed using H&E staining and immunohistological UCP1 staining. H&E staining illustrated that BAT from mice treated with T3-TRLs exhibited more multilocular lipid droplets compared to BAT from Vehicle-TRLs treated mice (Figures 34A and B). Notably, immunohistochemical UCP1 staining also revealed a greater abundance of UCP1 in BAT of T3-TRLs treated mice than the Vehicle-TRLs treated mice, suggesting that treatment with T3-TRLs induced a higher UCP1 level in BAT (Figures 34C and D).

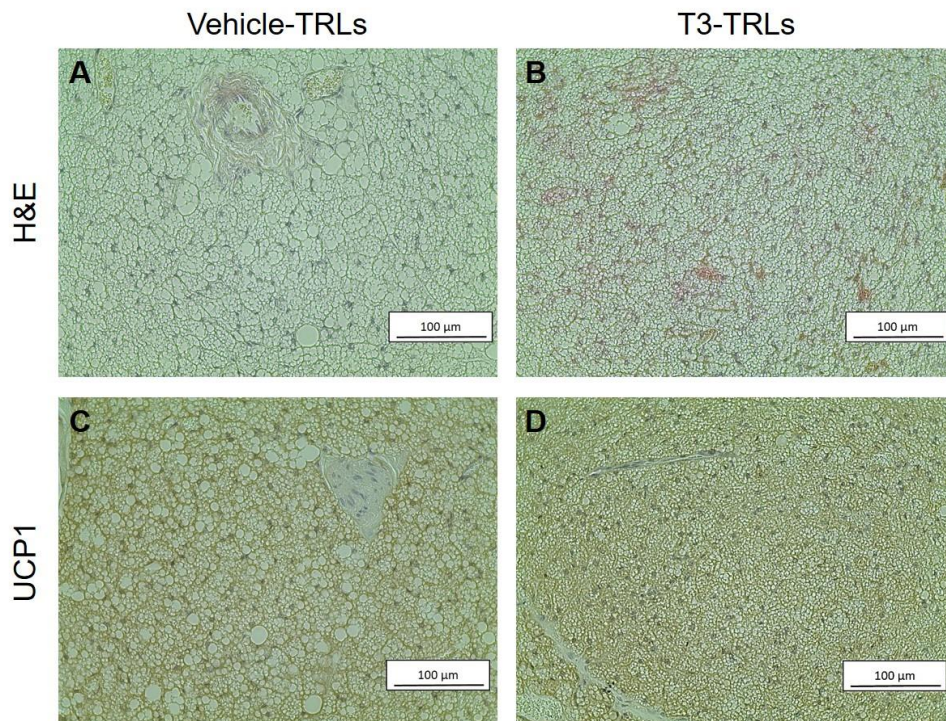


Figure 34. H&E staining and immunohistochemical UCP1 staining of BAT after treatments with Vehicle-TRLs and T3-TRLs. (A) H&E staining of BAT in vehicle-TRLs treated mice, (B) H&E staining of BAT in T3-TRLs treated mice, (C) Immunohistochemical UCP1 staining of BAT in vehicle-TRLs treated mice, (D) Immunohistochemical UCP1 staining of BAT in T3-TRLs treated mice ($n = 3 - 4$). Scale bar, 100 μm .

Next, H&E staining was conducted in the liver of mice treated with T3-TRLs and Vehicle-TRLs. As shown in Figures 35A and B, H&E staining did not show significant differences in the liver between the group treated with T3-TRLs and the group treated with Vehicle-TRLs. Only a slight reduction in the sinusoid size of mice treated with Vehicle-TRLs was observed (Figure 35A, arrows). The diameter of the sinusoid exhibited slightly larger compared to that of mice treated with T3-TRLs. Kostka et al. demonstrated that the hepatocyte volume and the diameter of the sinusoid might be affected by VLDL or other treatments in the liver (Kostka et al. 1999). According to the results, it is hypothesized that mice treated with T3-TRLs reduced blood flow by reducing sinusoids, which in turn increased the concentration of liver enzymes to metabolize the extra T3 encapsulated in T3-TRLs.

Figures 35 C and D exhibited representative images of transverse sections of the heart stained with H&E from Vehicle-TRLs treated mice and T3-TRLs treated mice. The left ventricle (LV) and right ventricle (RV) can be distinguished. No significant differences were observed between the two groups, which was consistent with the results of gene expressions in the heart.

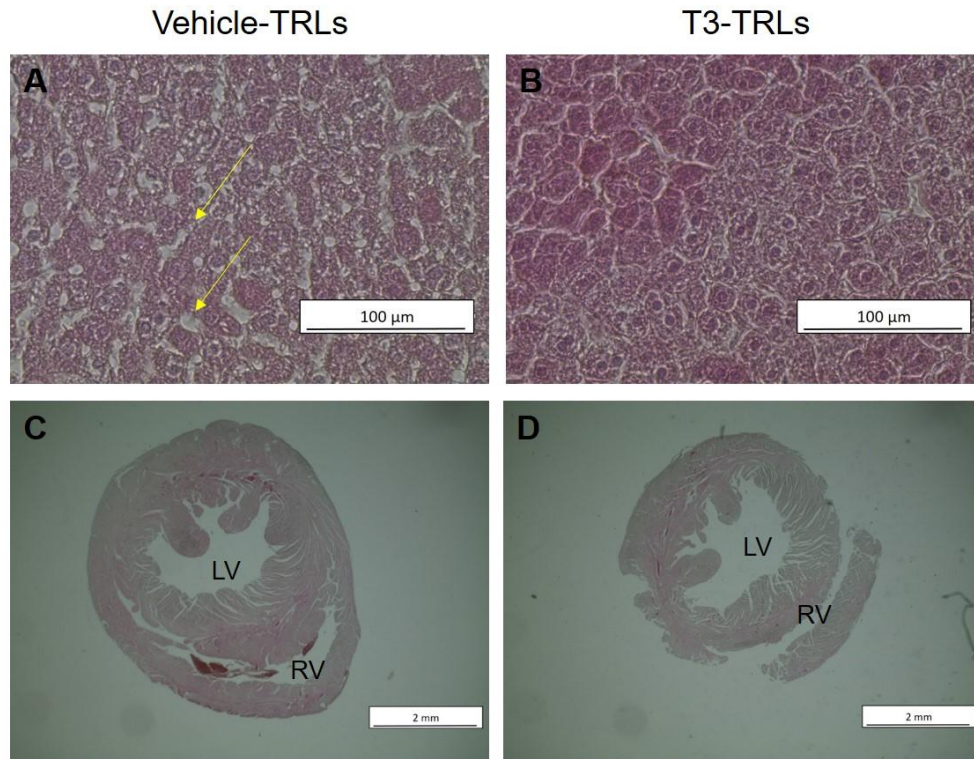


Figure 35. H&E staining of liver and heart of mice treated with Vehicle-TRLs and T3-TRLs. (A) H&E staining of the liver in vehicle-TRLs treated mice, (B) H&E staining of the liver in T3-TRLs treated mice, (C) H&E staining of the heart in vehicle-TRLs treated mice, (D) H&E staining of the heart in T3-TRLs treated mice. $n = 3 - 4$. LV: left ventricle, RV: right ventricle, arrow: hepatic sinusoid. (A - B) Scale bar, 100 μm . (C - D) Scale bar, 2 mm.

6 Discussion

6.1 Project I: MIR-loaded PLGA microparticles

6.1.1 A novel combination of PLGA microparticles and MIR

Nano/microparticle therapies have been receiving a surge of interest recently. FDA approved 51 Nano/microparticle therapies by 2016 while 77 products were already in clinical trials (Bobo et al. 2016). From 2016 to 2019, over 75 new trials were further initiated, and more than 15 new nano/microparticle technologies started clinical trials, indicating an increasing demand for nano/microparticle therapies (Anselmo and Mitragotri 2019).

Several studies have investigated the combination of off-label effects of FDA-approved drugs and nano/microparticle techniques for treating obesity. A study has attempted to use nanoparticle platforms to deliver rosiglitazone to AT vasculature, which binds to the nuclear PPAR γ receptor and upregulates *Ppar γ* expression as well as causes WAT beiging (Xue et al. 2016). Dibenzazepine (DBZ), a γ -secretase inhibitor, was used in another study to inhibit Notch signaling and promote the beiging of WAT (Jiang et al. 2017). Although Rosi is an FDA-approved drug for diabetes, Rosi's cardiovascular safety issues cannot be ignored (Nissen and Wolski 2007; Cohen 2010). Moreover, whether the use of Rosi for treating obesity could induce side effects in other organs such as the liver, kidney, and brain still needs to be explored (Hemmerlyckx et al. 2013; Ahmadian et al. 2013). As an iminostilbene, DBZ is mainly used in schizophrenia (SZ) (Meltzer et al. 1989). The effect of DBZ on WA beiging has been found in a recent study (Bi et al. 2014), but ADRB3 agonists have superior efficacy on WA beiging than DBZ (Merlin et al. 2018).

It has been decades since PLGA was first applied as a biodegradable and biocompatible device for drug delivery in medical fields (Kulkarni et al. 1971). PLGA has not only been successfully used to encapsulate and deliver hydrophobic and hydrophilic small molecule drugs such as steroids (Beck et al. 1979; Barichello et al. 1999), but also large molecules such as peptides, proteins, DNA, and RNA for potential medical uses (Wischke and Schwendeman 2008). In the aspect of pharmacological treatment for obesity, MIR showed promising effects on activating BA and beiging WA (Warren, Burden, and Abrams 2016; O'Mara et al. 2020). Clinical trials regarding the use of MIR to treat obesity have focused mainly on oral administration, which requires patients to take high doses of MIR daily and chronically (200 mg/day for weeks) (Cypess et al. 2015; Finlin et al. 2018; O'Mara et al. 2020). However, Nitti and Chapple *et al.* demonstrated that increases in blood pressure (0.4 - 0.6 mmHg) were strongly associated with MIR oral administrations (50

mg/day, 12 weeks) (Nitti et al. 2014). So far, MIR has seldom been reported to be encapsulated in PLGA devices to achieve its pharmacological effects on WA being. Therefore, using PLGA microparticles to control the release of MIR to WA and minimize its potential cardiovascular side effects could be a novel combination to treat obesity.

6.1.2 The release profile of MIR-loaded PLGA microparticles

The releasing profile of PLGA microparticles is influenced by several factors including drug characteristics, the lactic acid content of PLGA polymers, releasing medium, pH, surface-active agents, etc. (Parikh et al. 1993; Cowsar et al. 1985; Leelarasamee et al. 1986). To encapsulate the hydrophobic drug MIR in PLGA, the oil-in-water (o/w) emulsion/solvent evaporation technique was used. Here, adding a small amount of DMSO for assisting in dissolving MIR significantly increased the solubility of MIR in DCM. However, SEM images show that the formulation with increased DMSO exhibited pores on the surface of MIR-MPs. It is hypothesized that DMSO might diffuse into aqueous surroundings from newly hardened MIR-MPs during evaporation. This phenomenon may alter the release profile of MIR-MPs. Surprisingly, the results of the release profile showed that increased DMSO did not significantly change the release profile of MIR-MPs.

Using high molecular weight PLGA to prepare PLGA microparticles can significantly prolong the release profile (Sousa-Batista et al. 2019). The amount of MIR released from MIR-MPs should be enough to induce pharmacological effects on adipocytes and AT within an acceptable period in *in vitro* and *ex vivo* studies. Based on the results in this thesis, the optimized MIR-MPs contain 6% of MIR (w/w) and the kinetic release profile of MIR-MPs showed a sustainable release of MIR within 2 weeks in PBS (pH 7.4) as well as in similar aqueous mediums. Therefore, this formulation of MIR-MPs can be used *in vitro* and *ex vivo* to sustainably release MIR and induce pharmacological effects on adipocytes and AT. However, the *in vivo* release profile of MIR-MPs at the site of WAT after administration might differ from that in an aqueous medium. The *in vivo* release profile of MIR-MPs should be investigated by further pharmacokinetic studies.

6.1.3 Non-toxicity of MIR-loaded PLGA microparticles in adipocytes

Given the importance of the non-toxicity of MIR-MPs, efforts were undertaken to investigate the potential toxicity induced by MIR-MPs in adipocytes. Several studies have previously illustrated that PLGA microparticles do not cause significant cellular toxicity at a concentration of up to 300 g/ml (Xiong et al. 2013). In this thesis, two toxicity assays, the MTT assay and the ATP assay, were used to test MIR-MPs toxicity in adipocytes. Given the results shown in **4.3**, treatment with MIR and MIR-MPs generally did not induce cellular toxicity nor reduce the viability of adipocytes. However, BA showed a higher OD value than the other adipocytes in the MTT assay, and a reduction was observed in BA treated with MIR and MIR-MPs compared to the control groups. Since the MTT assay is a colorimetric assay for evaluating cellular metabolic activity, a high OD value indicates a high metabolic rate (Denizot and Lang 1986). BA are responsible for thermogenesis, they have a high basal metabolic rate (Carpentier et al. 2018). It is also known that the MTT assay is dependent on NADPH oxidoreductase enzymes. Cells with lower metabolic activities such as pre-BA and WA could reduce OD value less than those with a high metabolic rate (Kumar, Nagarajan, and Uchil 2018). The reduction of OD value in BA was possibly due to the high metabolic activity in BA rather than the toxicity of MIR and MIR-MPs. This point was further proved in the ATP assay, which showed no significant difference in cell viability between MIR-treated BA and non-treated BA. Therefore, it is clear that treatment with MIR and MIR-MPs did not induce cytotoxicity in adipocytes.

6.1.4 MIR-loaded PLGA microparticles induced effects in iWA

CL-316,243, a hydrophilic ADRB3 agonist, has been utilized as a gold stimulator to induce thermogenic and beiging gene expression in BAT and WAT (Commins et al. 1999). As a promising WAT beiging agent, treatment with MIR has been investigated mostly via oral administration on experimental animals or human beings (Bel et al. 2021). Nevertheless, a systematic *in vitro* study exploring the effects of MIR on iWA has not been properly investigated so far. Therefore, this thesis first systematically investigated the effects induced by treatment with MIR and MIR-MPs on adipocytes.

Ucp1, *Cidea*, *Ppargc1α*, and *Prdm16* have been reported as thermogenic markers and beiging markers in adipocytes after cold exposure or stimulations (Garcia, Roemmich, and Claycombe 2016; Dewal and Stanford 2019). Notably, the results in this thesis show that *Ucp1* gene

expression and UCP1 protein expression were significantly upregulated after 3-hour treatment with MIR-MPs in iWA and BA. Additional beiging markers such as *Ppargc1α*, *Dio2*, and *Cidea* also exhibited an increasing trend in iWA after treatments with MIR-MPs. Therefore, it is suggested that MIR released from MIR-MPs can successfully increase the expression of beiging markers in iWA.

Furthermore, previous studies have demonstrated that chronic treatments with CL-316,243 could elevate the lipolytic rate in adipocytes (Atgié et al. 1998). In line with these studies, the results in this thesis confirmed that the lipolysis level in both BA and iWA can be upregulated by treatment with MIR and MIR-MPs. In iWA, the fold change in lipolysis was greater than in BA, suggesting that MIR accelerates lipolysis more effectively in iWA than in BA. Indeed, treatment with CL-316,243 has previously been shown to be associated with a decrease in the lipid droplet size of adipocytes (Ghorbani, Claus, and Himms-Hagen 1997). This thesis also found that iWA exhibited a morphology of drained lipid droplets and less density of Oil Red O staining after treatment with MIR-MPs, which was consistent with the upregulated expression of beiging markers. Therefore, those findings indicate that MIR showed comparable effects on inducing lipolysis and beiging in iWA as CL-316,243, and treatment with MIR-MPs had a promising potential in beiging iWA and increasing iWA lipolysis.

6.1.5 MIR-loaded PLGA microparticles induced oxygen consumption in adipocytes

Since treatment with MIR-MPs increased lipolysis rate and *Ucp1* expression in adipocytes, efforts were further undertaken to investigate the oxygen consumption induced by MIR-MPs in adipocytes. A recent study performed a MIR-induced mitochondrial stress assay in BA and showed that MIR increased cAMP and UCP1 levels resulting in increased UCP1-mediated oxygen consumption (Dehvari et al. 2020). Despite this, using MIR-MPs to induce the beiging and increase oxygen consumption in iWA has not been conducted yet. The results in this thesis revealed that treatment with MIR and MIR-MPs can elevate the level of basal respiration and maximal respiration in iWA. Unfortunately, the UCP1-mediated oxygen consumption did not significantly increase after treatment with MIR and MIR-MPs. This was probably due to the limited treatment period (3 hours) with MIR and MIR-MPs before being measured by Seahorse XF24 Analyzer, which was not long enough to significantly alter UCP1-mediated oxygen consumption.

6.1.6 MIR-loaded PLGA microparticles induced effects in adipose tissue

The effects of MIR-MPs on adipocytes have been demonstrated in 4.2. Given the expression of thermogenic marker and beige markers, as well as the lipolysis level induced by treatment with MIR and MIR-MPs in adipocytes, efforts were further undertaken to explore the effects of MIR-MPs in explanted murine AT and human subcutaneous white adipose tissue (scWAT). Since *ADRB3* is expressed dominantly in murine AT (Evans et al. 2019; S. Collins et al. 1994), it is clear that treatment with MIR and MIR-MPs showed the same significant effects on murine BAT, iWAT, and gWAT (Figure 22). However, a previous study has shown that treatment with *ADRB3* agonist at a high dose might induce a cross-talk effect between other β -adrenergic receptors (Susulic et al. 1995). In this thesis, to eliminate the cross-talk effects between other beta-adrenergic receptors, CGP and ICI were applied to block *ADRB1* and *ADRB2* respectively. Importantly, either adding CGP and ICI individually or together did not attenuate the increased lipolysis induced by treatment with MIR and MIR-MPs in murine iWAT. These results strongly support that the selectivity of MIR to *ADRB3* and the effects induced by MIR and MIR-MPs in murine adipocytes and AT were mainly via *ADRB3*.

Given a lower *ADRB3* expression level in human WAT than in murine WAT (Evans et al. 2019), comparing the expression of *ADRB3* and *ADRB2* between human scWAT and murine iWAT could help to evaluate whether the therapeutic effects induced in murine AT can be further transferred to human scWAT. The results in this thesis were in the line with the previous findings that both human scWAT and murine iWAT expressed *ADRB3*, but human scWAT predominantly expressed *ADRB2* rather than *ADRB3*. However, the same treatment with MIR and MIR-MPs did not induce a comparable effect in human scWAT after a 3-hour incubation.

Considering cumulative glycerol release over a certain period integratively represents lipolysis level, human scWAT likely needs a prolonged period of incubation to induce robust lipolysis possibly because of a low expression of *ADRB3* in human scWAT. Prolonging the incubation period of *ex vivo* lipolysis led to a higher concentration of MIR in the MIR-MPs treated groups due to continuous release. As the incubation time was prolonged, the non-treated group and Ctrl-MPs treated group did not show significant changes in glycerol release in both murine iWAT and gWAT compared to the 3-hour incubation lipolysis, indicating that prolonging incubation did not increase basal lipolysis level. Interestingly, a higher glycerol release was observed in both murine iWAT and gWAT treated with MIR and MIR-MPs when the incubation period was prolonged. Here, the

glycerol release in the group treated with MIR showed no difference from the group treated with MIR-MPs (Figure 24). These results indicate that glycerol release from murine iWAT can be further enhanced by prolonging the incubation only if MIR or MIR-MPs have already been administrated. This point was further supported in human scWAT. As the incubation period was prolonged, the lipolysis level in human scWAT was significantly elevated after treatment with MIR or MIR-MPs, while the basal level of lipolysis remained unchanged in the control groups.

Blondin et al. recently reported that thermogenesis might be conducted via ADRB2 in human BA (Blondin et al. 2020). Since the expression pattern of *ADRB3* is different in human scWAT, the cross-talk effect with ADRB2 in human scWAT after treatment with MIR-MPs remains to be investigated. To prove that the upregulated lipolysis in human scWAT was induced by MIR mainly via ADRB3, SAL (an ADRB2 agonist) and ICI (an ADRB2 antagonist) were further applied. The results show that treatment with SAL and MIR both increased the lipolysis level in explanted human scWAT. Notably, the inhibitory effect of ICI was only observed in the SAL-treated human scWAT, but ICI did not attenuate the increased lipolysis after treatment with MIR and MIR-MPs (Figure 25). These results provide further evidence that treatment with MIR-MPs could increase human scWAT lipolysis mainly via ADRB3.

Additionally, ADRB2 agonists could be potential drug candidates to induce lipolysis and beiging in human WAT as well. Since the expression of *ADRB2* is more promiscuous in various human organs, however, it might cause more side effects if treatment is not specifically targeted (Bellinger et al. 2021; Lulich et al. 1986). Therefore, it would be extremely important to use pharmaceutical methods to specifically deliver ADRB2 agonists.

While it is clear that treatment with MIR and MIR-MPs upregulated lipolysis in human scWAT via co-culturing, a method that directly injects MIR-MPs into human scWAT has not been studied. Therefore, MIR-MPs were injected directly into human scWAT. Since the environment inside scWAT contains more lipids that completely differ from an *in vitro* aqueous environment, the release profile of MIR-MPs might also alter after direct injection. Interestingly, an increase in lipolysis level of human scWAT after direct injection of MIR-MPs was also observed as well as the increased expression of *UCP1* (Figure 27). Considering the therapeutic effects of MIR-MPs, a feasible application of MIR-MPs as described could be a potential and novel therapeutic approach for the treatment of obesity.

6.2 Project II: T3-loaded TRLs

6.2.1 Optimization of T3-TRLs

As the administration of nonencapsulated T3 can increase the free T3 level in plasma and induce undesirable pharmacological effects such as hyperthyroidism (Danzi and Klein 2003), it is tempting to optimize T3-TRLs in terms of removing nonencapsulated T3. However, so far, removing nonencapsulated drugs from drug-loaded TRLs or drug-loaded liposomes remains a challenge (Dimov et al. 2017). There are several methods for eliminating nonencapsulated API mainly including dialysis, centrifugation, column chromatography, and ultrafiltration (Ingebrigtsen et al. 2017; Yamamoto et al. 2018; Mayer and St-Onge 1995). Correspondingly, each method has its advantages and disadvantages. The advantages of dialysis include a large quantity of samples, being well reproducible, and easy operation, but adhesion may lead to product loss (M. Lin and Qi 2018). Centrifugation for purification is flexible due to its controllable centrifugal force, but it might cause particle membrane fusion and result in aggregation and drug leakage (M. Lin and Qi 2018). In this present work, Sephadex G25 matrix columns were used to remove nonencapsulated T3 from T3-TRLs based on their different sizes. This method is considered to have the advantages of good reproducibility and easy operation with high recovery, but it avoids causing product loss compared to dialysis (Gimlette 1967). However, a dilution was inevitable to purify T3-TRLs using a Sephadex G25 matrix column. The results in this thesis show that the concentration of T3 dropped spectacularly each time of Sephadex G25 filtration, reducing from 14000 ng/ml to 167 ng/ml after two times of Sephadex G25 filtration (Figure 28). Since the total T3 concentration reduced almost 80-fold compared to the technical dilution factor, it is unlikely that Sephadex G25 filtration only diluted the original T3-TRLs. Additionally, this thesis further demonstrates that Sephadex G25 matrix columns proved to be effective in removing nonencapsulated FR from FR-TRLs as well.

The surface charge of TRLs plays a critical role in particle clearance and cellular interactions *in vivo*. It is known that cationic TRLs (> 20 mV zeta potential) could be captured by anionic surfaces of blood vessel walls through non-specific cellular interaction, resulting in rapid clearance from the circulation by the reticuloendothelial system (RES) after administration (F. Campbell et al. 2018). Interestingly, some previous studies have reported that TRLs with negative charges (< -20 mV zeta potential) showed a significantly longer half-life in circulation (Blanco, Shen, and Ferrari 2015; F. Campbell et al. 2018). All formulations of TRLs involved in this thesis were

negatively charged (< -18 mV zeta potential), indicating that they have better stability and a longer half-life in circulation than cationic TRLs.

Previous studies have also shown that the size of TRLs can also affect the delivery efficiency and *in vivo* fate. It is known that TRLs larger than 200 nm in diameter might increase the risk of spleen accumulation (Blanco, Shen, and Ferrari 2015). Unfortunately, the size of TRLs in this thesis was in the range of 250 nm to 450 nm, indicating that some TRLs might accumulate in the spleen after administration. Hildebrand et al. have verified that a small number of IRON-TRLs in the same size as TRLs prepared in this thesis were detected in the spleen following i.v. injection, but the majority were taken up by BAT after cold exposure (Hildebrand et al. 2021). Therefore, it could be postulated that optimizing the size of TRLs might further increase the delivery efficiency to the target tissue and attenuate the accumulation of TRLs in the spleen.

6.2.2 *In vivo* effects of T3-TRLs

Given the potential therapeutic effects of T3-TRLs, efforts were first undertaken to increase T3-TRLs *in vivo* uptake in BAT. Artificial TRLs have previously been shown to act like natural chylomicrons, allowing materials to be transported in the circulation and reach the liver and other peripheral tissues including AT (Bartelt et al. 2011; Lusi, Fogelman, and Fonarow 2004). It has been recently illustrated that using a radioactive-labeling-independent method (MPI method) to trace IRON-TRLs uptake in peripheral tissues (Hildebrand et al. 2021). Given the major role of activated BAT in postprandial TG clearance (Khedoe et al. 2015; Bartelt et al. 2011) and an increase in fuel demand after BAT activation, cold exposure during treatment with T3-TRLs can further accelerate TRLs uptake in BAT (Cypess et al. 2009; Bartelt et al. 2011). Importantly, previous studies have revealed that cold exposure can elicit the expression of CD36, a protein involved in lipid disposal, on the surface of endothelial cells in BAT, and TRLs internalization in BAT depends on the presence of CD36 on endothelial cells (Fischer et al. 2021; Bartelt et al. 2011). Moreover, treatment with TRLs activates reactive oxygen species (ROS)-dependent hypoxia-inducible factor 1- α (HIF1 α) in endothelial cells, which further promotes thermogenic remodeling of BAT and beiging of WAT (Fischer et al. 2021). Therefore, it can be postulated that cold exposure acts as a trigger in a “domino effect”. It first activates BAT and increases T3-TRLs uptake in BAT. The increased uptake of T3-TRLs further increases the thermogenic remodeling of BAT and energy consumption.

Given cold exposure is a feasible method to switch on the uptake of T3-TRLs in BAT, elucidating the expression of thermogenic marker *Ucp1* in BAT could evaluate the effects of T3-TRLs. Previous studies have shown that treatment with T3 via intraperitoneal injection (i.p.) can stimulate BAT and upregulate the expression of *Ucp1* (Yau et al. 2019). Notably, in this thesis, mice treated with T3-TRLs via i.v. injection showed a significant increase in the expression of thermogenic markers (*Ucp1* and *Dio2*) (Figure 31). The immunohistological UCP1 staining of BAT also confirmed this finding (Figure 34). However, nonencapsulated T3 might also lead to an increase in the expression of thermogenic markers. Since the nonencapsulated T3 in T3-TRLs showed a lower concentration level than the normal T3 level in WT mouse plasma (Figure 28), it is suggested that the nonencapsulated T3 could not be enough to mediate the upregulation of thermogenic markers in BAT. Therefore, it is likely that the uptake of T3-TRLs is responsible for the increased T3-mediated expression of thermogenic markers in BAT.

While it is clear that the liver is the main organ that metabolizes TRLs in circulation (Heeren and Scheja 2021), the effect induced by treatment with drug-loaded TRLs on the liver has not been investigated. The expression of *Dio1* and *Me1* in the liver has been previously shown to be highly related to the hepatic T3 level (Zavacki et al. 2005; Goldberg et al. 2012). Furthermore, T3 also regulates the expression of FA oxidation genes (*Cpt1a* and *Ppara*) in the liver (Simcox et al. 2017). Importantly, this thesis found that treatment with T3-TRLs significantly upregulated the expression of *Dio1*, *Me1*, *Cpt1a*, and *Ppara* in the liver (Figure 32). Therefore, it is clear that T3 has been successfully delivered to the liver by T3-TRLs and induced the expression of T3-related genes in the liver. Additionally, the liver is the main player in lipoprotein metabolism, and TRL remnants are taken up by hepatocytes via endocytosis (Heeren and Scheja 2021). Accordingly, it could also be postulated that utilizing TRLs as carriers to deliver T3 to the liver could provide an additional promising approach for liver-targeted delivery and treat metabolic syndromes such as NAFLD and hepatocellular carcinoma (HCC) (Marta A. Kowalik, Columbano, and Perra 2018; Marta Anna Kowalik et al. 2020; Tanase et al. 2020; Perra et al. 2008).

However, the effects of T3-TRLs on whole-body metabolism and the duration of treatment remain to be further investigated and improved. The concentration of thyroid hormone in the circulation is controlled by a negative feedback mechanism in which raising thyroid hormone levels inhibits the secretion of TSH (Snyder and Utiger 1972). Examining TSH concentrations in serum after treatments might provide more insights into the advantages of applying T3-TRLs than traditional administrations. Moreover, the differences in oxygen consumption between the treated group and

the control group were not significant, underlining that the duration of treatment with T3-TRLs might not be long enough to induce significant changes in oxygen consumption.

Additionally, Than et al. developed a T3-loaded microneedle patch and observed an increase in the expression of *Ucp1* after applying T3-loaded microneedle patches to the iWAT of mice (Than et al. 2017). Nevertheless, the application of the microneedle patch slightly raised serum T3 levels. The treatment showed less specific tissue targeting, and it remains to be seen whether this effect differs from direct T3 injections. Taken together, combining thyroid hormones with pharmaceutical technologies is still considered a novel and challenging therapeutic approach in obesity therapies. So far, the data in this thesis show that T3-TRLs could be a potential therapeutic option to target the BAT and the liver.

7 Summary

AT plays an essential role in controlling metabolic activities. WAT stores energy and possesses endocrine functions, while BAT is responsible for energy expenditure as well as glucose and lipids uptake showing a thermogenic capacity (Pfeifer and Hoffmann 2015). However, in obese individuals, WAT can become dysfunctional, inflamed, and unable to store the excessive energy properly, leading to symptoms such as fatty liver and systemic inflammation (Ellulu et al. 2017; Longo et al. 2019; Fabbrini, Sullivan, and Klein 2010; Zatterale et al. 2019). Moreover, obese patients have less active BAT than lean healthy individuals (Leitner et al. 2017). Due to the very limited amount of BAT in adult obese patients, activating BAT to increase energy consumption for obese patients faces many challenges. Interestingly, several drugs have been utilized as promising candidates for treating obesity in clinical trials, such as T3 (a thyroid hormone) in the 1980s (Moore et al. 1980) and MIR (an ADRB3 agonist) in 2020 (O'Mara et al. 2020). Nevertheless, they may elicit some inadvertent adverse effects from conventional oral administration at a high dose (Cypess et al. 2009; Kaptein, Beale, and Chan 2009). Therefore, due to the growing number of obese patients worldwide, there is an urgent need to develop novel anti-obesity therapies that combine pharmaceutical technologies with marketed drugs to induce WAT beiging and activate BAT, while minimizing side effects.

Here, this thesis demonstrates two drug delivery systems (Figure 36): i) a controlled drug delivery system with poly (lactic-co-glycolic acid) PLGA microparticles (PLGA MPs) as carriers and ii) a targeted drug delivery system using triglyceride-rich lipoproteins (TRLs). MIR and T3 are loaded into PLGA MPs and TRLs to induce WAT beiging and BAT activation, respectively. Interestingly, data in the first part of this thesis suggest that MIR-MPs measured with a size of 30 μm can successfully induce WA beiging and also increase lipolysis *in vitro* and *ex vivo* both in murine iWAT and human scWAT via ADRB3. The second part of this thesis focuses on establishing drug-loaded TRLs. Developed TRLs can encapsulate T3 with an encapsulation efficiency of $40.8 \pm 1.8\%$. As the most promising feature of T3-TRLs, T3-TRLs possess not only a targeted delivery function to the liver and the BAT but also present promising *in vivo* therapeutic effects involving BAT activation. These two methods combine FDA-approved drugs and pharmaceutical technologies intending to reduce the side effects induced by the “off-label” uses of drugs and inspire new strategies for the treatment of obesity and its associated metabolic diseases.

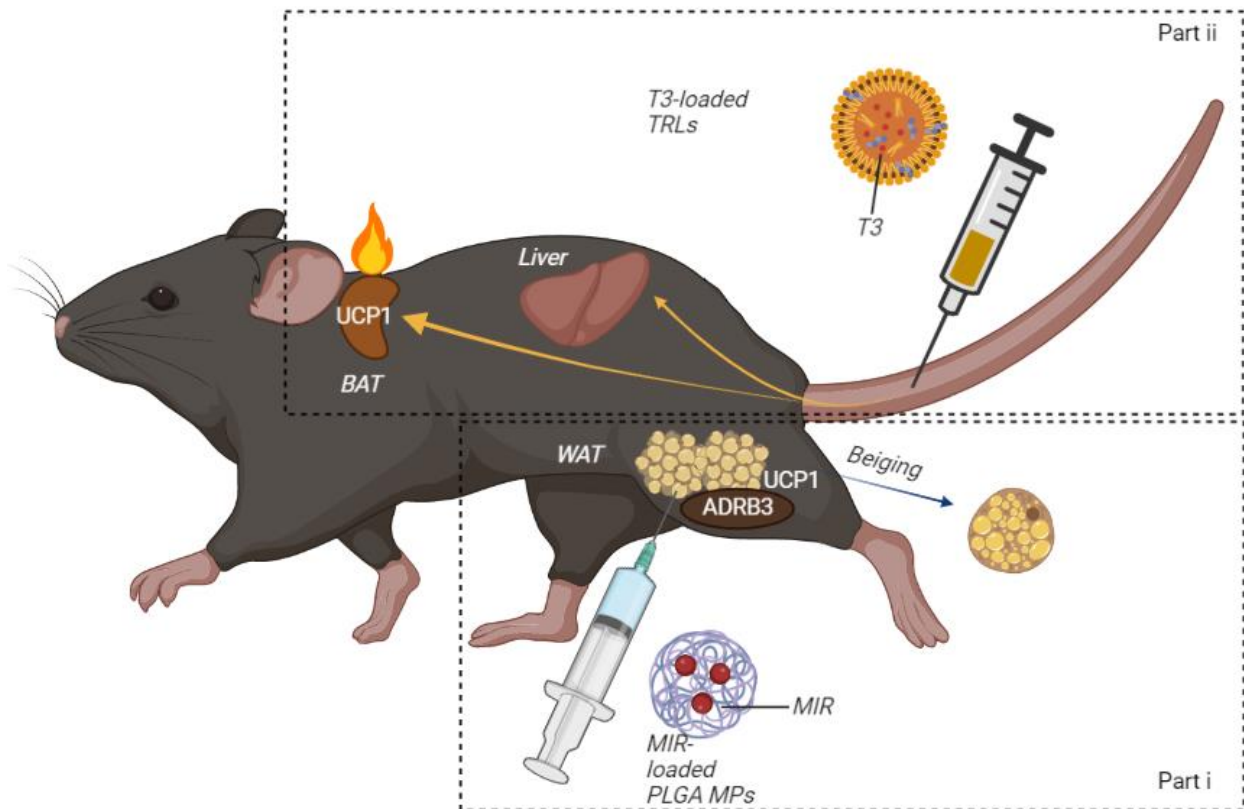


Figure 36. Scheme illustration of mechanisms of MIR-MPs and T3-TRLs. The scheme is generated using Bio render. ADRB3: beta 3-adrenergic receptors, UCP1: Uncoupling Protein 1, BAT: brown adipose tissue, WAT: white adipose tissue, T3: Triiodothyronine, TRLs: triglyceride-rich lipoproteins, MIR: mirabegron, PLGA MPs: poly (lactic-co-glycolic acid) PLGA microparticles.

8 References

- Adams, Andrew C., Inna Astapova, Ffolliott M. Fisher, Michael K. Badman, Katherine E. Kurgansky, Jeffrey S. Flier, Anthony N. Hollenberg, and Eleftheria Maratos-Flier. 2010. "Thyroid Hormone Regulates Hepatic Expression of Fibroblast Growth Factor 21 in a PPAR α -Dependent Manner." *The Journal of Biological Chemistry* 285 (19): 14078–82. <https://doi.org/10.1074/jbc.C110.107375>.
- Adeyo, O., C. N. Goulbourne, A. Bensadoun, A. P. Beigneux, L. G. Fong, and S. G. Young. 2012. "Glycosylphosphatidylinositol-Anchored High-Density Lipoprotein-Binding Protein 1 and the Intravascular Processing of Triglyceride-Rich Lipoproteins." *Journal of Internal Medicine* 272 (6): 528–40. <https://doi.org/10.1111/joim.12003>.
- Agrahari, Vibhuti, Vivek Agrahari, and Ashim K Mitra. 2016. "Nanocarrier Fabrication and Macromolecule Drug Delivery: Challenges and Opportunities." *Therapeutic Delivery* 7 (4): 257–78. <https://doi.org/10.4155/tde-2015-0012>.
- Ahmadian, Maryam, Jae Myoung Suh, Nasun Hah, Christopher Liddle, Annette R. Atkins, Michael Downes, and Ronald M. Evans. 2013. "PPAR γ Signaling and Metabolism: The Good, the Bad and the Future." *Nature Medicine* 19 (5): 557–66. <https://doi.org/10.1038/nm.3159>.
- Ahmadian, Maryam, Yuhui Wang, and Hei Sook Sul. 2010. "Medicine in Focus: Lipolysis in Adipocytes." *The International Journal of Biochemistry & Cell Biology* 42 (5): 555–59. <https://doi.org/10.1016/j.biocel.2009.12.009>.
- Amoyav, Ben Zion, and Ofra Benny. 2019. "Microfluidic Based Fabrication and Characterization of Highly Porous Polymeric Microspheres." *Polymers* 11 (3). <https://doi.org/10.3390/polym11030419>.
- Andreotti, P. E., I. A. Cree, C. M. Kurbacher, D. M. Hartmann, D. Linder, G. Harel, I. Gleiberman, P. A. Caruso, S. H. Ricks, and M. Untch. 1995. "Chemosensitivity Testing of Human Tumors Using a Microplate Adenosine Triphosphate Luminescence Assay: Clinical Correlation for Cisplatin Resistance of Ovarian Carcinoma." *Cancer Research* 55 (22): 5276–82.
- Anselmo, Aaron C., and Samir Mitragotri. 2019. "Nanoparticles in the Clinic: An Update." *Bioengineering & Translational Medicine* 4 (3): e10143. <https://doi.org/10.1002/btm2.10143>.
- Arch, J. R., and S. Wilson. 1996. "Beta 3-Adrenoceptors and the Regulation of Metabolism in Adipose Tissues." *Biochemical Society Transactions* 24 (2): 412–18. <https://doi.org/10.1042/bst0240412>.
- Arch, Jonathan R. S. 2011. "Challenges in B3-Adrenoceptor Agonist Drug Development." *Therapeutic Advances in Endocrinology and Metabolism* 2 (2): 59–64. <https://doi.org/10.1177/2042018811398517>.
- Argyropoulos, George, and Mary-Ellen Harper. 2002. "Uncoupling Proteins and Thermoregulation." *Journal of Applied Physiology (Bethesda, Md.: 1985)* 92 (5): 2187–98. <https://doi.org/10.1152/japplphysiol.00994.2001>.
- Atgié, C., G. Faintrenie, C. Carpéne, L. J. Bukowiecki, and A. Gélœn. 1998. "Effects of Chronic Treatment with Noradrenaline or a Specific Beta3-Adrenergic Agonist, CL 316 243, on Energy Expenditure and Epididymal Adipocyte Lipolytic Activity in Rat." *Comparative Biochemistry and Physiology. Part A, Molecular & Integrative Physiology* 119 (2): 629–36. [https://doi.org/10.1016/s1095-6433\(97\)00476-5](https://doi.org/10.1016/s1095-6433(97)00476-5).
- Attia, Ramy R., Sara Connaughton, Lindsey R. Boone, Fang Wang, Marshall B. Elam, Gene C. Ness, George A. Cook, and Edwards A. Park. 2010. "Regulation of Pyruvate Dehydrogenase Kinase 4 (PDK4) by Thyroid Hormone: Role of the Peroxisome

- Proliferator-Activated Receptor Gamma Coactivator (PGC-1 Alpha)." *The Journal of Biological Chemistry* 285 (4): 2375–85. <https://doi.org/10.1074/jbc.M109.039081>.
- Azzu, Vian, and Martin D. Brand. 2010. "The on/off Switches of the Mitochondrial Uncoupling Proteins." *Trends in Biochemical Sciences* 35 (5): 298–307. <https://doi.org/10.1016/j.tibs.2009.11.001>.
- Bagchi, Devika P., and Ormond A. MacDougald. 2019. "Identification and Dissection of Diverse Mouse Adipose Depots." *Journal of Visualized Experiments : JoVE*, no. 149 (July): 10.3791/59499. <https://doi.org/10.3791/59499>.
- Ballinger, A. 2000. "Orlistat in the Treatment of Obesity." *Expert Opinion on Pharmacotherapy* 1 (4): 841–47. <https://doi.org/10.1517/14656566.1.4.841>.
- Barbatelli, G., I. Murano, L. Madsen, Q. Hao, M. Jimenez, K. Kristiansen, J. P. Giacobino, R. De Matteis, and S. Cinti. 2010. "The Emergence of Cold-Induced Brown Adipocytes in Mouse White Fat Depots Is Determined Predominantly by White to Brown Adipocyte Transdifferentiation." *American Journal of Physiology. Endocrinology and Metabolism* 298 (6): E1244–1253. <https://doi.org/10.1152/ajpendo.00600.2009>.
- Barichello, J. M., M. Morishita, K. Takayama, and T. Nagai. 1999. "Encapsulation of Hydrophilic and Lipophilic Drugs in PLGA Nanoparticles by the Nanoprecipitation Method." *Drug Development and Industrial Pharmacy* 25 (4): 471–76. <https://doi.org/10.1081/ddc-100102197>.
- Bartelt, Alexander, Oliver T. Bruns, Rudolph Reimer, Heinz Hohenberg, Harald Ittrich, Kersten Peldschus, Michael G. Kaul, et al. 2011. "Brown Adipose Tissue Activity Controls Triglyceride Clearance." *Nature Medicine* 17 (2): 200–205. <https://doi.org/10.1038/nm.2297>.
- Bartelt, Alexander, and Joerg Heeren. 2014. "Adipose Tissue Browning and Metabolic Health." *Nature Reviews. Endocrinology* 10 (1): 24–36. <https://doi.org/10.1038/nrendo.2013.204>.
- Beck, L. R., D. R. Cowsar, D. H. Lewis, J. W. Gibson, and C. E. Flowers. 1979. "New Long-Acting Injectable Microcapsule Contraceptive System." *American Journal of Obstetrics and Gynecology* 135 (3): 419–26. [https://doi.org/10.1016/0002-9378\(79\)90717-8](https://doi.org/10.1016/0002-9378(79)90717-8).
- Bel, Jocelyn S., T. C. Tai, Neelam Khaper, and Simon J. Lees. 2021. "Mirabegron: The Most Promising Adipose Tissue Beiging Agent." *Physiological Reports* 9 (5): e14779. <https://doi.org/10.14814/phy2.14779>.
- Bellinger, Denise L., Carlo Wood, Jon E. Wergedal, and Dianne Lorton. 2021. "Driving B2-While Suppressing α -Adrenergic Receptor Activity Suppresses Joint Pathology in Inflammatory Arthritis." *Frontiers in Immunology* 12 (June): 628065. <https://doi.org/10.3389/fimmu.2021.628065>.
- Berbée, Jimmy F. P., Mariëtte R. Boon, P. Padmini S. J. Khedoe, Alexander Bartelt, Christian Schlein, Anna Worthmann, Sander Kooijman, et al. 2015. "Brown Fat Activation Reduces Hypercholesterolaemia and Protects from Atherosclerosis Development." *Nature Communications* 6 (March): 6356. <https://doi.org/10.1038/ncomms7356>.
- Berkowitz, D. E., N. A. Nardone, R. M. Smiley, D. T. Price, D. K. Kreutter, R. T. Freneau, and D. A. Schwinn. 1995. "Distribution of Beta 3-Adrenoceptor mRNA in Human Tissues." *European Journal of Pharmacology* 289 (2): 223–28. [https://doi.org/10.1016/0922-4106\(95\)90098-5](https://doi.org/10.1016/0922-4106(95)90098-5).
- Berridge, Michael V., Patries M. Herst, and An S. Tan. 2005. "Tetrazolium Dyes as Tools in Cell Biology: New Insights into Their Cellular Reduction." *Biotechnology Annual Review* 11: 127–52. [https://doi.org/10.1016/S1387-2656\(05\)11004-7](https://doi.org/10.1016/S1387-2656(05)11004-7).
- Bi, Pengpeng, Tizhong Shan, Weiye Liu, Feng Yue, Xin Yang, Xin-Rong Liang, Jinghua Wang, et al. 2014. "Inhibition of Notch Signaling Promotes Browning of White Adipose Tissue and Ameliorates Obesity." *Nature Medicine* 20 (8): 911–18. <https://doi.org/10.1038/nm.3615>.

- Bianco, A. C., and J. E. Silva. 1987a. "Intracellular Conversion of Thyroxine to Triiodothyronine Is Required for the Optimal Thermogenic Function of Brown Adipose Tissue." *The Journal of Clinical Investigation* 79 (1): 295–300. <https://doi.org/10.1172/JCI112798>.
- . 1987b. "Nuclear 3,5,3'-Triiodothyronine (T3) in Brown Adipose Tissue: Receptor Occupancy and Sources of T3 as Determined by in Vivo Techniques." *Endocrinology* 120 (1): 55–62. <https://doi.org/10.1210/endo-120-1-55>.
- Bianco, Antonio C., Domenico Salvatore, Balázs Gereben, Marla J. Berry, and P. Reed Larsen. 2002. "Biochemistry, Cellular and Molecular Biology, and Physiological Roles of the Iodothyronine Selenodeiodinases." *Endocrine Reviews* 23 (1): 38–89. <https://doi.org/10.1210/edrv.23.1.0455>.
- Billington, Charlotte K, and Raymond B Penn. 2003. "Signaling and Regulation of G Protein-Coupled Receptors in Airway Smooth Muscle." *Respiratory Research* 4 (1): 2.
- Biondi, Bernadette, Emiliano A. Palmieri, Gaetano Lombardi, and Serafino Fazio. 2002. "Effects of Thyroid Hormone on Cardiac Function: The Relative Importance of Heart Rate, Loading Conditions, and Myocardial Contractility in the Regulation of Cardiac Performance in Human Hyperthyroidism." *The Journal of Clinical Endocrinology and Metabolism* 87 (3): 968–74. <https://doi.org/10.1210/jcem.87.3.8302>.
- Birnbaumer, L. 1992. "Receptor-to-Effector Signaling through G Proteins: Roles for Beta Gamma Dimers as Well as Alpha Subunits." *Cell* 71 (7): 1069–72. [https://doi.org/10.1016/s0092-8674\(05\)80056-x](https://doi.org/10.1016/s0092-8674(05)80056-x).
- Birsoy, Kivanç, William T. Festuccia, and Mathieu Laplante. 2013. "A Comparative Perspective on Lipid Storage in Animals." *Journal of Cell Science* 126 (Pt 7): 1541–52. <https://doi.org/10.1242/jcs.104992>.
- Blanco, Elvin, Haifa Shen, and Mauro Ferrari. 2015. "Principles of Nanoparticle Design for Overcoming Biological Barriers to Drug Delivery." *Nature Biotechnology* 33 (9): 941–51. <https://doi.org/10.1038/nbt.3330>.
- Blondin, Denis P., Soren Nielsen, Eline N. Kuipers, Mai C. Severinsen, Verena H. Jensen, Stéphanie Miard, Naja Z. Jespersen, et al. 2020. "Human Brown Adipocyte Thermogenesis Is Driven by B2-AR Stimulation." *Cell Metabolism* 32 (2): 287-300.e7. <https://doi.org/10.1016/j.cmet.2020.07.005>.
- Bobo, Daniel, Kye J. Robinson, Jiaul Islam, Kristofer J. Thurecht, and Simon R. Corrie. 2016. "Nanoparticle-Based Medicines: A Review of FDA-Approved Materials and Clinical Trials to Date." *Pharmaceutical Research* 33 (10): 2373–87. <https://doi.org/10.1007/s11095-016-1958-5>.
- Brand, Martin D., and David G. Nicholls. 2011. "Assessing Mitochondrial Dysfunction in Cells." *Biochemical Journal* 435 (Pt 2): 297–312. <https://doi.org/10.1042/BJ20110162>.
- Briand, Olivier, Véronique Touche, Sophie Colin, Gemma Brufau, Alberto Davalos, Marleen Schonewille, Fabiola Bovenga, et al. 2016. "Liver X Receptor Regulates Triglyceride Absorption Through Intestinal Down-Regulation of Scavenger Receptor Class B, Type 1." *Gastroenterology* 150 (3): 650–58. <https://doi.org/10.1053/j.gastro.2015.11.015>.
- Bronnikov, G., T. Bengtsson, L. Kramarova, V. Golozoubova, B. Cannon, and J. Nedergaard. 1999. "Beta1 to Beta3 Switch in Control of Cyclic Adenosine Monophosphate during Brown Adipocyte Development Explains Distinct Beta-Adrenoceptor Subtype Mediation of Proliferation and Differentiation." *Endocrinology* 140 (9): 4185–97. <https://doi.org/10.1210/endo.140.9.6972>.
- Brown, N F, J K Hill, V Esser, J L Kirkland, B E Corkey, D W Foster, and J D McGarry. 1997. "Mouse White Adipocytes and 3T3-L1 Cells Display an Anomalous Pattern of Carnitine Palmitoyltransferase (CPT) I Isoform Expression during Differentiation. Inter-Tissue and Inter-Species Expression of CPT I and CPT II Enzymes." *Biochemical Journal* 327 (Pt 1): 225–31.

- Cahill, Thomas J., Alex R. B. Thomsen, Jeffrey T. Tarrasch, Bianca Plouffe, Anthony H. Nguyen, Fan Yang, Li-Yin Huang, et al. 2017. "Distinct Conformations of GPCR- β -Arrestin Complexes Mediate Desensitization, Signaling, and Endocytosis." *Proceedings of the National Academy of Sciences of the United States of America* 114 (10): 2562–67. <https://doi.org/10.1073/pnas.1701529114>.
- Campbell, Adrian P., and Alan V. Smrcka. 2018. "Targeting G Protein-Coupled Receptor Signalling by Blocking G Proteins." *Nature Reviews. Drug Discovery* 17 (11): 789–803. <https://doi.org/10.1038/nrd.2018.135>.
- Campbell, Frederick, Frank L. Bos, Sandro Sieber, Gabriela Arias-Alpizar, Bjørn E. Koch, Jörg Huwyler, Alexander Kros, and Jeroen Bussmann. 2018. "Directing Nanoparticle Biodistribution through Evasion and Exploitation of Stab2-Dependent Nanoparticle Uptake." *ACS Nano* 12 (3): 2138–50. <https://doi.org/10.1021/acsnano.7b06995>.
- Cannon, Barbara, and Jan Nedergaard. 2004. "Brown Adipose Tissue: Function and Physiological Significance." *Physiological Reviews* 84 (1): 277–359. <https://doi.org/10.1152/physrev.00015.2003>.
- Carpentier, André C., Denis P. Blondin, Kirsi A. Virtanen, Denis Richard, François Haman, and Éric E. Turcotte. 2018. "Brown Adipose Tissue Energy Metabolism in Humans." *Frontiers in Endocrinology* 9: 447. <https://doi.org/10.3389/fendo.2018.00447>.
- Casalini, Tommaso, Filippo Rossi, Andrea Castrovinci, and Giuseppe Perale. 2019. "A Perspective on Polylactic Acid-Based Polymers Use for Nanoparticles Synthesis and Applications." *Frontiers in Bioengineering and Biotechnology* 7: 259. <https://doi.org/10.3389/fbioe.2019.00259>.
- Casley-Smith, J. R. 1962. "The Identification of Chylomicra and Lipoproteins in Tissue Sections and Their Passage into Jejunal Lacteals." *The Journal of Cell Biology* 15 (November): 259–77. <https://doi.org/10.1083/jcb.15.2.259>.
- Cero, Cheryl, Hannah J. Lea, Kenneth Y. Zhu, Farnaz Shamsi, Yu-Hua Tseng, and Aaron M. Cypess. 2021. "B3-Adrenergic Receptors Regulate Human Brown/Beige Adipocyte Lipolysis and Thermogenesis." *JCI Insight* 6 (11): 139160. <https://doi.org/10.1172/jci.insight.139160>.
- Chang, Hung-Chun, and Leonard Guarente. 2014. "SIRT1 and Other Sirtuins in Metabolism." *Trends in Endocrinology and Metabolism: TEM* 25 (3): 138–45. <https://doi.org/10.1016/j.tem.2013.12.001>.
- Chen, Zhe, William D. Singer, Paul C. Sternweis, and Stephen R. Sprang. 2005. "Structure of the P115RhoGEF RgRGS Domain-G α 13/I1 Chimera Complex Suggests Convergent Evolution of a GTPase Activator." *Nature Structural & Molecular Biology* 12 (2): 191–97. <https://doi.org/10.1038/nsmb888>.
- Chusyd, Daniella E., Donghai Wang, Derek M. Huffman, and Tim R. Nagy. 2016. "Relationships between Rodent White Adipose Fat Pads and Human White Adipose Fat Depots." *Frontiers in Nutrition* 3 (April): 10. <https://doi.org/10.3389/fnut.2016.00010>.
- Cioffi, Federica, Alessandra Gentile, Elena Silvestri, Fernando Goglia, and Assunta Lombardi. 2018. "Effect of Iodothyronines on Thermogenesis: Focus on Brown Adipose Tissue." *Frontiers in Endocrinology* 9: 254. <https://doi.org/10.3389/fendo.2018.00254>.
- Cohen, Deborah. 2010. "Rosiglitazone: What Went Wrong?" *BMJ (Clinical Research Ed.)* 341 (September): c4848. <https://doi.org/10.1136/bmj.c4848>.
- Coleman, R. A., T. M. Lewin, and D. M. Muoio. 2000. "Physiological and Nutritional Regulation of Enzymes of Triacylglycerol Synthesis." *Annual Review of Nutrition* 20: 77–103. <https://doi.org/10.1146/annurev.nutr.20.1.77>.
- Collins, S., K. W. Daniel, E. M. Rohlf, V. Ramkumar, I. L. Taylor, and T. W. Gettys. 1994. "Impaired Expression and Functional Activity of the Beta 3- and Beta 1-Adrenergic Receptors in Adipose Tissue of Congenitally Obese (C57BL/6J Ob/Ob) Mice." *Molecular*

- Endocrinology (Baltimore, Md.)* 8 (4): 518–27.
<https://doi.org/10.1210/mend.8.4.7914350>.
- Collins, Sheila. 2012. “ β -Adrenoceptor Signaling Networks in Adipocytes for Recruiting Stored Fat and Energy Expenditure.” *Frontiers in Endocrinology* 2 (January): 102.
<https://doi.org/10.3389/fendo.2011.00102>.
- Colquitt, Jill L., Karen Pickett, Emma Loveman, and Geoff K. Frampton. 2014. “Surgery for Weight Loss in Adults.” *The Cochrane Database of Systematic Reviews*, no. 8 (August): CD003641. <https://doi.org/10.1002/14651858.CD003641.pub4>.
- Commins, S. P., D. J. Marsh, S. A. Thomas, P. M. Watson, M. A. Padgett, R. Palmiter, and T. W. Gettys. 1999. “Norepinephrine Is Required for Leptin Effects on Gene Expression in Brown and White Adipose Tissue.” *Endocrinology* 140 (10): 4772–78.
<https://doi.org/10.1210/endo.140.10.7043>.
- Cotecchia, S., D. A. Schwinn, R. R. Randall, R. J. Lefkowitz, M. G. Caron, and B. K. Kobilka. 1988. “Molecular Cloning and Expression of the cDNA for the Hamster Alpha 1-Adrenergic Receptor.” *Proceedings of the National Academy of Sciences of the United States of America* 85 (19): 7159. <https://doi.org/10.1073/pnas.85.19.7159>.
- Cowsar, D. R., T. R. Tice, R. M. Gilley, and J. P. English. 1985. “Poly(Lactide-Co-Glycolide) Microcapsules for Controlled Release of Steroids.” *Methods in Enzymology* 112: 101–16. [https://doi.org/10.1016/s0076-6879\(85\)12010-0](https://doi.org/10.1016/s0076-6879(85)12010-0).
- Cypess, Aaron M., Sanaz Lehman, Gethin Williams, Ilan Tal, Dean Rodman, Allison B. Goldfine, Frank C. Kuo, et al. 2009. “Identification and Importance of Brown Adipose Tissue in Adult Humans.” *The New England Journal of Medicine* 360 (15): 1509–17.
<https://doi.org/10.1056/NEJMoa0810780>.
- Cypess, Aaron M., Lauren S. Weiner, Carla Roberts-Toler, Elisa Franquet Elía, Skyler H. Kessler, Peter A. Kahn, Jeffrey English, et al. 2015. “Activation of Human Brown Adipose Tissue by a B3-Adrenergic Receptor Agonist.” *Cell Metabolism* 21 (1): 33–38.
<https://doi.org/10.1016/j.cmet.2014.12.009>.
- Dallinga-Thie, Geesje M., Remco Franssen, Hans L. Mooij, Maartje E. Visser, H. Carlijnne Hassing, Frank Peelman, John J. P. Kastelein, Miklós Péterfy, and Max Nieuwdorp. 2010. “The Metabolism of Triglyceride-Rich Lipoproteins Revisited: New Players, New Insight.” *Atherosclerosis* 211 (1): 1–8.
<https://doi.org/10.1016/j.atherosclerosis.2009.12.027>.
- Danzi, Sara, and Irwin Klein. 2003. “Thyroid Hormone and Blood Pressure Regulation.” *Current Hypertension Reports* 5 (6): 513–20. <https://doi.org/10.1007/s11906-003-0060-7>.
- Dastis, Negrin S., E. François, J. Deviere, A. Hittelet, A. Ilah Mehdi, M. Barea, and J.-M. Dumonceau. 2009. “Intragastric Balloon for Weight Loss: Results in 100 Individuals Followed for at Least 2.5 Years.” *Endoscopy* 41 (7): 575–80. <https://doi.org/10.1055/s-0029-1214826>.
- Dehvari, Nodi, Masaaki Sato, Muhammad Hamza Bokhari, Anastasia Kalinovich, Seungmin Ham, Jie Gao, Huong T. M. Nguyen, et al. 2020. “The Metabolic Effects of Mirabegron Are Mediated Primarily by B3-adrenoceptors.” *Pharmacology Research & Perspectives* 8 (5): e00643. <https://doi.org/10.1002/prp2.643>.
- Denizot, F., and R. Lang. 1986. “Rapid Colorimetric Assay for Cell Growth and Survival. Modifications to the Tetrazolium Dye Procedure Giving Improved Sensitivity and Reliability.” *Journal of Immunological Methods* 89 (2): 271–77.
[https://doi.org/10.1016/0022-1759\(86\)90368-6](https://doi.org/10.1016/0022-1759(86)90368-6).
- Dewal, Revati S., and Kristin I. Stanford. 2019. “Effects of Exercise on Brown and Beige Adipocytes.” *Biochimica Et Biophysica Acta. Molecular and Cell Biology of Lipids* 1864 (1): 71–78. <https://doi.org/10.1016/j.bbalip.2018.04.013>.
- Dhanasekaran, N., and J. M. Dermott. 1996. “Signaling by the G12 Class of G Proteins.” *Cellular Signalling* 8 (4): 235–45. [https://doi.org/10.1016/0898-6568\(96\)00048-4](https://doi.org/10.1016/0898-6568(96)00048-4).

- Dimov, Nikolay, Elisabeth Kastner, Maryam Hussain, Yvonne Perrie, and Nicolas Szita. 2017. "Formation and Purification of Tailored Liposomes for Drug Delivery Using a Module-Based Micro Continuous-Flow System." *Scientific Reports* 7 (1): 12045. <https://doi.org/10.1038/s41598-017-11533-1>.
- Dinarvand, R., N. Sepehri, S. Manoochehri, H. Rouhani, and F. Atyabi. 2011. "Polylactide-Co-Glycolide Nanoparticles for Controlled Delivery of Anticancer Agents." *International Journal of Nanomedicine* 6: 877–95. <https://doi.org/10.2147/IJN.S18905>.
- Divakaruni, Ajit S., Alexander Paradyse, David A. Ferrick, Anne N. Murphy, and Martin Jastroch. 2014. "Analysis and Interpretation of Microplate-Based Oxygen Consumption and PH Data." *Methods in Enzymology* 547: 309–54. <https://doi.org/10.1016/B978-0-12-801415-8.00016-3>.
- Dominiczak, Marek H., and Muriel J. Caslake. 2011. "Apolipoproteins: Metabolic Role and Clinical Biochemistry Applications." *Annals of Clinical Biochemistry* 48 (Pt 6): 498–515. <https://doi.org/10.1258/acb.2011.011111>.
- Driskell, Ryan, Colin A. B. Jahoda, Cheng-Ming Chuong, Fiona Watt, and Valerie Horsley. 2014. "Defining Dermal Adipose Tissue." *Experimental Dermatology* 23 (9): 629–31. <https://doi.org/10.1111/exd.12450>.
- Eisenstein, Anna, and Katya Ravid. 2014. "G Protein-Coupled Receptors and Adipogenesis: A Focus on Adenosine Receptors." *Journal of Cellular Physiology* 229 (4): 414–21. <https://doi.org/10.1002/jcp.24473>.
- Ellulu, Mohammed S., Ismail Patimah, Huzwah Khaza'ai, Asmah Rahmat, and Yehia Abed. 2017. "Obesity and Inflammation: The Linking Mechanism and the Complications." *Archives of Medical Science : AMS* 13 (4): 851–63. <https://doi.org/10.5114/aoms.2016.58928>.
- Eltink, Charlotte, Jennifer Lee, Marloes Schaddelee, Wenhui Zhang, Virginie Kerbusch, John Meijer, Sjoerd van Marle, et al. 2012. "Single-Dose Pharmacokinetics and Absolute Bioavailability of Mirabegron, a B₃-Adrenoceptor Agonist for Treatment of Overactive Bladder." *International Journal of Clinical Pharmacology and Therapeutics* 50 (11): 838–50. <https://doi.org/10.5414/CP201782>.
- Escobar-Morreale, H. F., M. J. Obregón, F. Escobar del Rey, and G. Morreale de Escobar. 1999. "Tissue-Specific Patterns of Changes in 3,5,3'-Triiodo-L-Thyronine Concentrations in Thyroidectomized Rats Infused with Increasing Doses of the Hormone. Which Are the Regulatory Mechanisms?" *Biochimie* 81 (5): 453–62. [https://doi.org/10.1016/s0300-9084\(99\)80095-9](https://doi.org/10.1016/s0300-9084(99)80095-9).
- Evans, Bronwyn A., Jon Merlin, Tore Bengtsson, and Dana S. Hutchinson. 2019. "Adrenoceptors in White, Brown, and Brite Adipocytes." *British Journal of Pharmacology* 176 (14): 2416–32. <https://doi.org/10.1111/bph.14631>.
- Fabbrini, Elisa, Shelby Sullivan, and Samuel Klein. 2010. "Obesity and Nonalcoholic Fatty Liver Disease: Biochemical, Metabolic and Clinical Implications." *Hepatology (Baltimore, Md.)* 51 (2): 679–89. <https://doi.org/10.1002/hep.23280>.
- Fan, Jingqian, Yuangang Liu, Shibin Wang, Yulu Liu, Siming Li, Ruimin Long, Ran Zhang, and Ranjith Kumar Kankala. 2017. "Synthesis and Characterization of Innovative Poly(Lactide- Co -Glycolide)-(Poly- l -Ornithine/Fucoidan) Core-Shell Nanocarriers by Layer-by-Layer Self-Assembly." *RSC Advances* 7 (52): 32786–94. <https://doi.org/10.1039/C7RA04908K>.
- Fedorenko, Andriy, Polina V. Lishko, and Yuriy Kirichok. 2012. "Mechanism of Fatty-Acid-Dependent UCP1 Uncoupling in Brown Fat Mitochondria." *Cell* 151 (2): 400–413. <https://doi.org/10.1016/j.cell.2012.09.010>.
- Feingold, Kenneth R., and Carl Grunfeld. 2000. "Introduction to Lipids and Lipoproteins." In *Endotext*, edited by Kenneth R. Feingold, Bradley Anawalt, Alison Boyce, George

- Chrousos, Kathleen Dungan, Ashley Grossman, Jerome M. Hershman, et al. South Dartmouth (MA): MDText.com, Inc. <http://www.ncbi.nlm.nih.gov/books/NBK305896/>.
- Ferrannini, Giulia, Maria Namwanje, Bin Fang, Manashree Damle, Dylan Li, Qiongming Liu, Mitchell A. Lazar, and Li Qiang. 2016. "Genetic Backgrounds Determine Brown Remodeling of White Fat in Rodents." *Molecular Metabolism* 5 (10): 948–58. <https://doi.org/10.1016/j.molmet.2016.08.013>.
- Filippatos, Theodosios D., Christos S. Derdemezis, Irene F. Gazi, Eleni S. Nakou, Dimitri P. Mikhailidis, and Moses S. Elisaf. 2008. "Orlistat-Associated Adverse Effects and Drug Interactions: A Critical Review." *Drug Safety* 31 (1): 53–65. <https://doi.org/10.2165/00002018-200831010-00005>.
- Finlin, Brian S., Hasiyet Memetimin, Amy L. Confides, Ildiko Kasza, Beibei Zhu, Hemendra J. Vekaria, Brianna Harfmann, et al. 2018. "Human Adipose Beiging in Response to Cold and Mirabegron." *JCI Insight* 3 (15). <https://doi.org/10.1172/jci.insight.121510>.
- Fischer, Alexander W., Michelle Y. Jaekstein, Kristina Gottschling, Markus Heine, Frederike Sass, Nils Mangels, Christian Schlein, et al. 2021. "Lysosomal Lipoprotein Processing in Endothelial Cells Stimulates Adipose Tissue Thermogenic Adaptation." *Cell Metabolism* 33 (3): 547–564.e7. <https://doi.org/10.1016/j.cmet.2020.12.001>.
- Fisher, Ffolliott M., Sandra Kleiner, Nicholas Douris, Elliott C. Fox, Rina J. Mepani, Francisco Verdeguer, Jun Wu, et al. 2012. "FGF21 Regulates PGC-1 α and Browning of White Adipose Tissues in Adaptive Thermogenesis." *Genes & Development* 26 (3): 271–81. <https://doi.org/10.1101/gad.177857.111>.
- Flamant, Frédéric, John D. Baxter, Douglas Forrest, Samuel Refetoff, Herbert Samuels, Tom S. Scanlan, Bjorn Vennström, and Jacques Samarut. 2006. "International Union of Pharmacology. LIX. The Pharmacology and Classification of the Nuclear Receptor Superfamily: Thyroid Hormone Receptors." *Pharmacological Reviews* 58 (4): 705–11. <https://doi.org/10.1124/pr.58.4.3>.
- Flechtner-Mors, M., C. P. Jenkinson, A. Alt, G. Adler, and H. H. Ditschuneit. 2002. "In Vivo Alpha(1)-Adrenergic Lipolytic Activity in Subcutaneous Adipose Tissue of Obese Subjects." *The Journal of Pharmacology and Experimental Therapeutics* 301 (1): 229–33. <https://doi.org/10.1124/jpet.301.1.229>.
- Frühbeck, Gema, Leire Méndez-Giménez, José-Antonio Fernández-Formoso, Secundino Fernández, and Amaia Rodríguez. 2014. "Regulation of Adipocyte Lipolysis." *Nutrition Research Reviews* 27 (1): 63–93. <https://doi.org/10.1017/S095442241400002X>.
- Fujioka, Mamoru, Shigetaka Koda, Yuki Yoshi Morimoto, and Klaus Biemann. 1988. "Structure of FR900359, a Cyclic Depsipeptide from *Ardisia Crenata* Sims." *The Journal of Organic Chemistry* 53 (12): 2820–25. <https://doi.org/10.1021/jo00247a030>.
- Gallagher, Emily Jane, and Derek LeRoith. 2015. "Obesity and Diabetes: The Increased Risk of Cancer and Cancer-Related Mortality." *Physiological Reviews* 95 (3): 727–48. <https://doi.org/10.1152/physrev.00030.2014>.
- Garcia, Rolando A., James N. Roemmich, and Kate J. Claycombe. 2016. "Evaluation of Markers of Beige Adipocytes in White Adipose Tissue of the Mouse." *Nutrition & Metabolism* 13: 24. <https://doi.org/10.1186/s12986-016-0081-2>.
- GBD 2015 Obesity Collaborators, Ashkan Afshin, Mohammad H. Forouzanfar, Marissa B. Reitsma, Patrick Sur, Kara Estep, Alex Lee, et al. 2017. "Health Effects of Overweight and Obesity in 195 Countries over 25 Years." *The New England Journal of Medicine* 377 (1): 13–27. <https://doi.org/10.1056/NEJMoa1614362>.
- Gentile, Piergiorgio, Valeria Chiono, Irene Carmagnola, and Paul V. Hatton. 2014. "An Overview of Poly(Lactic-Co-Glycolic) Acid (PLGA)-Based Biomaterials for Bone Tissue Engineering." *International Journal of Molecular Sciences* 15 (3): 3640–59. <https://doi.org/10.3390/ijms15033640>.

- Gereben, Balázs, Ann Marie Zavacki, Scott Ribich, Brian W. Kim, Stephen A. Huang, Warner S. Simonides, Anikó Zeöld, and Antonio C. Bianco. 2008. "Cellular and Molecular Basis of Deiodinase-Regulated Thyroid Hormone Signaling." *Endocrine Reviews* 29 (7): 898–938. <https://doi.org/10.1210/er.2008-0019>.
- Ghorbani, M., T. H. Claus, and J. Himms-Hagen. 1997. "Hypertrophy of Brown Adipocytes in Brown and White Adipose Tissues and Reversal of Diet-Induced Obesity in Rats Treated with a Beta3-Adrenoceptor Agonist." *Biochemical Pharmacology* 54 (1): 121–31. [https://doi.org/10.1016/s0006-2952\(97\)00162-7](https://doi.org/10.1016/s0006-2952(97)00162-7).
- Gilman, A. G. 1987. "G Proteins: Transducers of Receptor-Generated Signals." *Annual Review of Biochemistry* 56: 615–49. <https://doi.org/10.1146/annurev.bi.56.070187.003151>.
- Gimlette, T. M. 1967. "Use of Sephadex Column Chromatography in the Assessment of Thyroid Status." *Journal of Clinical Pathology* 20 (2): 170–74. <https://doi.org/10.1136/jcp.20.2.170>.
- Goldberg, Ira J., Li-Shin Huang, Lesley A. Huggins, Shuiqing Yu, Prabhakara R. Nagareddy, Thomas S. Scanlan, and Joel R. Ehrenkranz. 2012. "Thyroid Hormone Reduces Cholesterol via a Non-LDL Receptor-Mediated Pathway." *Endocrinology* 153 (11): 5143–49. <https://doi.org/10.1210/en.2012-1572>.
- Goldstein, Joseph L., and Michael S. Brown. 2009. "The LDL Receptor." *Arteriosclerosis, Thrombosis, and Vascular Biology* 29 (4): 431–38. <https://doi.org/10.1161/ATVBAHA.108.179564>.
- Gordon, Scott M., Susanna Hofmann, David S. Askew, and W. Sean Davidson. 2011. "High-Density Lipoprotein: It's Not Just about Lipid Transport Anymore." *Trends in Endocrinology and Metabolism: TEM* 22 (1): 9–15. <https://doi.org/10.1016/j.tem.2010.10.001>.
- Goudriaan, Jeltje R., Marion A. M. den Boer, Patrick C. N. Rensen, Maria Febbraio, Folkert Kuipers, Johannes A. Romijn, Louis M. Havekes, and Peter J. Voshol. 2005. "CD36 Deficiency in Mice Impairs Lipoprotein Lipase-Mediated Triglyceride Clearance." *Journal of Lipid Research* 46 (10): 2175–81. <https://doi.org/10.1194/jlr.M500112-JLR200>.
- Gregoire, F. M., C. M. Smas, and H. S. Sul. 1998. "Understanding Adipocyte Differentiation." *Physiological Reviews* 78 (3): 783–809. <https://doi.org/10.1152/physrev.1998.78.3.783>.
- Grujic, D., V. S. Susulic, M. E. Harper, J. Himms-Hagen, B. A. Cunningham, B. E. Corkey, and B. B. Lowell. 1997. "Beta3-Adrenergic Receptors on White and Brown Adipocytes Mediate Beta3-Selective Agonist-Induced Effects on Energy Expenditure, Insulin Secretion, and Food Intake. A Study Using Transgenic and Gene Knockout Mice." *The Journal of Biological Chemistry* 272 (28): 17686–93. <https://doi.org/10.1074/jbc.272.28.17686>.
- Guerre-Millo, M. 2004. "Adipose Tissue and Adipokines: For Better or Worse." *Diabetes & Metabolism* 30 (1): 13–19. [https://doi.org/10.1016/s1262-3636\(07\)70084-8](https://doi.org/10.1016/s1262-3636(07)70084-8).
- Hall, Jessica A., Scott Ribich, Marcelo A. Christoffolete, Gordana Simovic, Mayrin Correa-Medina, Mary Elizabeth Patti, and Antonio C. Bianco. 2010. "Absence of Thyroid Hormone Activation during Development Underlies a Permanent Defect in Adaptive Thermogenesis." *Endocrinology* 151 (9): 4573–82. <https://doi.org/10.1210/en.2010-0511>.
- Hanoune, J., and N. Defer. 2001. "Regulation and Role of Adenylyl Cyclase Isoforms." *Annual Review of Pharmacology and Toxicology* 41: 145–74. <https://doi.org/10.1146/annurev.pharmtox.41.1.145>.
- Hauser, Alexander S., Misty M. Attwood, Mathias Rask-Andersen, Helgi B. Schiöth, and David E. Gloriam. 2017. "Trends in GPCR Drug Discovery: New Agents, Targets and Indications." *Nature Reviews. Drug Discovery* 16 (12): 829–42. <https://doi.org/10.1038/nrd.2017.178>.

- Heeren, Joerg, and Ludger Scheja. 2021. "Metabolic-Associated Fatty Liver Disease and Lipoprotein Metabolism." *Molecular Metabolism* 50 (August): 101238. <https://doi.org/10.1016/j.molmet.2021.101238>.
- Hemmerlyckx, Bianca, Marijke Gaekens, David J. Gallacher, Hua Rong Lu, and Henri Roger Lijnen. 2013. "Effect of Rosiglitazone on Liver Structure and Function in Genetically Diabetic Akita Mice." *Basic & Clinical Pharmacology & Toxicology* 113 (5): 353–60. <https://doi.org/10.1111/bcpt.12104>.
- Hildebrand, Staffan, Norbert Löwa, Hendrik Paysen, Raluca M. Fratila, Laia Reverte-Salisa, Thithawat Trakoolwilaiwan, Zheming Niu, et al. 2021. "Quantification of Lipoprotein Uptake in Vivo Using Magnetic Particle Imaging and Spectroscopy." *ACS Nano* 15 (1): 434–46. <https://doi.org/10.1021/acsnano.0c03229>.
- Himms-Hagen, J. 1984. "Nonshivering Thermogenesis." *Brain Research Bulletin* 12 (2): 151–60. [https://doi.org/10.1016/0361-9230\(84\)90183-7](https://doi.org/10.1016/0361-9230(84)90183-7).
- . 1989. "Brown Adipose Tissue Thermogenesis and Obesity." *Progress in Lipid Research* 28 (2): 67–115. [https://doi.org/10.1016/0163-7827\(89\)90009-x](https://doi.org/10.1016/0163-7827(89)90009-x).
- Hjemdahl, P., and B. Linde. 1983. "Influence of Circulating NE and Epi on Adipose Tissue Vascular Resistance and Lipolysis in Humans." *The American Journal of Physiology* 245 (3): H447–452. <https://doi.org/10.1152/ajpheart.1983.245.3.H447>.
- Hoeke, Geerte, Sander Kooijman, Mariëtte R. Boon, Patrick C. N. Rensen, and Jimmy F. P. Berbée. 2016. "Role of Brown Fat in Lipoprotein Metabolism and Atherosclerosis." *Circulation Research* 118 (1): 173–82. <https://doi.org/10.1161/CIRCRESAHA.115.306647>.
- Hoffmans, M. D., D. Kromhout, and C. de Lezenne Coulander. 1988. "The Impact of Body Mass Index of 78,612 18-Year Old Dutch Men on 32-Year Mortality from All Causes." *Journal of Clinical Epidemiology* 41 (8): 749–56. [https://doi.org/10.1016/0895-4356\(88\)90161-8](https://doi.org/10.1016/0895-4356(88)90161-8).
- Honor, R. C., G. S. Dhillon, and C. Londos. 1985. "CAMP-Dependent Protein Kinase and Lipolysis in Rat Adipocytes. II. Definition of Steady-State Relationship with Lipolytic and Antilipolytic Modulators." *The Journal of Biological Chemistry* 260 (28): 15130–38.
- Ibrahim, M. Mohsen. 2010. "Subcutaneous and Visceral Adipose Tissue: Structural and Functional Differences." *Obesity Reviews: An Official Journal of the International Association for the Study of Obesity* 11 (1): 11–18. <https://doi.org/10.1111/j.1467-789X.2009.00623.x>.
- Ingebrigtsen, Sveinung G., Nataša Škalko-Basnet, Cristiane de Albuquerque Cavalcanti Jacobsen, and Ann Mari Holsæter. 2017. "Successful Co-Encapsulation of Benzoyl Peroxide and Chloramphenicol in Liposomes by a Novel Manufacturing Method - Dual Asymmetric Centrifugation." *European Journal of Pharmaceutical Sciences: Official Journal of the European Federation for Pharmaceutical Sciences* 97 (January): 192–99. <https://doi.org/10.1016/j.ejps.2016.11.017>.
- Jain, R. A. 2000. "The Manufacturing Techniques of Various Drug Loaded Biodegradable Poly(Lactide-Co-Glycolide) (PLGA) Devices." *Biomaterials* 21 (23): 2475–90. [https://doi.org/10.1016/s0142-9612\(00\)00115-0](https://doi.org/10.1016/s0142-9612(00)00115-0).
- Jiang, Chunhui, Mario Alberto Cano-Vega, Feng Yue, Liangju Kuang, Naagarajan Narayanan, Gozde Uzunalli, Madeline P. Merkel, Shihuan Kuang, and Meng Deng. 2017. "Dibenzazepine-Loaded Nanoparticles Induce Local Browning of White Adipose Tissue to Counteract Obesity." *Molecular Therapy: The Journal of the American Society of Gene Therapy* 25 (7): 1718–29. <https://doi.org/10.1016/j.ymthe.2017.05.020>.
- Johansson, C., B. Vennström, and P. Thorén. 1998. "Evidence That Decreased Heart Rate in Thyroid Hormone Receptor-Alpha1-Deficient Mice Is an Intrinsic Defect." *The American Journal of Physiology* 275 (2): R640–646. <https://doi.org/10.1152/ajpregu.1998.275.2.R640>.

- Jung, Un Ju, and Myung-Sook Choi. 2014. "Obesity and Its Metabolic Complications: The Role of Adipokines and the Relationship between Obesity, Inflammation, Insulin Resistance, Dyslipidemia and Nonalcoholic Fatty Liver Disease." *International Journal of Molecular Sciences* 15 (4): 6184–6223. <https://doi.org/10.3390/ijms15046184>.
- Kang, Yanyong, X. Edward Zhou, Xiang Gao, Yuanzheng He, Wei Liu, Andrii Ishchenko, Anton Barty, et al. 2015. "Crystal Structure of Rhodopsin Bound to Arrestin by Femtosecond X-Ray Laser." *Nature* 523 (7562): 561–67. <https://doi.org/10.1038/nature14656>.
- Kannabiran, Sukanya Arcot, Dominic Gosejacob, Birte Niemann, Viacheslav O. Nikolaev, and Alexander Pfeifer. 2020. "Real-Time Monitoring of CAMP in Brown Adipocytes Reveals Differential Compartmentation of B1 and B3-Adrenoceptor Signalling." *Molecular Metabolism* 37 (July): 100986. <https://doi.org/10.1016/j.molmet.2020.100986>.
- Kaptein, Elaine M., Elizabeth Beale, and Linda S. Chan. 2009. "Thyroid Hormone Therapy for Obesity and Nonthyroidal Illnesses: A Systematic Review." *The Journal of Clinical Endocrinology and Metabolism* 94 (10): 3663–75. <https://doi.org/10.1210/jc.2009-0899>.
- Khedoe, P. Padmini S. J., Geerte Hoeke, Sander Kooijman, Wieneke Dijk, Jeroen T. Buijs, Sander Kersten, Louis M. Havekes, et al. 2015. "Brown Adipose Tissue Takes up Plasma Triglycerides Mostly after Lipolysis." *Journal of Lipid Research* 56 (1): 51–59. <https://doi.org/10.1194/jlr.M052746>.
- Kim, Ja-Young, Esther van de Wall, Mathieu Laplante, Anthony Azzara, Maria E. Trujillo, Susanna M. Hofmann, Todd Schraw, et al. 2007. "Obesity-Associated Improvements in Metabolic Profile through Expansion of Adipose Tissue." *The Journal of Clinical Investigation* 117 (9): 2621–37. <https://doi.org/10.1172/JCI31021>.
- Kinlaw, W. B., J. L. Church, J. Harmon, and C. N. Mariash. 1995. "Direct Evidence for a Role of the 'Spot 14' Protein in the Regulation of Lipid Synthesis." *The Journal of Biological Chemistry* 270 (28): 16615–18. <https://doi.org/10.1074/jbc.270.28.16615>.
- Kissel, T., Z. Brich, S. Bantle, I. Lancranjan, F. Nimmerfall, and P. Vit. 1991. "Parenteral Depot-Systems on the Basis of Biodegradable Polyesters." *Journal of Controlled Release* 16 (1): 27–41. [https://doi.org/10.1016/0168-3659\(91\)90028-C](https://doi.org/10.1016/0168-3659(91)90028-C).
- Klepac, Katarina, Ana Kilić, Thorsten Gnad, Loren M. Brown, Beate Herrmann, Andrea Wilderman, Aileen Balkow, et al. 2016. "The Gq Signalling Pathway Inhibits Brown and Beige Adipose Tissue." *Nature Communications* 7 (March). <https://doi.org/10.1038/ncomms10895>.
- Kohane, Daniel S. 2007. "Microparticles and Nanoparticles for Drug Delivery." *Biotechnology and Bioengineering* 96 (2): 203–9. <https://doi.org/10.1002/bit.21301>.
- Köhrle, J. 1999. "Local Activation and Inactivation of Thyroid Hormones: The Deiodinase Family." *Molecular and Cellular Endocrinology* 151 (1–2): 103–19. [https://doi.org/10.1016/s0303-7207\(99\)00040-4](https://doi.org/10.1016/s0303-7207(99)00040-4).
- Koley, Dipankar, and Allen J. Bard. 2010. "Triton X-100 Concentration Effects on Membrane Permeability of a Single HeLa Cell by Scanning Electrochemical Microscopy (SECM)." *Proceedings of the National Academy of Sciences of the United States of America* 107 (39): 16783–87. <https://doi.org/10.1073/pnas.1011614107>.
- Kostka, Grażyna, Danuta Palut, Joanna Kopeć-Szlęzak, and Jan K. Ludwicki. 1999. "Early Hepatic Changes in Rats Induced by Permethrin in Comparison with DDT." *Toxicology* 142 (2): 135–43. [https://doi.org/10.1016/S0300-483X\(99\)00164-X](https://doi.org/10.1016/S0300-483X(99)00164-X).
- Kotzbeck, Petra, Antonio Giordano, Eleonora Mondini, Incoronata Murano, Ilenia Severi, Wiebe Venema, Maria Paola Cecchini, et al. 2018. "Brown Adipose Tissue Whitening Leads to Brown Adipocyte Death and Adipose Tissue Inflammation." *Journal of Lipid Research* 59 (5): 784–94. <https://doi.org/10.1194/jlr.M079665>.
- Kowalik, Marta A., Amedeo Columbano, and Andrea Perra. 2018. "Thyroid Hormones, Thyromimetics and Their Metabolites in the Treatment of Liver Disease." *Frontiers in Endocrinology* 9 (July): 382. <https://doi.org/10.3389/fendo.2018.00382>.

- Kowalik, Marta Anna, Elisabetta Puliga, Lavinia Cabras, Pia Sulas, Annalisa Petrelli, Andrea Perra, Giovanna Maria Ledda-Columbano, et al. 2020. "Thyroid Hormone Inhibits Hepatocellular Carcinoma Progression via Induction of Differentiation and Metabolic Reprogramming." *Journal of Hepatology* 72 (6): 1159–69. <https://doi.org/10.1016/j.jhep.2019.12.018>.
- Krotkiewski, M. 2000. "Thyroid Hormones and Treatment of Obesity." *International Journal of Obesity and Related Metabolic Disorders: Journal of the International Association for the Study of Obesity* 24 Suppl 2 (June): S116–119. <https://doi.org/10.1038/sj.ijo.0801294>.
- Kulkarni, R. K., E. G. Moore, A. F. Hegyeli, and F. Leonard. 1971. "Biodegradable Poly(Lactic Acid) Polymers." *Journal of Biomedical Materials Research* 5 (3): 169–81. <https://doi.org/10.1002/jbm.820050305>.
- Kumar, Priti, Arvindhan Nagarajan, and Pradeep D. Uchil. 2018. "Analysis of Cell Viability by the MTT Assay." *Cold Spring Harbor Protocols* 2018 (6). <https://doi.org/10.1101/pdb.prot095505>.
- Kumari, Punita, Ashish Srivastava, Ramanuj Banerjee, Eshan Ghosh, Pragya Gupta, Ravi Ranjan, Xin Chen, et al. 2016. "Functional Competence of a Partially Engaged GPCR- β -Arrestin Complex." *Nature Communications* 7 (November): 13416. <https://doi.org/10.1038/ncomms13416>.
- Lafontan, M. 1994. "Differential Recruitment and Differential Regulation by Physiological Amines of Fat Cell Beta-1, Beta-2 and Beta-3 Adrenergic Receptors Expressed in Native Fat Cells and in Transfected Cell Lines." *Cellular Signalling* 6 (4): 363–92. [https://doi.org/10.1016/0898-6568\(94\)90085-x](https://doi.org/10.1016/0898-6568(94)90085-x).
- Lagrec, Elena, Valentina Onesto, Concetta Di Natale, Sara La Manna, Paolo Antonio Netti, and Raffaele Vecchione. 2020. "Recent Advances in the Formulation of PLGA Microparticles for Controlled Drug Delivery." *Progress in Biomaterials* 9 (4): 153–74. <https://doi.org/10.1007/s40204-020-00139-y>.
- Långberg, Ewa-Carin, Mohammed Seed Ahmed, Suad Efendic, Harvest F. Gu, and Claes-Göran Östenson. 2013. "Genetic Association of Adrenergic Receptor Alpha 2A with Obesity and Type 2 Diabetes." *Obesity (Silver Spring, Md.)* 21 (8): 1720–25. <https://doi.org/10.1002/oby.20162>.
- Lanni, A., M. De Felice, A. Lombardi, M. Moreno, C. Fleury, D. Ricquier, and F. Goglia. 1997. "Induction of UCP2 mRNA by Thyroid Hormones in Rat Heart." *FEBS Letters* 418 (1–2): 171–74. [https://doi.org/10.1016/s0014-5793\(97\)01375-6](https://doi.org/10.1016/s0014-5793(97)01375-6).
- Larsson, Susanna C., Alicja Wolk, Niclas Håkansson, and Magnus Bäck. 2017. "Overall and Abdominal Obesity and Incident Aortic Valve Stenosis: Two Prospective Cohort Studies." *European Heart Journal* 38 (28): 2192–97. <https://doi.org/10.1093/eurheartj/ehx140>.
- Lass, Achim, Robert Zimmermann, Guenter Haemmerle, Monika Riederer, Gabriele Schoiswohl, Martina Schweiger, Petra Kienesberger, Juliane G. Strauss, Gregor Gorkiewicz, and Rudolf Zechner. 2006. "Adipose Triglyceride Lipase-Mediated Lipolysis of Cellular Fat Stores Is Activated by CGI-58 and Defective in Chanarin-Dorfman Syndrome." *Cell Metabolism* 3 (5): 309–19. <https://doi.org/10.1016/j.cmet.2006.03.005>.
- Leelarasamee, N., S. A. Howard, C. J. Malanga, L. A. Luzzi, T. F. Hogan, S. J. Kandzari, and J. K. Ma. 1986. "Kinetics of Drug Release from Polylactic Acid-Hydrocortisone Microcapsules." *Journal of Microencapsulation* 3 (3): 171–79. <https://doi.org/10.3109/02652048609031571>.
- Leitner, Brooks P., Shan Huang, Robert J. Brychta, Courtney J. Duckworth, Alison S. Baskin, Suzanne McGehee, Ilan Tal, et al. 2017. "Mapping of Human Brown Adipose Tissue in Lean and Obese Young Men." *Proceedings of the National Academy of Sciences of the United States of America* 114 (32): 8649–54. <https://doi.org/10.1073/pnas.1705287114>.

- Leone Roberti Maggiore, Umberto, Linda Cardozo, Simone Ferrero, Filomena Sileo, Alice Cola, Fabio Del Deo, Marco Torella, Nicola Colacurci, Massimo Candiani, and Stefano Salvatore. 2014. "Mirabegron in the Treatment of Overactive Bladder." *Expert Opinion on Pharmacotherapy* 15 (6): 873–87. <https://doi.org/10.1517/14656566.2014.898752>.
- Li, Xin, and Kai Sun. 2018. "Regulation of Lipolysis in Adipose Tissue and Clinical Significance." In *Neural Regulation of Metabolism*, edited by Qi Wu and Ruimao Zheng, 199–210. *Advances in Experimental Medicine and Biology*. Singapore: Springer. https://doi.org/10.1007/978-981-13-1286-1_11.
- Li, Ying, Anthony W. Frei, Irayme M. Labrada, Yanan Rong, Jia-Pu Liang, Magdalena M. Samojlik, Chuqiao Sun, et al. 2021. "Immunosuppressive PLGA TGF-B1 Microparticles Induce Polyclonal and Antigen-Specific Regulatory T Cells for Local Immunomodulation of Allogeneic Islet Transplants." *Frontiers in Immunology* 12: 653088. <https://doi.org/10.3389/fimmu.2021.653088>.
- Lin, Hong-Ru, Chun-Jung Kuo, C. Y. Yang, Shyh-Yu Shaw, and Yu-Jun Wu. 2002. "Preparation of Macroporous Biodegradable PLGA Scaffolds for Cell Attachment with the Use of Mixed Salts as Porogen Additives." *Journal of Biomedical Materials Research* 63 (3): 271–79. <https://doi.org/10.1002/jbm.10183>.
- Lin, Meng, and Xian-Rong Qi. 2018. "Purification Method of Drug-Loaded Liposome." In *Liposome-Based Drug Delivery Systems*, edited by Wan-Liang Lu and Xiang-Rong Qi, 1–11. *Biomaterial Engineering*. Berlin, Heidelberg: Springer. https://doi.org/10.1007/978-3-662-49231-4_24-1.
- Loh, Rebecca K. C., Melissa F. Formosa, Andre La Gerche, Anne T. Reutens, Bronwyn A. Kingwell, and Andrew L. Carey. 2019. "Acute Metabolic and Cardiovascular Effects of Mirabegron in Healthy Individuals." *Diabetes, Obesity & Metabolism* 21 (2): 276–84. <https://doi.org/10.1111/dom.13516>.
- Longo, Michele, Federica Zatterale, Jamal Naderi, Luca Parrillo, Pietro Formisano, Gregory Alexander Raciti, Francesco Beguinot, and Claudia Miele. 2019. "Adipose Tissue Dysfunction as Determinant of Obesity-Associated Metabolic Complications." *International Journal of Molecular Sciences* 20 (9): E2358. <https://doi.org/10.3390/ijms20092358>.
- Lü, Jian-Ming, Xinwen Wang, Christian Marin-Muller, Hao Wang, Peter H. Lin, Qizhi Yao, and Changyi Chen. 2009. "Current Advances in Research and Clinical Applications of PLGA-Based Nanotechnology." *Expert Review of Molecular Diagnostics* 9 (4): 325–41. <https://doi.org/10.1586/erm.09.15>.
- Lulich, K. M., R. G. Goldie, G. Ryan, and J. W. Paterson. 1986. "Adverse Reactions to Beta 2-Agonist Bronchodilators." *Medical Toxicology* 1 (4): 286–99. <https://doi.org/10.1007/BF03259844>.
- Luong, Quyen, Jun Huang, and Kevin Y. Lee. 2019. "Deciphering White Adipose Tissue Heterogeneity." *Biology* 8 (2): E23. <https://doi.org/10.3390/biology8020023>.
- Lusis, Aldons J., Alan M. Fogelman, and Gregg C. Fonarow. 2004. "Genetic Basis of Atherosclerosis: Part I: New Genes and Pathways." *Circulation* 110 (13): 1868–73. <https://doi.org/10.1161/01.CIR.0000143041.58692.CC>.
- Madamanchi, Aasakiran. 2007. "β-Adrenergic Receptor Signaling in Cardiac Function and Heart Failure." *McGill Journal of Medicine : MJM* 10 (2): 99–104.
- Maeda, N., M. Takahashi, T. Funahashi, S. Kihara, H. Nishizawa, K. Kishida, H. Nagaretani, et al. 2001. "PPARγ Ligands Increase Expression and Plasma Concentrations of Adiponectin, an Adipose-Derived Protein." *Diabetes* 50 (9): 2094–99. <https://doi.org/10.2337/diabetes.50.9.2094>.
- Maffetone, Philip B., Ivan Rivera-Dominguez, and Paul B. Laursen. 2016. "Overfat and Underfat: New Terms and Definitions Long Overdue." *Frontiers in Public Health* 4: 279. <https://doi.org/10.3389/fpubh.2016.00279>.

- Magalhaes, Ana C., Henry Dunn, and Stephen Sg Ferguson. 2012. "Regulation of GPCR Activity, Trafficking and Localization by GPCR-Interacting Proteins." *British Journal of Pharmacology* 165 (6): 1717–36. <https://doi.org/10.1111/j.1476-5381.2011.01552.x>.
- Mahley, R. W., T. L. Innerarity, S. C. Rall, and K. H. Weisgraber. 1984. "Plasma Lipoproteins: Apolipoprotein Structure and Function." *Journal of Lipid Research* 25 (12): 1277–94.
- Makadia, Hirenkumar K., and Steven J. Siegel. 2011. "Poly Lactic-Co-Glycolic Acid (PLGA) as Biodegradable Controlled Drug Delivery Carrier." *Polymers* 3 (3): 1377–97. <https://doi.org/10.3390/polym3031377>.
- Malik, M., E. M. van Gelderen, J. H. Lee, D. L. Kowalski, M. Yen, R. Goldwater, S. K. Mujais, et al. 2012. "Proarrhythmic Safety of Repeat Doses of Mirabegron in Healthy Subjects: A Randomized, Double-Blind, Placebo-, and Active-Controlled Thorough QT Study." *Clinical Pharmacology and Therapeutics* 92 (6): 696–706. <https://doi.org/10.1038/clpt.2012.181>.
- Mansbach, Charles M., and Shadab A. Siddiqi. 2010. "The Biogenesis of Chylomicrons." *Annual Review of Physiology* 72: 315–33. <https://doi.org/10.1146/annurev-physiol-021909-135801>.
- Manzano, Jimena, Beatriz Morte, Thomas S. Scanlan, and Juan Bernal. 2003. "Differential Effects of Triiodothyronine and the Thyroid Hormone Receptor Beta-Specific Agonist GC-1 on Thyroid Hormone Target Genes in the b Ain." *Endocrinology* 144 (12): 5480–87. <https://doi.org/10.1210/en.2003-0633>.
- Marken Lichtenbelt, Wouter D. van, and Patrick Schrauwen. 2011. "Implications of Nonshivering Thermogenesis for Energy Balance Regulation in Humans." *American Journal of Physiology. Regulatory, Integrative and Comparative Physiology* 301 (2): R285-296. <https://doi.org/10.1152/ajpregu.00652.2010>.
- Martyniak, Kari, and Michal M. Masternak. 2017. "Changes in Adipose Tissue Cellular Composition during Obesity and Aging as a Cause of Metabolic Dysregulation." *Experimental Gerontology* 94 (August): 59–63. <https://doi.org/10.1016/j.exger.2016.12.007>.
- Matsuno, F., S. Chowdhury, T. Gotoh, K. Iwase, H. Matsuzaki, K. Takatsuki, M. Mori, and M. Takiguchi. 1996. "Induction of the C/EBP Beta Gene by Dexamethasone and Glucagon in Primary-Cultured Rat Hepatocytes." *Journal of Biochemistry* 119 (3): 524–32. <https://doi.org/10.1093/oxfordjournals.jbchem.a021273>.
- Mayer, L. D., and G. St-Onge. 1995. "Determination of Free and Liposome-Associated Doxorubicin and Vincristine Levels in Plasma under Equilibrium Conditions Employing Ultrafiltration Techniques." *Analytical Biochemistry* 232 (2): 149–57. <https://doi.org/10.1006/abio.1995.0001>.
- McCudden, C. R., M. D. Hains, R. J. Kimple, D. P. Siderovski, and F. S. Willard. 2005. "G-Protein Signaling: Back to the Future." *Cellular and Molecular Life Sciences: CMLS* 62 (5): 551–77. <https://doi.org/10.1007/s00018-004-4462-3>.
- Mehta, A., S. P. Marso, and I. J. Neeland. 2016. "Liraglutide for Weight Management: A Critical Review of the Evidence." *Obesity Science & Practice* 3 (1): 3–14. <https://doi.org/10.1002/osp4.84>.
- Meleka, Matthew M., Alethia J. Edwards, Jingsheng Xia, Shelby A. Dahlen, Ipsita Mohanty, Matthew Medcalf, Shaili Aggarwal, Kevin D. Moeller, Ole V. Mortensen, and Patrick Osei-Owusu. 2019. "Anti-Hypertensive Mechanisms of Cyclic Depsipeptide Inhibitor Ligands for Gq/11 Class G Proteins." *Pharmacological Research* 141 (March): 264–75. <https://doi.org/10.1016/j.phrs.2019.01.012>.
- Meltzer, H. Y., B. Bastani, K. Y. Kwon, L. F. Ramirez, S. Burnett, and J. Sharpe. 1989. "A Prospective Study of Clozapine in Treatment-Resistant Schizophrenic Patients. I. Preliminary Report." *Psychopharmacology* 99 Suppl: S68-72. <https://doi.org/10.1007/BF00442563>.

- Mendoza, Arturo, Catherine Tang, Jinyoung Choi, Mariana Acuña, Maya Logan, Adriana G. Martin, Lujain Al-Sowaimel, et al. 2021. "Thyroid Hormone Signaling Promotes Hepatic Lipogenesis through the Transcription Factor ChREBP." *Science Signaling* 14 (709): eabh3839. <https://doi.org/10.1126/scisignal.abh3839>.
- Menezes-Ferreira, M. M., P. A. Petrick, and B. D. Weintraub. 1986. "Regulation of Thyrotropin (TSH) Bioactivity by TSH-Releasing Hormone and Thyroid Hormone." *Endocrinology* 118 (5): 2125–30. <https://doi.org/10.1210/endo-118-5-2125>.
- Merlin, Jon, Masaaki Sato, Ling Yeong Chia, Richard Fahey, Mohsen Pakzad, Cameron J. Nowell, Roger J. Summers, Tore Bengtsson, Bronwyn A. Evans, and Dana S. Hutchinson. 2018. "Rosiglitazone and a B3-Adrenoceptor Agonist Are Both Required for Functional Browning of White Adipocytes in Culture." *Frontiers in Endocrinology* 9: 249. <https://doi.org/10.3389/fendo.2018.00249>.
- Milić, Sandra, Davorka Lulić, and Davor Štimac. 2014. "Non-Alcoholic Fatty Liver Disease and Obesity: Biochemical, Metabolic and Clinical Presentations." *World Journal of Gastroenterology* 20 (28): 9330–37. <https://doi.org/10.3748/wjg.v20.i28.9330>.
- Mishra, Alok, Xu-guang Zhu, Kai Ge, and Sheue-Yann Cheng. 2010. "Adipogenesis Is Differentially Impaired by Thyroid Hormone Receptor Mutant Isoforms." *Journal of Molecular Endocrinology* 44 (4): 247–55. <https://doi.org/10.1677/JME-09-0137>.
- Mitchell, Nia, Vicki Catenacci, Holly R. Wyatt, and James O. Hill. 2011. "OBESITY: OVERVIEW OF AN EPIDEMIC." *The Psychiatric Clinics of North America* 34 (4): 717–32. <https://doi.org/10.1016/j.psc.2011.08.005>.
- Mohamed, Farahidah, and Christopher F. van der Walle. 2008. "Engineering Biodegradable Polyester Particles with Specific Drug Targeting and Drug Release Properties." *Journal of Pharmaceutical Sciences* 97 (1): 71–87. <https://doi.org/10.1002/jps.21082>.
- Monami, Matteo, Ilaria Dicembrini, Niccolò Marchionni, Carlo M. Rotella, and Edoardo Mannucci. 2012. "Effects of Glucagon-like Peptide-1 Receptor Agonists on Body Weight: A Meta-Analysis." *Experimental Diabetes Research* 2012: 672658. <https://doi.org/10.1155/2012/672658>.
- Moore, R., A. M. Grant, A. N. Howard, and I. H. Mills. 1980. "Treatment of Obesity with Triiodothyronine and a Very-Low-Calorie Liquid Formula Diet." *Lancet (London, England)* 1 (8162): 223–26. [https://doi.org/10.1016/s0140-6736\(80\)90715-1](https://doi.org/10.1016/s0140-6736(80)90715-1).
- Mosmann, T. 1983. "Rapid Colorimetric Assay for Cellular Growth and Survival: Application to Proliferation and Cytotoxicity Assays." *Journal of Immunological Methods* 65 (1–2): 55–63. [https://doi.org/10.1016/0022-1759\(83\)90303-4](https://doi.org/10.1016/0022-1759(83)90303-4).
- Moura, E, J Afonso, L Hein, and M A Vieira-Coelho. 2006. "A2-Adrenoceptor Subtypes Involved in the Regulation of Catecholamine Release from the Adrenal Medulla of Mice." *British Journal of Pharmacology* 149 (8): 1049–58. <https://doi.org/10.1038/sj.bjp.0706950>.
- Moustaïd, N., and H. S. Sul. 1991. "Regulation of Expression of the Fatty Acid Synthase Gene in 3T3-L1 Cells by Differentiation and Triiodothyronine." *The Journal of Biological Chemistry* 266 (28): 18550–54.
- Mulder, Willem J. M., Mandy M. T. van Leent, Marnix Lameijer, Edward A. Fisher, Zahi A. Fayad, and Carlos Pérez-Medina. 2018. "High-Density Lipoprotein Nanobiologics for Precision Medicine." *Accounts of Chemical Research* 51 (1): 127–37. <https://doi.org/10.1021/acs.accounts.7b00339>.
- Mund, Ross A., and William H. Frishman. 2013. "Brown Adipose Tissue Thermogenesis: B3-Adrenoreceptors as a Potential Target for the Treatment of Obesity in Humans." *Cardiology in Review* 21 (6): 265–69. <https://doi.org/10.1097/CRD.0b013e31829cabff>.
- Nawrocki, Andrea R., Michael W. Rajala, Eva Tomas, Utpal B. Pajvani, Asish K. Saha, Myrna E. Trumbauer, Zhen Pang, et al. 2006. "Mice Lacking Adiponectin Show Decreased Hepatic Insulin Sensitivity and Reduced Responsiveness to Peroxisome Proliferator-

- Activated Receptor Gamma Agonists." *The Journal of Biological Chemistry* 281 (5): 2654–60. <https://doi.org/10.1074/jbc.M505311200>.
- Nedergaard, Jan, and Barbara Cannon. 2014. "The Browning of White Adipose Tissue: Some Burning Issues." *Cell Metabolism* 20 (3): 396–407. <https://doi.org/10.1016/j.cmet.2014.07.005>.
- Neves, Susana R., Prahlad T. Ram, and Ravi Iyengar. 2002. "G Protein Pathways." *Science (New York, N.Y.)* 296 (5573): 1636–39. <https://doi.org/10.1126/science.1071550>.
- Nicholls, David G. 2006. "The Physiological Regulation of Uncoupling Proteins." *Biochimica Et Biophysica Acta* 1757 (5–6): 459–66. <https://doi.org/10.1016/j.bbabbio.2006.02.005>.
- Nicoloff, J. T., J. C. Low, J. H. Dussault, and D. A. Fisher. 1972. "Simultaneous Measurement of Thyroxine and Triiodothyronine Peripheral Turnover Kinetics in Man." *The Journal of Clinical Investigation* 51 (3): 473–83. <https://doi.org/10.1172/JCI106835>.
- Nissen, Steven E., and Kathy Wolski. 2007. "Effect of Rosiglitazone on the Risk of Myocardial Infarction and Death from Cardiovascular Causes." *New England Journal of Medicine* 356 (24): 2457–71. <https://doi.org/10.1056/NEJMoa072761>.
- Nitti, V. W., C. R. Chapple, C. Walters, M. B. Blauwet, S. Herschorn, I. Milsom, S. Auerbach, and P. Radziszewski. 2014. "Safety and Tolerability of the B3 -Adrenoceptor Agonist Mirabegron, for the Treatment of Overactive Bladder: Results of a Prospective Pooled Analysis of Three 12-Week Randomised Phase III Trials and of a 1-Year Randomised Phase III Trial." *International Journal of Clinical Practice* 68 (8): 972–85. <https://doi.org/10.1111/ijcp.12433>.
- Nitti, V. W., V. Khullar, P. van Kerrebroeck, S. Herschorn, J. Cambronero, J. C. Angulo, M. B. Blauwet, C. Dorrepaal, E. Siddiqui, and N. E. Martin. 2013. "Mirabegron for the Treatment of Overactive Bladder: A Prespecified Pooled Efficacy Analysis and Pooled Safety Analysis of Three Randomised, Double-Blind, Placebo-Controlled, Phase III Studies." *International Journal of Clinical Practice* 67 (7): 619–32. <https://doi.org/10.1111/ijcp.12194>.
- Ó'Fágáin, Ciarán, Philip M. Cummins, and Brendan F. O'Connor. 2010. "Gel-Filtration Chromatography." *Protein Chromatography* 681 (June): 25–33. https://doi.org/10.1007/978-1-60761-913-0_2.
- Offermanns, S, L P Zhao, A Gohla, I Sarosi, M I Simon, and T M Wilkie. 1998. "Embryonic Cardiomyocyte Hypoplasia and Craniofacial Defects in G Alpha q/G Alpha 11-Mutant Mice." *The EMBO Journal* 17 (15): 4304–12. <https://doi.org/10.1093/emboj/17.15.4304>.
- Offermanns, Stefan. 2006. "Activation of Platelet Function through G Protein-Coupled Receptors." *Circulation Research* 99 (12): 1293–1304. <https://doi.org/10.1161/01.RES.0000251742.71301.16>.
- Olivecrona, Gunilla. 2016. "Role of Lipoprotein Lipase in Lipid Metabolism." *Current Opinion in Lipidology* 27 (3): 233–41. <https://doi.org/10.1097/MOL.0000000000000297>.
- O'Mara, Alana E., James W. Johnson, Joyce D. Linderman, Robert J. Brychta, Suzanne McGehee, Laura A. Fletcher, Yael A. Fink, et al. 2020. "Chronic Mirabegron Treatment Increases Human Brown Fat, HDL Cholesterol, and Insulin Sensitivity." *The Journal of Clinical Investigation* 130 (5): 2209–19. <https://doi.org/10.1172/JCI131126>.
- Onken, Michael D., Carol M. Makepeace, Kevin M. Kaltenbronn, Joelle Choi, Leonel Hernandez-Aya, Katherine N. Weilbaecher, Kisha D. Piggott, et al. 2021. "Targeting Primary and Metastatic Uveal Melanoma with a G Protein Inhibitor." *The Journal of Biological Chemistry* 296 (February): 100403. <https://doi.org/10.1016/j.jbc.2021.100403>.
- Oppenheimer, J. H., H. L. Schwartz, J. T. Lane, and M. P. Thompson. 1991. "Functional Relationship of Thyroid Hormone-Induced Lipogenesis, Lipolysis, and Thermogenesis in the Rat." *The Journal of Clinical Investigation* 87 (1): 125–32. <https://doi.org/10.1172/JCI114961>.

- Ossoli, Alice, Sara Simonelli, Cecilia Vitali, Guido Franceschini, and Laura Calabresi. 2016. "Role of LCAT in Atherosclerosis." *Journal of Atherosclerosis and Thrombosis* 23 (2): 119–27. <https://doi.org/10.5551/jat.32854>.
- Panyam, Jayanth, Manisha M. Dali, Sanjeeb K. Sahoo, Wenxue Ma, Sudhir S. Chakravarthi, Gordon L. Amidon, Robert J. Levy, and Vinod Labhasetwar. 2003. "Polymer Degradation and in Vitro Release of a Model Protein from Poly(D, L-Lactide-Co-Glycolide) Nano- and Microparticles." *Journal of Controlled Release: Official Journal of the Controlled Release Society* 92 (1–2): 173–87. [https://doi.org/10.1016/s0168-3659\(03\)00328-6](https://doi.org/10.1016/s0168-3659(03)00328-6).
- Parikh, B. V., S. M. Upadrashta, S. H. Neau, and N. O. Nuessle. 1993. "Oestrone Loaded Poly(L-Lactic Acid) Microspheres: Preparation, Evaluation and in Vitro Release Kinetics." *Journal of Microencapsulation* 10 (2): 141–53. <https://doi.org/10.3109/02652049309104380>.
- Pavlov, G. M., O. A. Dommes, I. V. Aver'yanov, G. F. Kolbina, O. V. Okatova, V. A. Korzhikov, A. V. Dobrodumov, and T. B. Tennikova. 2015. "Conformational Differences of Poly(L-Lactic Acid) and Poly(D, L-Lactic Acid) in Dilute Solutions." *Doklady Chemistry* 465 (1): 261–64. <https://doi.org/10.1134/S0012500815110038>.
- Perez, D. M., M. T. Piascik, and R. M. Graham. 1991. "Solution-Phase Library Screening for the Identification of Rare Clones: Isolation of an Alpha 1D-Adrenergic Receptor cDNA." *Molecular Pharmacology* 40 (6): 876–83.
- Perra, Andrea, Gabriella Simbula, Michela Simbula, Monica Pibiri, Marta A. Kowalik, Pia Sulas, Maria T. Cocco, Giovanna M. Ledda-Columbano, and Amedeo Columbano. 2008. "Thyroid Hormone (T3) and TRbeta Agonist GC-1 Inhibit/Reverse Nonalcoholic Fatty Liver in Rats." *FASEB Journal: Official Publication of the Federation of American Societies for Experimental Biology* 22 (8): 2981–89. <https://doi.org/10.1096/fj.08-108464>.
- Petersen, Rasmus Koefoed, Lise Madsen, Lone Møller Pedersen, Philip Hallenborg, Hanne Hagland, Kristin Viste, Stein Ove Døskeland, and Karsten Kristiansen. 2008. "Cyclic AMP (cAMP)-Mediated Stimulation of Adipocyte Differentiation Requires the Synergistic Action of Epac- and cAMP-Dependent Protein Kinase-Dependent Processes." *Molecular and Cellular Biology* 28 (11): 3804–16. <https://doi.org/10.1128/MCB.00709-07>.
- Petrovic, Natasa, Tomas B. Walden, Irina G. Shabalina, James A. Timmons, Barbara Cannon, and Jan Nedergaard. 2010. "Chronic Peroxisome Proliferator-Activated Receptor γ (PPAR γ) Activation of Epididymally Derived White Adipocyte Cultures Reveals a Population of Thermogenically Competent, UCP1-Containing Adipocytes Molecularly Distinct from Classic Brown Adipocytes." *The Journal of Biological Chemistry* 285 (10): 7153–64. <https://doi.org/10.1074/jbc.M109.053942>.
- Pfeifer, Alexander, and Linda S. Hoffmann. 2015. "Brown, Beige, and White: The New Color Code of Fat and Its Pharmacological Implications." *Annual Review of Pharmacology and Toxicology* 55: 207–27. <https://doi.org/10.1146/annurev-pharmtox-010814-124346>.
- Plitzko, Birte, and Sandra Loesgen. 2018. "Measurement of Oxygen Consumption Rate (OCR) and Extracellular Acidification Rate (ECAR) in Culture Cells for Assessment of the Energy Metabolism." *Bio-Protocol* 8 (10): e2850. <https://doi.org/10.21769/BioProtoc.2850>.
- Pouleur, Anne-Catherine, Stefan Anker, Dulce Brito, Oana Brosteanu, Dirk Hasenclever, Barbara Casadei, Frank Edelmann, et al. 2018. "Rationale and Design of a Multicentre, Randomized, Placebo-Controlled Trial of Mirabegron, a Beta3-Adrenergic Receptor Agonist on Left Ventricular Mass and Diastolic Function in Patients with Structural Heart Disease Beta3-Left Ventricular Hypertrophy (Beta3-LVH)." *ESC Heart Failure* 5 (5): 830–41. <https://doi.org/10.1002/ehf2.12306>.
- Powell-Wiley, Tiffany M., Paul Poirier, Lora E. Burke, Jean-Pierre Després, Penny Gordon-Larsen, Carl J. Lavie, Scott A. Lear, et al. 2021. "Obesity and Cardiovascular Disease: A

- Scientific Statement From the American Heart Association." *Circulation* 143 (21): e984–1010. <https://doi.org/10.1161/CIR.0000000000000973>.
- Qi, Feng, Jie Wu, Qingze Fan, Fan He, Guifang Tian, Tingyuan Yang, Guanghui Ma, and Zhiguo Su. 2013. "Preparation of Uniform-Sized Exenatide-Loaded PLGA Microspheres as Long-Effective Release System with High Encapsulation Efficiency and Bio-Stability." *Colloids and Surfaces. B, Biointerfaces* 112 (December): 492–98. <https://doi.org/10.1016/j.colsurfb.2013.08.048>.
- Queiroz, Marcia Silva, Yvonne Shao, and Faramarz Ismail-Beigi. 2004. "Effect of Thyroid Hormone on Uncoupling Protein-3 mRNA Expression in Rat Heart and Skeletal Muscle." *Thyroid: Official Journal of the American Thyroid Association* 14 (3): 177–85. <https://doi.org/10.1089/105072504773297849>.
- Radhika, V., and N. Dhanasekaran. 2001. "Transforming G Proteins." *Oncogene* 20 (13): 1607–14. <https://doi.org/10.1038/sj.onc.1204274>.
- Reaven, Gerald M. 2011. "Relationships among Insulin Resistance, Type 2 Diabetes, Essential Hypertension, and Cardiovascular Disease: Similarities and Differences." *Journal of Clinical Hypertension (Greenwich, Conn.)* 13 (4): 238–43. <https://doi.org/10.1111/j.1751-7176.2011.00439.x>.
- Revelli, J. P., P. Muzzin, A. Paoloni, M. Moinat, and J. P. Giacobino. 1993. "Expression of the Beta 3-Adrenergic Receptor in Human White Adipose Tissue." *Journal of Molecular Endocrinology* 10 (2): 193–97. <https://doi.org/10.1677/jme.0.0100193>.
- Ribeiro, M. O., S. D. Carvalho, J. J. Schultz, G. Chiellini, T. S. Scanlan, A. C. Bianco, and G. A. Brent. 2001. "Thyroid Hormone--Sympathetic Interaction and Adaptive Thermogenesis Are Thyroid Hormone Receptor Isoform--Specific." *The Journal of Clinical Investigation* 108 (1): 97–105. <https://doi.org/10.1172/JCI12584>.
- Richardson, Paul E., Medha Manchekar, Nassrin Dashti, Martin K. Jones, Anne Beigneux, Stephen G. Young, Stephen C. Harvey, and Jere P. Segrest. 2005. "Assembly of Lipoprotein Particles Containing Apolipoprotein-B: Structural Model for the Nascent Lipoprotein Particle." *Biophysical Journal* 88 (4): 2789–2800. <https://doi.org/10.1529/biophysj.104.046235>.
- Rong, James X., Yang Qiu, Michael K. Hansen, Lei Zhu, Vivian Zhang, Mi Xie, Yuji Okamoto, et al. 2007. "Adipose Mitochondrial Biogenesis Is Suppressed in Db/Db and High-Fat Diet-Fed Mice and Improved by Rosiglitazone." *Diabetes* 56 (7): 1751–60. <https://doi.org/10.2337/db06-1135>.
- Rosen, Evan D., and Ormond A. MacDougald. 2006. "Adipocyte Differentiation from the inside Out." *Nature Reviews. Molecular Cell Biology* 7 (12): 885–96. <https://doi.org/10.1038/nrm2066>.
- Rosenwald, Matthias, Alike Perdikari, Thomas Röllicke, and Christian Wolfrum. 2013. "Bi-Directional Interconversion of Brite and White Adipocytes." *Nature Cell Biology* 15 (6): 659–67. <https://doi.org/10.1038/ncb2740>.
- Sacco, Emilio, and Riccardo Bientinesi. 2012. "Mirabegron: A Review of Recent Data and Its Prospects in the Management of Overactive Bladder." *Therapeutic Advances in Urology* 4 (6): 315–24. <https://doi.org/10.1177/1756287212457114>.
- Sacco, Emilio, Riccardo Bientinesi, Daniele Tienforti, Marco Racioppi, Gaetano Gulino, Daniele D'Agostino, Matteo Vittori, and Pierfrancesco Bassi. 2014. "Discovery History and Clinical Development of Mirabegron for the Treatment of Overactive Bladder and Urinary Incontinence." *Expert Opinion on Drug Discovery* 9 (4): 433–48. <https://doi.org/10.1517/17460441.2014.892923>.
- Salans, L. B., J. L. Knittle, and J. Hirsch. 1968. "The Role of Adipose Cell Size and Adipose Tissue Insulin Sensitivity in the Carbohydrate Intolerance of Human Obesity." *The Journal of Clinical Investigation* 47 (1): 153–65. <https://doi.org/10.1172/JCI105705>.

- Samuels, H. H., and J. S. Tsai. 1974. "Thyroid Hormone Action. Demonstration of Similar Receptors in Isolated Nuclei of Rat Liver and Cultured GH1 Cells." *The Journal of Clinical Investigation* 53 (2): 656–59. <https://doi.org/10.1172/JCI107601>.
- Saponaro, Federica, Simona Sestito, Massimiliano Runfola, Simona Rapposelli, and Grazia Chiellini. 2020. "Selective Thyroid Hormone Receptor-Beta (TR β) Agonists: New Perspectives for the Treatment of Metabolic and Neurodegenerative Disorders." *Frontiers in Medicine* 7 (July): 331. <https://doi.org/10.3389/fmed.2020.00331>.
- Schilperoort, Maaïke, Geerte Hoeke, Sander Kooijman, and Patrick C. N. Rensen. 2016. "Relevance of Lipid Metabolism for Brown Fat Visualization and Quantification." *Current Opinion in Lipidology* 27 (3): 242–48. <https://doi.org/10.1097/MOL.0000000000000296>.
- Schliecker, Gesine, Carsten Schmidt, Stefan Fuchs, and Thomas Kissel. 2003. "Characterization of a Homologous Series of D,L-Lactic Acid Oligomers; a Mechanistic Study on the Degradation Kinetics in Vitro." *Biomaterials* 24 (21): 3835–44. [https://doi.org/10.1016/s0142-9612\(03\)00243-6](https://doi.org/10.1016/s0142-9612(03)00243-6).
- Schmittgen, Thomas D., and Kenneth J. Livak. 2008. "Analyzing Real-Time PCR Data by the Comparative C T Method." *Nature Protocols* 3 (6): 1101–8. <https://doi.org/10.1038/nprot.2008.73>.
- Schrage, Ramona, Anna-Lena Schmitz, Evelyn Gaffal, Suvi Annala, Stefan Kehraus, Daniela Wenzel, Katrin M. Büllersbach, et al. 2015. "The Experimental Power of FR900359 to Study Gq-Regulated Biological Processes." *Nature Communications* 6 (December): 10156. <https://doi.org/10.1038/ncomms10156>.
- Seale, Patrick. 2015. "Transcriptional Regulatory Circuits Controlling Brown Fat Development and Activation." *Diabetes* 64 (7): 2369–75. <https://doi.org/10.2337/db15-0203>.
- Seale, Patrick, Bryan Bjork, Wenli Yang, Shingo Kajimura, Sherry Chin, Shihuan Kuang, Anthony Scimè, et al. 2008. "PRDM16 Controls a Brown Fat/Skeletal Muscle Switch." *Nature* 454 (7207): 961–67. <https://doi.org/10.1038/nature07182>.
- Shabalina, Irina G., Natasa Petrovic, Jasper M. A. de Jong, Anastasia V. Kalinovich, Barbara Cannon, and Jan Nedergaard. 2013. "UCP1 in Brite/Beige Adipose Tissue Mitochondria Is Functionally Thermogenic." *Cell Reports* 5 (5): 1196–1203. <https://doi.org/10.1016/j.celrep.2013.10.044>.
- Shimizu, Ippei, and Kenneth Walsh. 2015. "The Whitening of Brown Fat and Its Implications for Weight Management in Obesity." *Current Obesity Reports* 4 (2): 224–29. <https://doi.org/10.1007/s13679-015-0157-8>.
- Silva, J. E., T. E. Dick, and P. R. Larsen. 1978. "The Contribution of Local Tissue Thyroxine Monodeiodination to the Nuclear 3,5,3'-Triiodothyronine in Pituitary, Liver, and Kidney of Euthyroid Rats." *Endocrinology* 103 (4): 1196–1207. <https://doi.org/10.1210/endo-103-4-1196>.
- Simcox, Judith, Gisela Geoghegan, John Alan Maschek, Claire L. Bensard, Marzia Pasquali, Ren Miao, Sanghoon Lee, et al. 2017. "Global Analysis of Plasma Lipids Identifies Liver-Derived Acylcarnitines as a Fuel Source for Brown Fat Thermogenesis." *Cell Metabolism* 26 (3): 509–522.e6. <https://doi.org/10.1016/j.cmet.2017.08.006>.
- Simonds, W. F. 1999. "G Protein Regulation of Adenylate Cyclase." *Trends in Pharmacological Sciences* 20 (2): 66–73. [https://doi.org/10.1016/s0165-6147\(99\)01307-3](https://doi.org/10.1016/s0165-6147(99)01307-3).
- Singh, Amar M., Liang Zhang, John Avery, Amelia Yin, Yuhong Du, Hui Wang, Zibo Li, Haian Fu, Hang Yin, and Stephen Dalton. 2020. "Human Beige Adipocytes for Drug Discovery and Cell Therapy in Metabolic Diseases." *Nature Communications* 11 (1): 2758. <https://doi.org/10.1038/s41467-020-16340-3>.
- Singh, Rajesh, and James W. Lillard. 2009. "Nanoparticle-Based Targeted Drug Delivery." *Experimental and Molecular Pathology* 86 (3): 215–23. <https://doi.org/10.1016/j.yexmp.2008.12.004>.

- Sinha, Rohit A., Brijesh K. Singh, and Paul M. Yen. 2014. "Thyroid Hormone Regulation of Hepatic Lipid and Carbohydrate Metabolism." *Trends in Endocrinology and Metabolism: TEM* 25 (10): 538–45. <https://doi.org/10.1016/j.tem.2014.07.001>.
- Smolina, Natalia, Joseph Bruton, Anna Kostareva, and Thomas Sejersen. 2017. "Assaying Mitochondrial Respiration as an Indicator of Cellular Metabolism and Fitness." *Methods in Molecular Biology (Clifton, N.J.)* 1601: 79–87. https://doi.org/10.1007/978-1-4939-6960-9_7.
- Snyder, Peter J., and Robert D. Utiger. 1972. "Inhibition of Thyrotropin Response to Thyrotropin-Releasing Hormone by Small Quantities of Thyroid Hormones." *Journal of Clinical Investigation* 51 (8): 2077–84.
- Soomherun, Nopparuj, Narumol Kreua-Ongarjnkool, Sorayouth Chumnavej, and Saowapa Thumsing. 2017. "Encapsulation of Nicardipine Hydrochloride and Release from Biodegradable Poly(D, L-Lactic-Co-Glycolic Acid) Microparticles by Double Emulsion Process: Effect of Emulsion Stability and Different Parameters on Drug Entrapment." *International Journal of Biomaterials* 2017: 1743765. <https://doi.org/10.1155/2017/1743765>.
- Sousa-Batista, Ariane J., Wallace Pacienza-Lima, Maria Inês Ré, and Bartira Rossi-Bergmann. 2019. "Novel and Safe Single-Dose Treatment of Cutaneous Leishmaniasis with Implantable Amphotericin B-Loaded Microparticles." *International Journal for Parasitology. Drugs and Drug Resistance* 11 (December): 148–55. <https://doi.org/10.1016/j.ijpddr.2019.06.001>.
- Steinberg, D., and J. K. Huttunen. 1972. "The Role of Cyclic AMP in Activation of Hormone-Sensitive Lipase of Adipose Tissue." *Advances in Cyclic Nucleotide Research* 1: 47–62.
- Sugden, M. C., M. L. Langdown, R. A. Harris, and M. J. Holness. 2000. "Expression and Regulation of Pyruvate Dehydrogenase Kinase Isoforms in the Developing Rat Heart and in Adulthood: Role of Thyroid Hormone Status and Lipid Supply." *The Biochemical Journal* 352 Pt 3 (December): 731–38.
- Susulic, Vedrana S., Robert C. Frederich, Joel Lawitts, Effie Tozzo, Barbara B. Kahn, Mary-Ellen Harper, Jean Himms-Hagen, Jeffrey S. Flier, and Bradford B. Lowell. 1995. "Targeted Disruption of the B3-Adrenergic Receptor Gene *." *Journal of Biological Chemistry* 270 (49): 29483–92. <https://doi.org/10.1074/jbc.270.49.29483>.
- Sze, Alice, David Erickson, Liqing Ren, and Dongqing Li. 2003. "Zeta-Potential Measurement Using the Smoluchowski Equation and the Slope of the Current-Time Relationship in Electroosmotic Flow." *Journal of Colloid and Interface Science* 261 (2): 402–10. [https://doi.org/10.1016/S0021-9797\(03\)00142-5](https://doi.org/10.1016/S0021-9797(03)00142-5).
- Tailleux, Anne, Patrick Duriez, Jean-Charles Fruchart, and Véronique Clavey. 2002. "Apolipoprotein A-II, HDL Metabolism and Atherosclerosis." *Atherosclerosis* 164 (1): 1–13. [https://doi.org/10.1016/s0021-9150\(01\)00751-1](https://doi.org/10.1016/s0021-9150(01)00751-1).
- Takasu, Toshiyuki, Masashi Ukai, Shuichi Sato, Tetsuo Matsui, Itsuro Nagase, Tatsuya Maruyama, Masao Sasamata, Keiji Miyata, Hisashi Uchida, and Osamu Yamaguchi. 2007. "Effect of (R)-2-(2-Aminothiazol-4-Yl)-4'-{2-[(2-Hydroxy-2-Phenylethyl)Amino]Ethyl} Acetanilide (YM178), a Novel Selective Beta3-Adrenoceptor Agonist, on Bladder Function." *The Journal of Pharmacology and Experimental Therapeutics* 321 (2): 642–47. <https://doi.org/10.1124/jpet.106.115840>.
- Takusagawa, Shin, Kanako Yajima, Aiji Miyashita, Shotaro Uehara, Takafumi Iwatsubo, and Takashi Usui. 2012. "Identification of Human Cytochrome P450 Isoforms and Esterases Involved in the Metabolism of Mirabegron, a Potent and Selective B3-Adrenoceptor Agonist." *Xenobiotica; the Fate of Foreign Compounds in Biological Systems* 42 (10): 957–67. <https://doi.org/10.3109/00498254.2012.675095>.
- Tall, A. R. 1998. "An Overview of Reverse Cholesterol Transport." *European Heart Journal* 19 Suppl A (February): A31-35.

- Tanase, Daniela Maria, Evelina Maria Gosav, Ecaterina Neculae, Claudia Florida Costea, Manuela Ciocoiu, Loredana Liliana Hurjui, Claudia Cristina Tarniceriu, and Mariana Floria. 2020. "Hypothyroidism-Induced Nonalcoholic Fatty Liver Disease (HIN): Mechanisms and Emerging Therapeutic Options." *International Journal of Molecular Sciences* 21 (16): E5927. <https://doi.org/10.3390/ijms21165927>.
- Thaker, Vidhu V. 2017. "GENETIC AND EPIGENETIC CAUSES OF OBESITY." *Adolescent Medicine: State of the Art Reviews* 28 (2): 379–405.
- Thakran, Shalini, Pragya Sharma, Ramy R. Attia, Roderick T. Hori, Xiong Deng, Marshall B. Elam, and Edwards A. Park. 2013. "Role of Sirtuin 1 in the Regulation of Hepatic Gene Expression by Thyroid Hormone." *The Journal of Biological Chemistry* 288 (2): 807–18. <https://doi.org/10.1074/jbc.M112.437970>.
- Than, Aung, Ke Liang, Shaohai Xu, Lei Sun, Hongwei Duan, Fengna Xi, Chenjie Xu, and Peng Chen. 2017. "Transdermal Delivery of Anti-Obesity Compounds to Subcutaneous Adipose Tissue with Polymeric Microneedle Patches." *Small Methods* 1 (11): 1700269. <https://doi.org/10.1002/smtd.201700269>.
- Thonberg, Håkan, J. Magnus Fredriksson, Jan Nedergaard, and Barbara Cannon. 2002. "A Novel Pathway for Adrenergic Stimulation of CAMP-Response-Element-Binding Protein (CREB) Phosphorylation: Mediation via Alpha1-Adrenoceptors and Protein Kinase C Activation." *The Biochemical Journal* 364 (Pt 1): 73–79. <https://doi.org/10.1042/bj3640073>.
- Torchilin, Vladimir P. 2005. "Recent Advances with Liposomes as Pharmaceutical Carriers." *Nature Reviews Drug Discovery* 4 (2): 145–60. <https://doi.org/10.1038/nrd1632>.
- Trujillo, Maria E., and Philipp E. Scherer. 2006. "Adipose Tissue-Derived Factors: Impact on Health and Disease." *Endocrine Reviews* 27 (7): 762–78. <https://doi.org/10.1210/er.2006-0033>.
- Tsibulnikov, Sergey, Leonid Maslov, Nikita Voronkov, and Peter Oeltgen. 2020. "Thyroid Hormones and the Mechanisms of Adaptation to Cold." *Hormones (Athens, Greece)* 19 (3): 329–39. <https://doi.org/10.1007/s42000-020-00200-2>.
- Tu, H. M., S. W. Kim, D. Salvatore, T. Bartha, G. Legradi, P. R. Larsen, and R. M. Lechan. 1997. "Regional Distribution of Type 2 Thyroxine Deiodinase Messenger Ribonucleic Acid in Rat Hypothalamus and Pituitary and Its Regulation by Thyroid Hormone." *Endocrinology* 138 (8): 3359–68. <https://doi.org/10.1210/endo.138.8.5318>.
- Varde, Neelesh K., and Daniel W. Pack. 2004. "Microspheres for Controlled Release Drug Delivery." *Expert Opinion on Biological Therapy* 4 (1): 35–51. <https://doi.org/10.1517/14712598.4.1.35>.
- Vargas-Uricoechea, Hernando, Anilsa Bonelo-Perdomo, and Carlos Hernán Sierra-Torres. 2014. "Effects of Thyroid Hormones on the Heart." *Clinica E Investigacion En Arteriosclerosis: Publicacion Oficial De La Sociedad Espanola De Arteriosclerosis* 26 (6): 296–309. <https://doi.org/10.1016/j.arteri.2014.07.003>.
- Vaughan, M., J. E. Berger, and D. Steinberg. 1964. "HORMONE-SENSITIVE LIPASE AND MONOGLYCERIDE LIPASE ACTIVITIES IN ADIPOSE TISSUE." *The Journal of Biological Chemistry* 239 (February): 401–9.
- Villarroya, F., R. Cereijo, A. Gavaldà-Navarro, J. Villarroya, and M. Giralt. 2018. "Inflammation of Brown/Beige Adipose Tissues in Obesity and Metabolic Disease." *Journal of Internal Medicine* 284 (5): 492–504. <https://doi.org/10.1111/joim.12803>.
- Villicev, Cássio M., Fatima R. S. Freitas, Marcelo S. Aoki, Cássio Taffarel, Thomas S. Scanlan, Anselmo S. Moriscot, Miriam O. Ribeiro, Antonio C. Bianco, and Cecília H. A. Gouveia. 2007. "Thyroid Hormone Receptor Beta-Specific Agonist GC-1 Increases Energy Expenditure and Prevents Fat-Mass Accumulation in Rats." *The Journal of Endocrinology* 193 (1): 21–29. <https://doi.org/10.1677/joe.1.07066>.

- Wadman, Meredith. 2006. "Rimonabant Adds Appetizing Choice to Slim Obesity Market." *Nature Medicine* 12 (1): 27–27. <https://doi.org/10.1038/nm0106-27>.
- Wall, M. A., B. A. Posner, and S. R. Sprang. 1998. "Structural Basis of Activity and Subunit Recognition in G Protein Heterotrimers." *Structure (London, England: 1993)* 6 (9): 1169–83. [https://doi.org/10.1016/s0969-2126\(98\)00117-8](https://doi.org/10.1016/s0969-2126(98)00117-8).
- Wang, J., C. W. Ng, K. Y. Win, P. Shoemakers, T. K. Y. Lee, S. S. Feng, and C. H. Wang. 2003. "Release of Paclitaxel from Polylactide-Co-Glycolide (PLGA) Microparticles and Discs under Irradiation." *Journal of Microencapsulation* 20 (3): 317–27. <https://doi.org/10.1080/0265204021000058401>.
- Warren, Katherine, Helena Burden, and Paul Abrams. 2016. "Mirabegron in Overactive Bladder Patients: Efficacy Review and Update on Drug Safety." *Therapeutic Advances in Drug Safety* 7 (5): 204–16. <https://doi.org/10.1177/2042098616659412>.
- Wassen, Frank W. J. S., Willem Klootwijk, Ellen Kaptein, Dirk J. Duncker, Theo J. Visser, and George G. J. M. Kuiper. 2004. "Characteristics and Thyroid State-Dependent Regulation of Iodothyronine Deiodinases in Pigs." *Endocrinology* 145 (9): 4251–63. <https://doi.org/10.1210/en.2004-0356>.
- Wettschureck, Nina, and Stefan Offermanns. 2005. "Mammalian G Proteins and Their Cell Type Specific Functions." *Physiological Reviews* 85 (4): 1159–1204. <https://doi.org/10.1152/physrev.00003.2005>.
- Wiersinga, Wilmar M., Leonidas Duntas, Valentin Fadeyev, Birte Nygaard, and Mark P. J. Vanderpump. 2012. "2012 ETA Guidelines: The Use of L-T4 + L-T3 in the Treatment of Hypothyroidism." *European Thyroid Journal* 1 (2): 55–71. <https://doi.org/10.1159/000339444>.
- Wing, Rena R., and Suzanne Phelan. 2005. "Long-Term Weight Loss Maintenance." *The American Journal of Clinical Nutrition* 82 (1 Suppl): 222S–225S. <https://doi.org/10.1093/ajcn/82.1.222S>.
- Wischke, Christian, and Steven P. Schwendeman. 2008. "Principles of Encapsulating Hydrophobic Drugs in PLA/PLGA Microparticles." *International Journal of Pharmaceutics* 364 (2): 298–327. <https://doi.org/10.1016/j.ijpharm.2008.04.042>.
- Wooltorton, Eric. 2002. "Obesity Drug Sibutramine (Meridia): Hypertension and Cardiac Arrhythmias." *CMAJ: Canadian Medical Association Journal* 166 (10): 1307–8.
- Wu, Jun, Pontus Boström, Lauren M. Sparks, Li Ye, Jang Hyun Choi, An-Hoa Giang, Melin Khandekar, et al. 2012. "Beige Adipocytes Are a Distinct Type of Thermogenic Fat Cell in Mouse and Human." *Cell* 150 (2): 366–76. <https://doi.org/10.1016/j.cell.2012.05.016>.
- Wu, Jun, Paul Cohen, and Bruce M. Spiegelman. 2013. "Adaptive Thermogenesis in Adipocytes: Is Beige the New Brown?" *Genes & Development* 27 (3): 234–50. <https://doi.org/10.1101/gad.211649.112>.
- Wu, X. S., and N. Wang. 2001. "Synthesis, Characterization, Biodegradation, and Drug Delivery Application of Biodegradable Lactic/Glycolic Acid Polymers. Part II: Biodegradation." *Journal of Biomaterials Science. Polymer Edition* 12 (1): 21–34. <https://doi.org/10.1163/156856201744425>.
- Xiao, R. P. 2001. "Beta-Adrenergic Signaling in the Heart: Dual Coupling of the Beta2-Adrenergic Receptor to G(s) and G(i) Proteins." *Science's STKE: Signal Transduction Knowledge Environment* 2001 (104): re15. <https://doi.org/10.1126/stke.2001.104.re15>.
- Xiong, Sijing, Saji George, Haiyang Yu, Robert Damoiseaux, Bryan France, Kee Woei Ng, and Joachim Say-Chye Loo. 2013. "Size Influences the Cytotoxicity of Poly (Lactic-Co-Glycolic Acid) (PLGA) and Titanium Dioxide (TiO₂) Nanoparticles." *Archives of Toxicology* 87 (6): 1075–86. <https://doi.org/10.1007/s00204-012-0938-8>.
- Xu, Jiang, Shusheng Zhang, Anais Machado, Sébastien Lecommandoux, Olivier Sandre, Frank Gu, and Annie Colin. 2017. "Controllable Microfluidic Production of Drug-Loaded PLGA

- Nanoparticles Using Partially Water-Miscible Mixed Solvent Microdroplets as a Precursor." *Scientific Reports* 7 (1): 4794. <https://doi.org/10.1038/s41598-017-05184-5>.
- Xue, Yuan, Xiaoyang Xu, Xue-Qing Zhang, Omid C. Farokhzad, and Robert Langer. 2016. "Preventing Diet-Induced Obesity in Mice by Adipose Tissue Transformation and Angiogenesis Using Targeted Nanoparticles." *Proceedings of the National Academy of Sciences of the United States of America* 113 (20): 5552–57. <https://doi.org/10.1073/pnas.1603840113>.
- Y, Hiramatsu, Muraoka R, Kigoshi S, and Muramatsu I. 1994. "Identification of Alpha 1-Adrenoceptor Subtypes in Rat Lung by Binding of [3H]-Prazosin and [3H]-WB4101." *Journal of Receptor Research* 14 (2). <https://doi.org/10.3109/10799899409066998>.
- Yamaguchi, Osamu, and Christopher R. Chapple. 2007. "Beta3-Adrenoceptors in Urinary Bladder." *Neurourology and Urodynamics* 26 (6): 752–56. <https://doi.org/10.1002/nau.20420>.
- Yamamoto, Eiichi, Shota Miyazaki, Chiaki Aoyama, and Masaru Kato. 2018. "A Simple and Rapid Measurement Method of Encapsulation Efficiency of Doxorubicin Loaded Liposomes by Direct Injection of the Liposomal Suspension to Liquid Chromatography." *International Journal of Pharmaceutics* 536 (1): 21–28. <https://doi.org/10.1016/j.ijpharm.2017.11.035>.
- Yau, Winifred W., Brijesh K. Singh, Ronny Lesmana, Jin Zhou, Rohit A. Sinha, Kiraely A. Wong, Yajun Wu, et al. 2019. "Thyroid Hormone (T3) Stimulates Brown Adipose Tissue Activation via Mitochondrial Biogenesis and MTOR-Mediated Mitophagy." *Autophagy* 15 (1): 131–50. <https://doi.org/10.1080/15548627.2018.1511263>.
- Yazdi, Fereshteh T., Susanne M. Clee, and David Meyre. 2015. "Obesity Genetics in Mouse and Human: Back and Forth, and Back Again." *PeerJ* 3 (March). <https://doi.org/10.7717/peerj.856>.
- Young, Stephen G., and Rudolf Zechner. 2013. "Biochemistry and Pathophysiology of Intravascular and Intracellular Lipolysis." *Genes & Development* 27 (5): 459–84. <https://doi.org/10.1101/gad.209296.112>.
- Zatterale, Federica, Michele Longo, Jamal Naderi, Gregory Alexander Raciti, Antonella Desiderio, Claudia Miele, and Francesco Beguinot. 2019. "Chronic Adipose Tissue Inflammation Linking Obesity to Insulin Resistance and Type 2 Diabetes." *Frontiers in Physiology* 10: 1607. <https://doi.org/10.3389/fphys.2019.01607>.
- Zavacki, Ann Marie, Hao Ying, Marcelo A. Christoffolete, Goele Aerts, Edward So, John W. Harney, Sheue-Yann Cheng, P. Reed Larsen, and Antonio C. Bianco. 2005. "Type 1 Iodothyronine Deiodinase Is a Sensitive Marker of Peripheral Thyroid Status in the Mouse." *Endocrinology* 146 (3): 1568–75. <https://doi.org/10.1210/en.2004-1392>.
- Zhao, J., L. Unelius, T. Bengtsson, B. Cannon, and J. Nedergaard. 1994. "Coexisting Beta-Adrenoceptor Subtypes: Significance for Thermogenic Process in Brown Fat Cells." *The American Journal of Physiology* 267 (4 Pt 1): C969-979. <https://doi.org/10.1152/ajpcell.1994.267.4.C969>.
- Zimmermann, Robert, Achim Lass, Guenter Haemmerle, and Rudolf Zechner. 2009. "Fate of Fat: The Role of Adipose Triglyceride Lipase in Lipolysis." *Biochimica Et Biophysica Acta* 1791 (6): 494–500. <https://doi.org/10.1016/j.bbaliip.2008.10.005>.
- Zimmermann, Robert, Juliane G. Strauss, Guenter Haemmerle, Gabriele Schoiswohl, Ruth Birner-Gruenberger, Monika Riederer, Achim Lass, et al. 2004. "Fat Mobilization in Adipose Tissue Is Promoted by Adipose Triglyceride Lipase." *Science (New York, N.Y.)* 306 (5700): 1383–86. <https://doi.org/10.1126/science.1100747>.

Publications and abstracts

Publications

Quantification of Lipoprotein Uptake *in Vivo* Using Magnetic Particle Imaging and Spectroscopy.

Hildebrand S, Löwa N, Paysen H, Fratila RM, Reverte-Salisa L, Trakoolwilaiwan T, **Niu Z**, Kasparis G, Preuss SF, Kosch O, M de la Fuente J, Thanh NTK, Wiekhorst F, Pfeifer A.

ACS Nano. 2021 Jan 26;15(1):434-446. doi: 10.1021/acsnano.0c03229. Epub 2020 Dec 11. PMID: 33306343.

Abstracts

Targeted transport of therapeutic nanoparticles into adipose tissue.

Zheming Niu, Alexander Pfeifer.

The 2nd International Conference and Exhibition on Nanomedicine and Drug Delivery, May 21-23, 2018 Tokyo, Japan.

Poster prize.